NASA CR-174922

National Aeronautics and Space Administration

ENVIRONMENTALLY-INDUCED DISCHARGE TRANSIENT COUPLING TO SPACECRAFT

by R. Viswanathan, G. Barbay, and N. J. Stevens

HUGHES AIRCRAFT COMPANY
SPACE AND COMMUNICATIONS GROUP
TECHNOLOGY DIVISION

prepared for

NATIONAL AERONAUTICS AND SPACE ADMINISTRATION

NASA Lewis Research Center
Contract NAS 3-23869

1. Report No.	2. Government Accession No.	3. Recipient's Catalog No.
NASA CR-174922		

4. Title and Subtitle	5. Report Date
Environmentally-Induced Discharge Transient Coupling to Spacecraft	May 1985
	6. Performing Organization Code

7. Author(s)	8. Performing Organization Report No.
R. Viswanathan, G. Barbay and N. J. Stevens	
	10. Work Unit No.

9. Performing Organization Name and Address	11. Contract or Grant No.
Hughes Aircraft Company Space and Communications Group Technology Division P. O. Box 92919, Los Angeles, CA 90009	NAS 3-23869
	13. Type of Report and Period Covered
12. Sponsoring Agency Name and Address	Final Report
National Aeronautics and Space Administration Lewis Research Center 21000 Brookpark Rd, Cleveland, OH 44135	14. Sponsoring Agency Code

15. Supplementary Notes

Project Manager, Mr. John V. Staskus
NASA Lewis Research Center, Cleveland, Ohio

16. Abstract

The Hughes "SCREENS" (Space Craft Response to Environments of Space) technique was applied to generic spin and 3-axis stabilized spacecraft models. It involved the NASCAP modeling for surface charging and lumped element modeling for transients Coupling into Spacecraft.

A differential voltage between antenna and spun shelf of ~ 400 V and current of 12 A resulted from discharge at antenna for the spinner and ~ 3 kv and 0.3 A from a discharge at solar panels for the 3-axis stabilized Spacecraft.

A typical interface circuit response was analyzed to show that the transients would couple into the Spacecraft System through ground points, which are most vulnerable.

A compilation and review was performed on 15 years of available data for electron and ion current collection phenomena. Empirical models were developed to match data and compared with flight data of Pix-1 and Pix-2 mission. It was found large space power systems would float negative and discharge if operated at or above 300 V. Several recommendations are given to impove the models and to apply them to large space systems.

17. Key Words (Suggested by Author(s))	18. Distribution Statement
NASCAP, Spacecraft Charging, Space Environments, Coupling, Lumped Element Model, Pix-1, Pix-2, High Voltage Solar Array, Plasma Interactions, Transients	Unclassified-Unlimited

19. Security Classif. (of this report)	20. Security Classif. (of this page)	21. No. of pages	22. Price*
Unclassified	Unclassified	86	

*For sale by the National Technical Information Service, Springfield, Virginia 22161

TABLE OF CONTENTS

TABLE OF CONTENTS - CONTINUED

TABLE OF FIGURES

TABLE OF FIGURES

1. SUMMARY

This contract study of environmentally-induced discharge transients coupling into Spacecraft Systems consists of two tasks.

In the first task is evaluated the transients that could occur in geosynchronous environments, using the NASA Charging Analyzer Program and lumped element modeling for transients coupling into wires. In the second task is evaluated the available data pertinent to high voltage solar arrays, collected from laboratory and space experiments, to develop and apply empirical models for large Space Systems.

It is shown that discharges on the exterior of Satellites can cause structural potentials to change, which is oscillatory and which creates differential voltages between different portions of the Spacecraft.

In a typical Spin Stabilized Spacecraft the differential voltages are smaller (~400 V) but currents are higher (~12 A) compared to a 3-axis Stabilized Spacecraft (V ~ 3 kv, current ~ 300 mA).

We have shown that it is possible to construct a simplified lumped element model, with judicious selection of parameters, which can be used to evaluate the response of a given spacecraft in a gross quick way. This will help locate areas of concern in a given design for further analysis.

A typical interface circuit response to discharge pulses was analyzed to show that the coupling through the ground point is a serious threat for Spacecraft electronic units.

In the high voltage solar array task of the study, it was found that the data available is inadequate to provide an absolute set of equations for electron and ion current collection phenomena. It is necessary to investigate systematically under well-controlled laboratory conditions with all of the plasma properties identified, to clarify the existing discrepencies between data from one laboratory to another.

The empirical models developed, however, reasonably explain flight data and give, in turn, information on the plasma characteristics during flight.

The current models developed here indicate that discharges are quite likely for systems operated at or above 300 V. It is necessary to conduct a test with a self generated voltage solar array to verify that the system could discharge and, if it does, to characterize the discharge pulse.

2. INTRODUCTION

This contract study of environmentally-induced discharge transient coupling into spacecraft systems was divided into two tasks. The first task involved the evaluation of transients that could occur in geosynchronous environments and the second concerned with high voltage solar array discharge transients that occur primarily in low Earth orbits.

The approach used in the spacecraft charging coupling study was to apply the Hughes SCREENS (Space Craft Response to Environments of Space) technique to generic spin and 3-axis stablized spacecraft models. This technique involved the use of NASCAP modeling studies to predict surface charging and charge stored in dielectrics and lumped element modeling to predict structure and cable currents and voltages resulting from possible exterior discharges. The goal of this study was to demonstrate plausable explanations on how spacecraft systems could be upset by exterior discharges.

The approach used in the high voltage solar array transient study was to review existing ground simulation data and develop simple current collection models to match the data. These models were then compared to available space experiment data. Finally, the models were used to conduct a preliminary evaluation of large power system behavior in space environments. The impacts of possible discharges on the power system operation were assessed. Recommendations were made for improving the state-of-knowledge of these environmentally-induced interactions.

3. BACKGROUND - ELECTROSTATIC DISCHARGE TRANSIENTS IN GEOSYNCHRONOUS ENVIRONMENT

3.1 Spacecraft Charging Phenomena

In the early 70's geosynchronous spacecraft began experiencing a series of unexplained electronic switching anomalies. These events were initially considered to be nuisances and were corrected by ground commands, logged in the operations records and forgotten. In June, 1973 an AF geosynchronous satellite failed and the subsequent review board found that the failure could have been caused by an encounter with a severe geomagnetic substorm.

It had been known for years prior to this failure that substorm environments could charge satellite surfaces to substantial negative voltages[2-5] but now this charging apparently could be responsible for catastrophic failures. Reviews of satellite operational records reinforced the opinion that geomagnetic substorms could be responsible for the switching anomalies as well as the failure. The term, "spacecraft charging", was applied to this process of geosynchronous satellite surfaces being charged by geomagnetic substorm environments.[4]

A cooperative Air Force and NASA technology investigation was launched late in 1975 to evaluate spacecraft charging phenomena.[6] The objective of this investigation was to develop the criteria necessary to control the absolute and differential charging of spacecraft surfaces by geomagnetic substorms. The principal outputs of this technology and space flight program were to be three documents; an environmental atlas, a specification for testing spacecraft to determine susceptability to upset by charging environments, and a design guideline document to provide criteria for designing immunity into spacecraft. This investigation was ambitious in that, over a five year period, it was to define the substorm environmental characteristics, develop computer tools necessary to predict complex spacecraft surface charging in that environment, determine the location and characteristics of discharges and predict transient coupling into the structure and subsystems. The results of this program have been documented in the preceedings of the biennial Spacecraft Charging Technology Conferences[7-9] and in AIAA conferences.[10-11]

From these published reports, it is apparent that substantial progress has been made although it has taken longer than anticipated to complete the task. The environmental atlas has been published[12], the NASA Charging Analyzer Program (NASCAP) has been validated against ground test and space flight data[13,14] and preliminary versions of a military standard[15,16] and design guidelines[17] are available. However, the study of discharge characteristic and transient pulse coupling into systems has been lagging behind other areas. It is recognized that a considerable effort went into the studies of discharges initiated under strong voltage gradients - the so-called "big bang" dis-

charges - before it became apparent that such gradients need not occur on spacecraft.[18] Subsequent studies have identified conditions which could produce lower energy discharges and have approximated possible characteristics.[19-21]

The status of the environmental models and surface charging analyzer computer codes is reviewed in the following sections. Finally, the approach used at Hughes Aircraft Company is discussed.

3.2 Geomagnetic Substorm Environmental Model

The composition and time evolution of the space plasma environment are quite complex.[17] It is standard practice to represent the environment in terms of a temperature and density, assuming a Maxwell-Boltzman distribution. In that characterization the geosynchronous environment is typified as a cold, dense plasma (with a temperature of about 1 eV and a density of up to 100 particles/cm^3). During a geomagnetic substorm the high-density, low-energy plasma near local midnight is replaced by a cloud of low-density plasmas (1 to 10 particles/ cm^3) with energies from 1 to 50 keV. It is this environment that can charge spacecraft dielectric surfaces to the extent that they may break down in an electostatic discharge. The hot plasma cloud diffuses in a few hours but it is replaced many times during the life of a storm (which may last a day or longer).

If the spacecraft is near local noon when the cloud appears, it may never see the hot plasma and will not charge. If the spacecraft is near midnight, it may experience charging and upsets. If the spacecraft is near local evening, as it moves towards midnight, it will pass into the diffusing cloud and a more severe charging environment. If the spacecraft is near local dawn, it may be over taken by the hot plasma. The problem in defining a substorm environment is that each of the above situations represents a unique set of plasma conditions as viewed by a spacecraft and results in a markedly different charging history.

That the charging of spacecraft surfaces occurs only at satellite local times of 2000 to 1000 hours[22] has been demonstrated by the AF SCATHA data. The data clearly shows the limited charging region experienced over a nine month period[23,24] (see Figure 1). Interior transients that were monitored by that spacecraft are also shown as open and closed dots. It should be noted that transients can occur even when there is no surface charging (local noon to local evening).

The environmental model for geomagnetic substorms is taken from a statistical approach to estimate the yearly percentage of occurrence of the plasma parameters.[17] These occurrence frequencies were derived by fitting the observed distributions of

electron and ion temperature from ATS-5/6 and SCATHA data. The distribution for the electron temperature is shown in Figure 2. The plasma parameters used (corresponding to a severe substorm) are:

Electron Temperature:	12 keV	Electron Density:	1.1 cm^{-3}
Ion Temperature:	20 keV	Ion Density:	0.4 cm^{-3}

The ion density is lower than the electron to account for the effect of different species of ions in the incident current terms. This type of substorm could occur in geosynchronous environments about 10% of time per year. Since these statistics concern only the environment, a spacecraft still may not be in the proper position to encounter this storm. Hence, for a given spacecraft, the percentage of time per year of orbit that it would encounter such a severe substorm could be significantly less.

The duration of time that a spacecraft would encounter such a severe substorm is relatively short. A severe substorm like this generally develops rapidly and dissipates to a lower level. This is demonstrated by the fact that spacecraft potentials in sunlight charging cases are limited to a few hundred volts negative for spinners[25] and to -2.3 kV for 3-axis stabilized spacecraft.[26] These levels of ground potential can be reached in about 10 minutes of charging in such storms. Hence, to be safe, all charging analyses will be run for 15 minutes.

3.3 NASA Charging Analyzer Program (NASCAP)

The NASCAP computer code was developed specifically to predict the charging of complex 3-dimensional spacecraft by geomagnetic substorms. It has been described in detail in the literature[27-29] and will only be summarized here.

NASCAP is a quasi-static computational code; that is, it assumes that a current balance exists at each instant of time. It is capable of analyzing the charging of 3-dimensional spacecraft as a function of time for given space environmental conditions. It includes consideration of conductive and dielectric materials properties (e.g. secondary emission, backscatter, photoemission, bulk, and surface conduction), electrostatic potentials and magnetic fields. It uses these considerations to compute currents to and from these surfaces and predict potential distributions around the body. The body must be defined in terms of rectangular parallelepiped sections of parallelepipeds, flat plates or booms within a 17 x 17 x 33 point grid. Up to 15 separate conductors can be specified with the first conductor capable of floating with respect to space. The others can be resistively or capacitively coupled or biased (with respect to the first). Environments

FIGURE 1. SCATHA CHARGING/DISCHARGING DATA

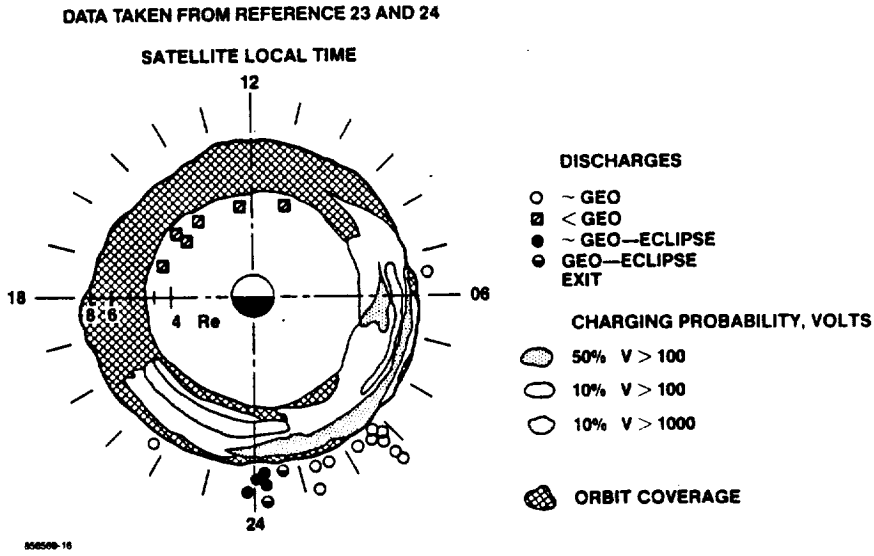

FIGURE 2. SUBSTORM STATISTICAL CHARACTERIZATION

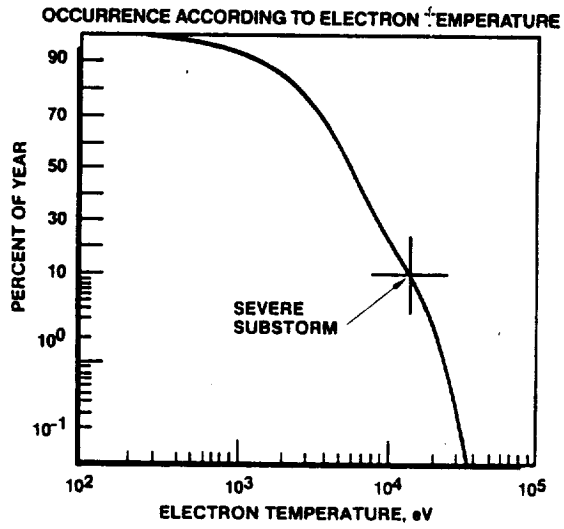

can be specified in terms of single or double Maxwellian distributions. The code outputs a variety of graphic displays showing the model used, the voltage distributions for given environments at specific times and particle trajectories (if desired). Tabular output is also available.

3.4 Discharge and Transient Coupling Processes

That a geomagnetic substorm can charge spacecraft and its dielectric surfaces to a point where discharges can occur has been demonstrated by SCATHA[30] and is generally accepted. What is not known is why discharges are initiated and how can this pulse induce a simulated switching transient.

It was first believed that discharges were the result of large differential charging between the dielectric surface and the substrate enhanced by edges, gaps or cracks in the dielectric. When differential voltages of about -15 kV were generated across 5 mil teflon and kapton test samples, spectacular lightning-like flashes could be observed.[31] These discharges damaged the dielectrics and could explain both the electronic upsets and thermal problems observed in space. However, analysis and flight data soon showed that differential voltages of -5 kV across 5 mil dielectrics were the maximum expected in space and these types of driving voltages would not trigger discharges. The present-day use of 1 and 2 mil dielectric films would reduce this maximum differential voltage further.

Discharge models were proposed in which charge was buried within the dielectric material[32-33]. Under these models the charge layer would build up until it would exceed a threshold (probably at a dielectric edge) and breakdown, emitting charge to space. The threshold was given in terms of an electric field ($\sim 2 \times 10^5$ volts/cm)[33] which could be easily reached with layers buried a few microns under the surface. Discharges could occur at any time according to this model and were not tied to the encounter with substorms. This could explain the transients observed by SCATHA and others[34] in the non-charging period of this orbit.

Another possible mechanism is the "inverted" charging type of discharge.[19-21] In this mechanism the conductor is charged negative with respect to the surrounding dielectrics.

This gives rise to an electron emitter surface coupled to an accelerating, extraction field. Discharges of this type occur more frequently in gaps (like solar arrays or OSR's), metallized dielectric films where the grounding of the metal film has failed, or painted metallic surfaces within cavities.

Finally, a discharge may occur because of an imperfection on the surface. This provides a trigger and the breakdown is across the capacitor between the spacecraft and the space plasma potential.

Once a discharge starts (for whatever reason) it stops eventually because it has emitted all of the available charge. With the large differential charge type of discharge, there was sufficient driving potential to move almost all of the charge to the discharge point and eject it to space. With the lower energy discharge only the charge in the region of the discharge is involved. The process is believed to be as follows:

a. Discharge is initiated and charge is ejected to space.

b. The spacecraft ground voltage becomes much more positive due to this change loss. ($\Delta V \simeq \Delta Q/C_{space}$)

c. Charge is moved throughout the structure to the discharge site due to the now unbalanced polarization charge in the dielectric.

d. The more positive spacecraft conductive surfaces collect particles from space (either attracting back the emitted particles or others). This enhances the current flow in structure. Eventually, the vehicle recharges.

e. The transient current flow in the structure creates a magnetic field which couples an electric field into the cables. This transient was believed to cause the upset. Filtering the input lines was then believed to be the answer to prevent upsets.

Experiments[35] and analysis[36] seemed to demonstrate that items a through d were probable. Item e could not be conclusively demonstrated. Testing of Voyager seemed to show that SEMCAP could explain coupling possibilities[37,38] but when applied to communications satelltites in Earth orbit, no hazard could be identified.[39,40] It is this area that really needs the study.

3.5 Hughes "SCREENS" Approach

The Space and Communications Group at Hughes Aircraft Company has been interested in electronic switching anomalies since the mid-seventies. It has developed, a technique called SCREENS (Space Craft Response to Environments of Space) to predict behavior in space and to try to localize coupling paths into electronic systems. This technique was initiated with analytical and experimental studies on the Intelsat VI spacecraft and has been expanded and improved continuously since then.

SCREENS is really several elements tied together to satisfy engineering requirements in spacecraft designs. The SCREENS flow chart for ESD survivability is shown in Figure 3. First step is to determine the surface charging. For a detailed study, the NASCAP code is used. For a quick response question, a simplified 1-dimensional code with an approximation for surface resistivity is used. The purpose is to determine where electric fields are concentrated and to estimate the total charge stored in dielectrics. The implicit assumption here is that the NASCAP data would bound the charge storage regardless of the discharge mechanism. Hence, there is a quantifiable means of bounding a discharge. With the buried charge concept, there is no known means to accomplish this.

The next step is to estimate the discharge pulse. This is usually treated as an over damped current pulse that accounts for the charge lost. The coupling of this transient into the structure and cables is computed by means of a lumped element, circuit-analysis model or LEM. For any spacecraft configuration each value of capacitance, resistance and inductance has to be computed, measured or estimated. For most spacecraft this can be a large task. Selected cable LEM's are included with the structure LEM. The advantage in the SCREENS approach is that the spacecraft ground can be floated and biased to the predetermined NASCAP value. The dielectrics can also be biased according to the NASCAP predictions. The model is run using the SPICE2 computer code by triggering discharges at selected sites in the model (based on NASCAP) and viewing the response at selected locations.

For a quick, engineering decision, simplified single and dual-path models were available. These are gross models used to determine whether or not a detailed study of a suspected region in the spacecraft should be undertaken.

Finally, there is an experimental element in SCREENS. This includes determination of the charge/discharge characteristics of selected materials to be used in a design. These tests are run whenever the are questions about a material or configuration effect in the design. Unit and spacecraft level transient pulse respond testing would also be an element of SCREENS.

4. NASCAP MODELING

4.1 Model Descriptions

Models of spin-stabilized and 3-axis stabilized spacecraft were constructed in the NASCAP code for this study. Two versions of the 3-axis stabilized spacecraft, one for dawn and another for midnight, were used.

FIGURE 3. "SCREENS" TECHNIQUE FLOW CHART
FOR ELECTROSTATIC DISCHARGE SURVIVABILITY

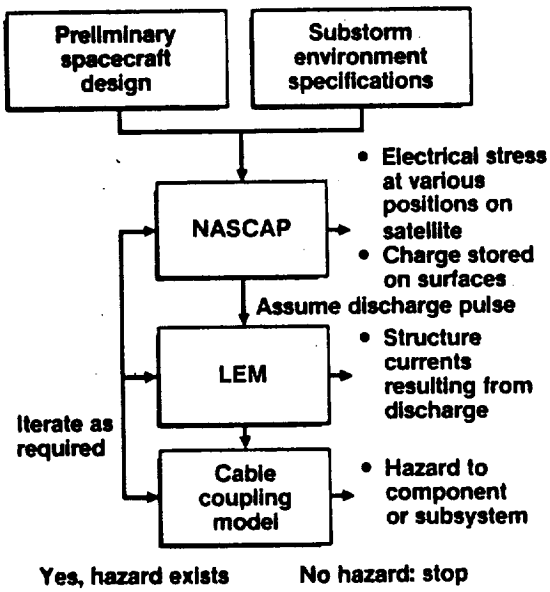

4.1.1 Spin-Stabilized Spacecraft

The spin stabilized spacecraft is shown in Figure 4. This represents a generic Hughes-type spacecraft with an extendable solar array. When extended this array formed a 2.7 m deep cavity. The solar array walls were coated with a quasi-conductive paint but the aft close-out barrier usually had a dielectric black paint over part if not all of the surface. This paint completely covered the barrier in this model and was also used around the bottom rim of the array. The properties used matched those obtained in charging tests of this paint. The same black paint was used on the top rim and top cavity wall. The top barrier was assumed to be 2 mil silvered teflon. The solar cells were assumed to be covered with ceria doped coversheets and the optical solar reflectors (OSR) on the radiator band are 8 mil fused silica. Interconnects in the solar array were simulated by a sprinkling of silver cells througout the array. The interconnect area corresponded roughly to 10% of the total solar array area. This cylindrical section was assumed to spin at a rate fast compared to the charging rate.

The despun antenna section used a germanium coated kapton film as sun shield. This material is semi-conductive. The rear side was assumed to be covered with 2 mil kapton over which a metallized grid was attached. At the potentials anticipated, this material responds as kapton. The boom was covered with kapton and the feed had an aluminum face (arbitrary selection) and kapton coated sides.

The dimensions of this spacecraft are shown in Figure 4. Note that each NASCAP cell corresponds to 30 cm x 30 cm squares. The solar array has a capability of generating about 1800 watts of which about 1/3 is usable at any one time due to spin.

4.1.2 Three-Axis Stabilized Spacecraft

The generic 3-axis stabilized spacecraft is shown in Figure 5. This spacecraft had 1 kW solar array constructed in two panels. Each array was assumed to be mounted on a kapton substrate and used fused silica solar cell covers. The interconnects were simulated by silver cells sprinkled throughout the area and represented approximately 10% of the array area. The array attachment supports were assumed to be kapton covered.

The spacecraft body had a single large antenna. The exposed base of the antenna was covered with white paint whose properties matched those obtained in charging tests. The rim of the antenna was a transparent mesh. The feed was kapton covered. The side of the antenna by the body and the antenna support were assumed to be covered by kapton blankets. The body radiator panels were covered with optical solar reflectors and the rest of the body had kapton blankets. The thruster simulator at the bottom of the body had a conductive base.

Due to operational characteristics of this type of spacecraft (sun fixed solar arrays with Earth facing antennas) two different NASCAP models had to be constructed. The first simulated the configuration at local midnight while the second, which had the body rotated 90°, simulated the configuration at local dawn. Configurations between midnight and dawn can not be simulated with the present versions of NASCAP but this approach should allow the charging characteristics to be bounded.

4.2 Charging Characteristics

The spin-stabilized and 3-axis stabilized spacecraft models were run in the severe environment substorm defined in section 2.2 to obtain the voltage distributions on the surfaces and around the craft. Both midnight and dawn simulations were analyzed for the first 15 minutes of substorm encounters. While the predictions indicated that the vehicle was still charging, the ground potentials were larger than known values actually measured on spacecraft. Hence, this analysis is sufficient to predict the maximum stresses within the spacecraft materials.

FIGURE 4. NASCAP MODEL - SPIN STABILIZED SPACECRAFT

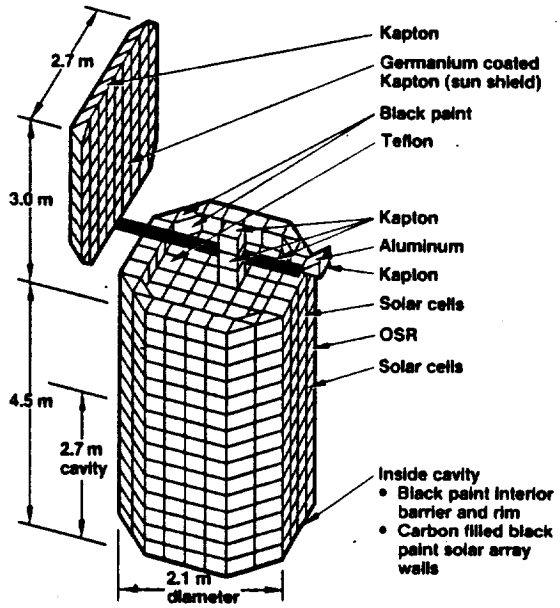

FIGURE 5. NASCAP MODELS - 3 AXIS STABILIZED SPACECRAFT

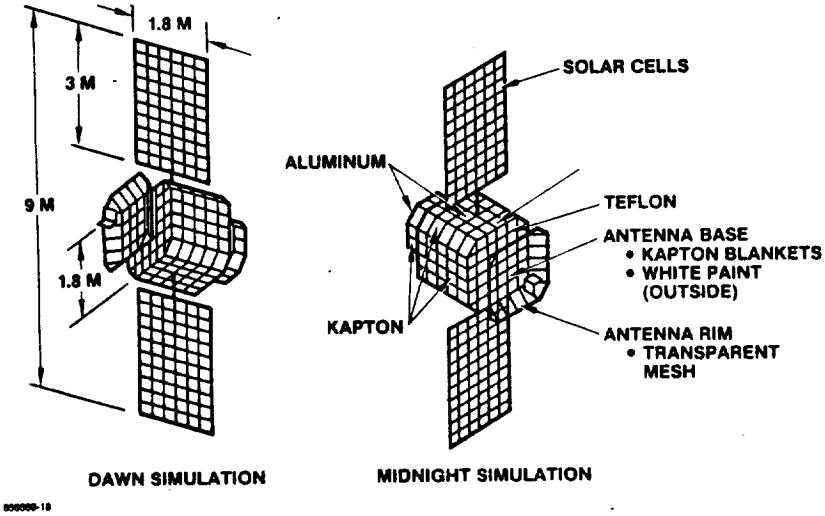

4.2.1 Spin-Stabilized Spacecraft Results

In both the midnight and dawn simulation, sunlight was directly incident upon the cylindrical solar array surfaces. The code was run in the spin mode which inputs average sun intensity into all surfaces exposed to sunlight. The despun antenna was simulated by assigning a zero photemission to those antenna surface that should be dark and increasing the photoemission by a factor of 3 for those antenna surfaces that should be in constant sunlight. The increase in photoemission was to compensate for the averaging of the solar intesity.

4.2.1.1 Midnight Simulation

The voltage distributions for the midnight simulation after 16 minutes are shown in Figure 6. For this simulation the sun illuminated the front surface of the feed and antenna while the backsides of both were dark. The charging history of the spacecraft ground is shown in Figure 7 while the differential voltages of selected surfaces are shown in Figure 8. After 16 minutes the ground potential reached about -1.5 kV and the maximum differential was about -2.0 kV on the dark kapton.

The voltage distributions from the dark kapton antenna extended into the back side of the solar array. This gave rise to a cirumferential voltage distribution around the body made up of solar array and the radiator OSR's. The body solar array differentials varied from -70 to +200 volts around the circumference relative to the structure potential.

The OSR's varied +350 to +800 volts. The lower solar array distribution ranged from -27 volts to +500 volts relative to the structure. Hence, the fields from the dark antenna should prevent discharges from the body array but would not prevent discharges from the OSR's and lower solar array. These would occur because the structure was more negative than the surrounding dielectrics (inverted gradient). Other areas of concern were the kapton used on the antenna and antenna pivot and the teflon forward barrier and black paint because the voltage difference relative to the structure was > -1.5 kV. The lower cavity was a concern because of a possible hollow cathode effect that could exist. The lower baffle was very negative (about -1.5 kV relative to the structure) while the rest of the cavity was essentially field free at a more positive value. Any discharge initiated at the barrier would be accelerated out to space.

FIGURE 6. PREDICTED CHARGING LEVELS - SPIN STABILIZED SPACECRAFT

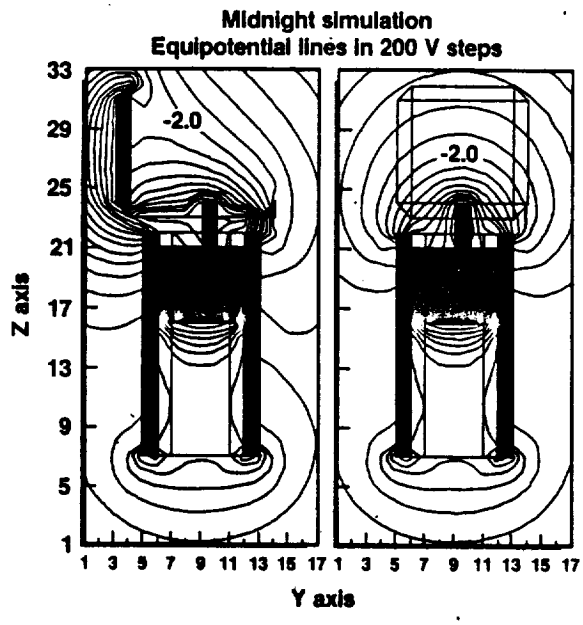

FIGURE 7. SPIN STABILIZED SPACECRAFT GROUND POTENTIAL (SEVERE SUBSTORM)

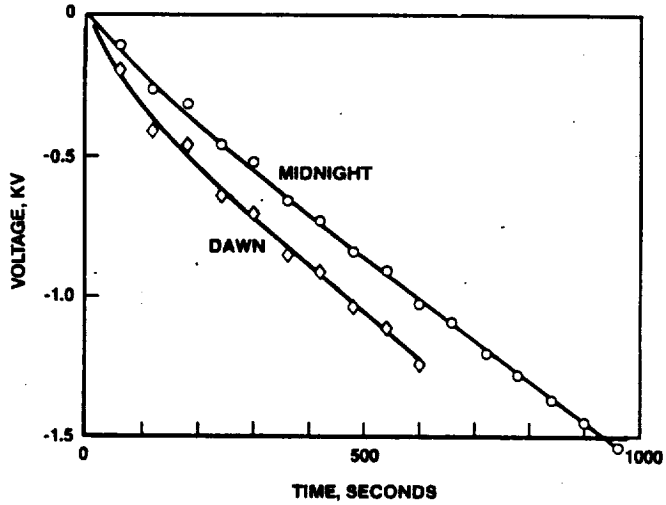

FIGURE 8. SPIN STABILIZED SPACECRAFT - MIDNIGHT SIMULATION DIELECTRIC DIFFERENTIAL VOLTAGES

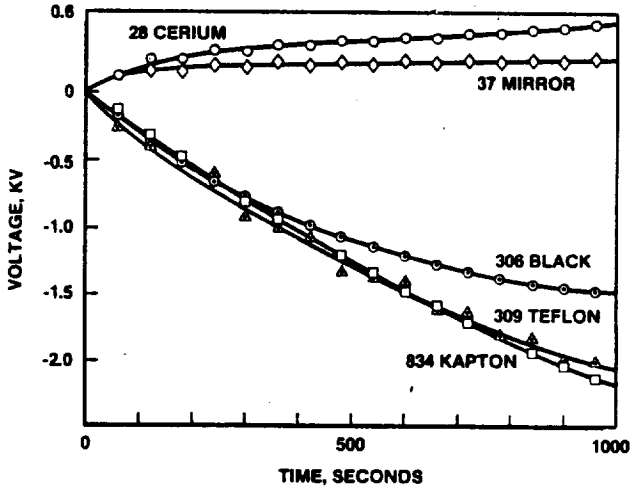

A summary of discharge sites is given in Table 1. Also listed is the differential voltage and the possible charge stored in each NASCAP cell computed from:

$$Q = \frac{\varepsilon}{d}[8.85\times10^{-14}]\ 900\ \Delta V = 7.965\times10^{-11}\ \frac{\varepsilon}{d}\ \Delta V \text{ coulumbs/NASCAP CELL}$$

where ε = dielectric constant and d is material thickness (cm). An approximation for the possible charge lost in a discharge is also listed. This is based solely on the assumption that only one cell would discharge at a time and that at most 10% of the total charge could be lost to space. These numbers were rounded down and were used in the lumped element modeling.

TABLE I

SUMMARY OF CHARGE STORED IN DIELECTRICS AND POSSIBLE DISCHARGE LOSSES

NASCAP RUNS FOR SPIN STABILIZED SPACECRAFT

Simulation	Site	Voltage Differential (kV)	Charge Stored (μC)*	Discharge Loss (μC)
Midnight	Kapton (2 mil)	-2.15	101	10
	Ceria Solar Cells (6 mil)	+0.5	10.5	1
	Optical Solar Reflectors (8 mil)	+0.8	12.5	1
	Teflon (2 mil)	-2.0	78.5	8
	Black Paint-Cavity	-1.5	70.6	7
Dawn	Kapton (2 mil)	-2.11	99	10
	Ge-Gated Kapton (2 mil)	-2.11	99	10
	Ceria Solar Cells (6 mil)	+0.65	13.6	1.5
	Optical Solar Reflectors (8 mil)	+0.65	10.2	1
	Teflon (2 mil)	-2.0	78.5	8
	Black Paint-Cavity	-1.5	70.6	7

* Per NASCAP CELL of 900 cm^2

4.2.1.2 Dawn Simulation

To simulate this condition the photoemission on one edge of the antenna, the exposed pivot and feed was increased while all other antenna surfaces were made to have zero photoemission. The voltage distribution resulting from this simulation after 16 minutes in the substorm is shown in Figure 9. The charging history of the ground potential is shown in Figure 7 while selected surface differential voltages are shown in Figure 10. The ground potential was slightly over - 2 kV in the back side kapton.

The principal difference that occurred here is that the fields around the antenna were more intense: both sides were charging. The fields also extended into the solar array as before giving rise to a circumferential variation. The distribution within the top cavity was not significantly different and the voltage distribution in the bottom cavity was identical to the midnight simulation.

The summary of charge stored and possible loss in discharges is given in Table I.

4.2.2 Three-Axis Stabilized Spacecraft

In this simulation two separate models of the same spacecraft were used for the midnight and dawn simulation. The solar intensity was held at unity and there was no need to adjust the photoemission of any surfaces.

4.2.2.1 Midnight Simulation

The voltage distribution due to running this model in a severe substorm for 16 minutes is shown in Figure 11. The charging history of the ground potential is shown in Figure 12. The differential voltages of selected surfaces are shown in Figure 13. After the 16 minutes of this simulation the ground potential reached -2.7 kV while the maximum differential was again about -2 kV in the shaded kapton and teflon surfaces.

These distributions indicate that breakdowns could exist in several locations due to voltage gradients. First, in the shaded region behind the antenna, there are intense fields with differential voltages of about -2 kV. However, the mesh portions of the antenna allowed sunlight to part of the forward enclosure. These surfaces charged differentially to only about -200 volts. Hence, across this surface there is about 1.8 kV differential. A discharge in this surface could release considerable charge from the dielectric.

FIGURE 9. PREDICTED CHARGING LEVELS - SPIN STABILIZED SPACECRAFT DAWN SIMULATION

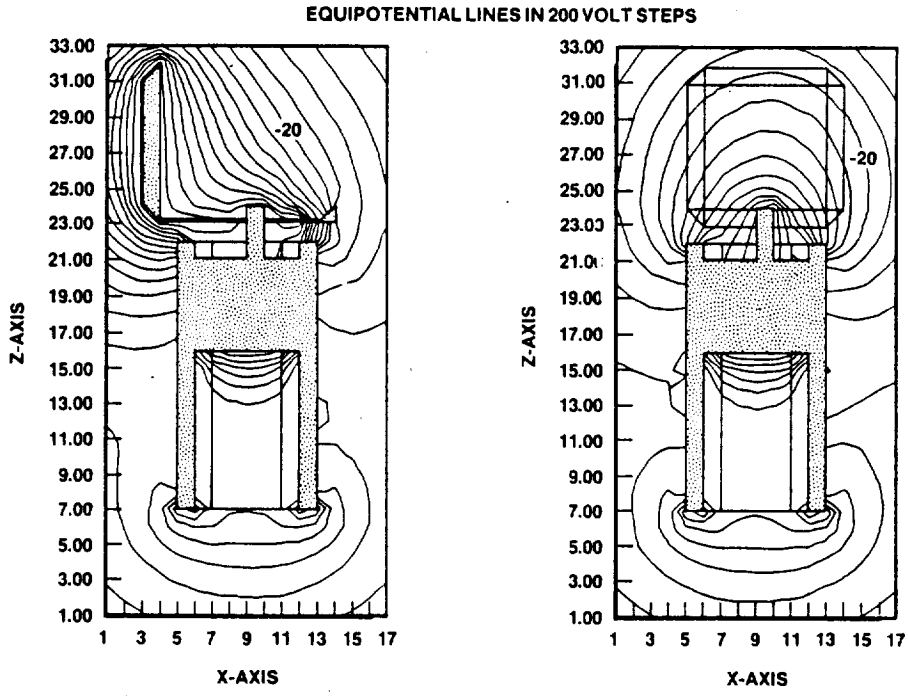

FIGURE 10. SPIN STABILIZED SPACECRAFT - DAWN SIMULATION DIELECTRIC DIFFERENTIAL VOLTAGES

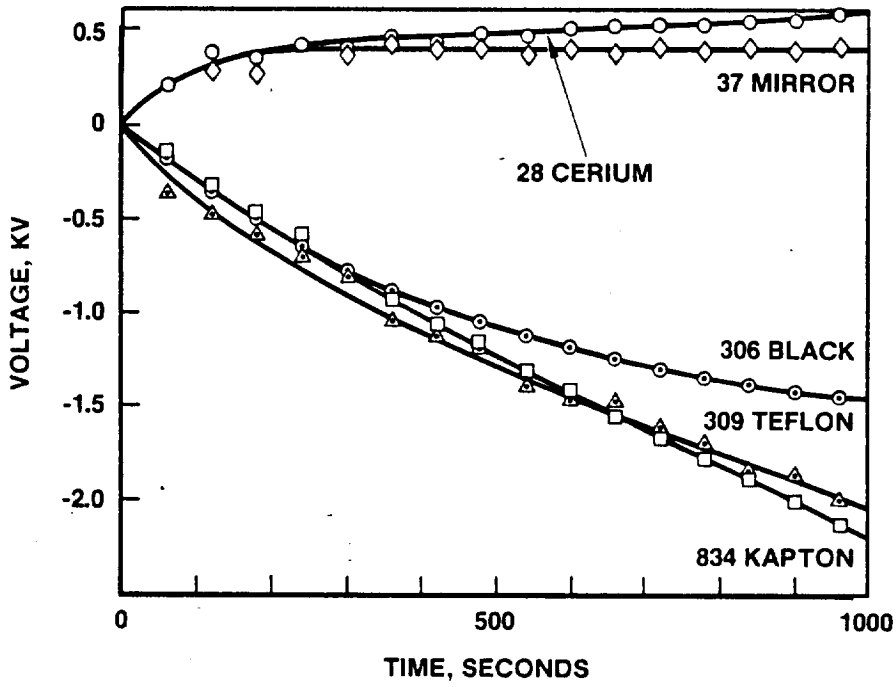

FIGURE 11. PREDICTED VOLTAGE DISTRIBUTIONS - 3 AXIS STABILIZED SPACECRAFT
-MIDNIGHT SIMULATION-

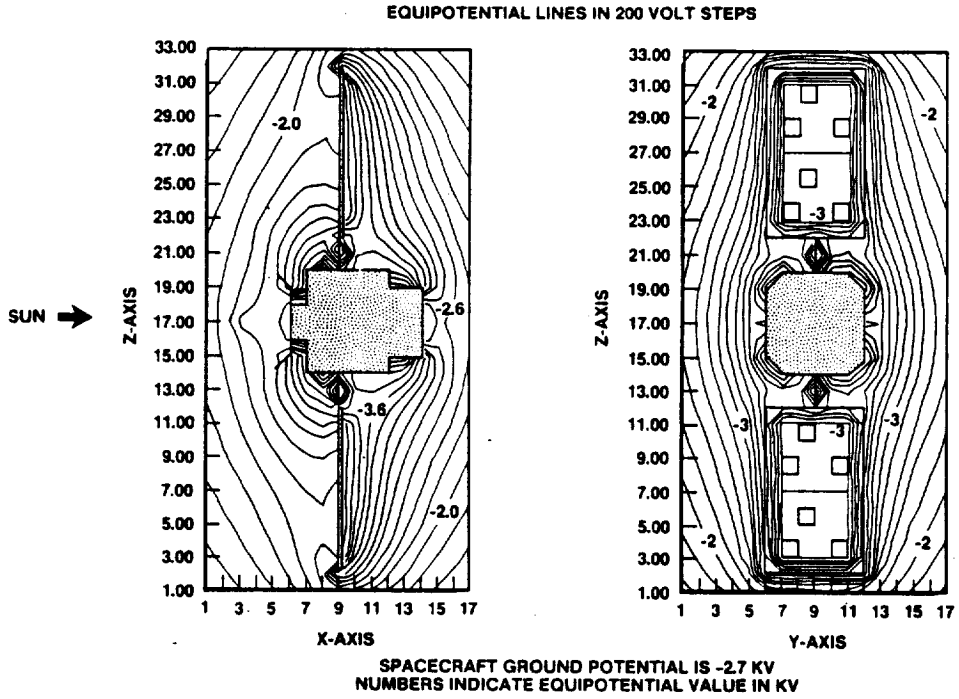

FIGURE 12. 3 AXIS STABILIZED SPACECRAFT - GROUND POTENTIALS

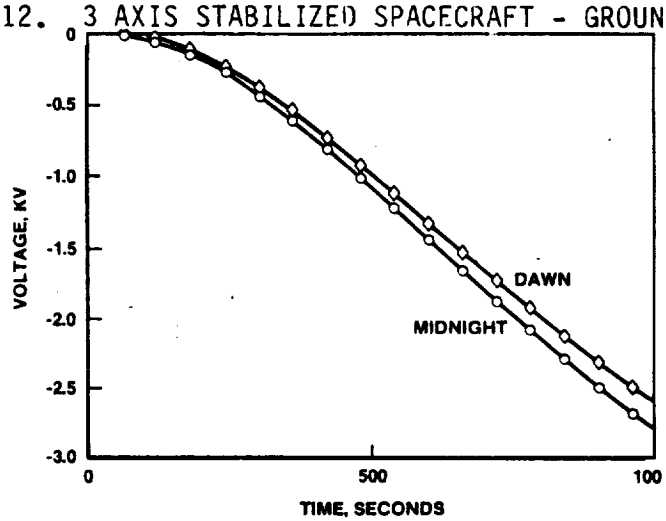

FIGURE 13. 3 AXIS STABILIZED S/C - MIDNIGHT SIMULATION
DIELECTRIC DIFFERENTIAL VOLTAGES

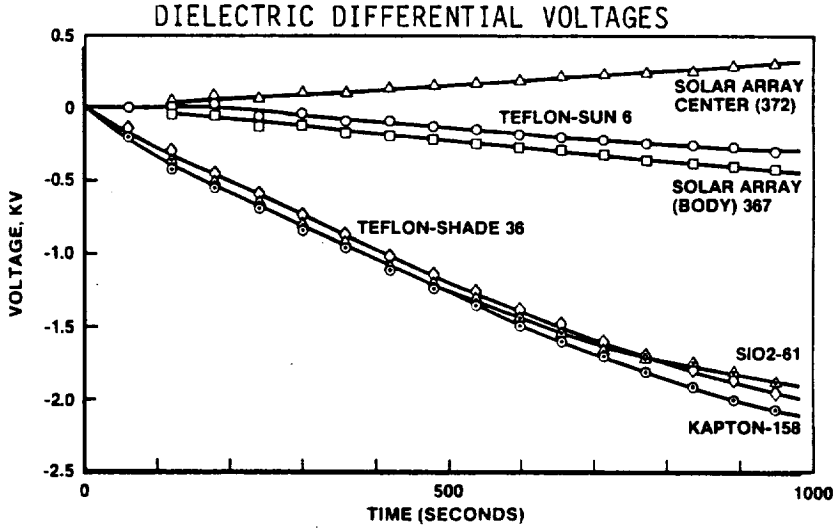

At the rear of the spacecraft body, the thruster enclosure was assumed to be conductive while the surrounding kapton blanket was at -4.8 kV. This means that the gradient is very severe at this interface (-2 kV). This voltage exists across the two mil thickness of kapton which means the electric field is 3.9×10^5 volts/cm. Discharges can occur.

Finally, a gradient in the solar cells exists at the panel edges. The majority of the cover glass surfaces was charged to ~-2 kV. This is slightly positive with respect to structure ground (~200 volts), but there was a 1 kV gradient around the edges. This could also breakdown.

The OSR's on both radiator panels had differential voltages greater than 1.5 kV. These also must be considered as possible discharge sites.

The summary of charge storage per NASCAP cell in areas of concern and the assumed possible charge loss per cell is given in Table II. For these areas where the surface voltage difference between cells is greater than 1 kV, the charge loss in a discharge is assumed to be 30%.

4.2.2.2 Dawn Simulation

The voltage distribution due to running this model in a severe substorm for 16 minutes is shown in Figure 14. The charging history of the ground potential is shown in Figure 12. Differential charging history of selected surfaces is shown in Figure 15. After the 16 minutes of this simulation, the ground potential reached -2.5 kV while the maximum differential still was -2 kV for shaded kapton and teflon surfaces.

There are considerable differences between the dawn and midnight simulations. In the dawn case, the sunlight is into the side of the antenna. This eliminates the severe sun-shaded conditions that existed in the forward barrier. However, discharges could still occur here with an estimated maximum charge loss of 10% maximum of the total charge.

Another area of difference was in the solar arrays. Here, the voltage distribution extended further into the array panels. The voltage gradient across the panels are now 1.5 kV and still are considered a likely discharge source.

The OSR's on the radiator panel were now differentially charged to -2 kV. Again they are possible discharge sites. The rear of the spacecraft body had a strong differential voltage and must be considered as a probable discharge location.

The summary of charge storage and possible discharge losses from these areas of concern is given in Table II. As before, charge loss in discharges of up to 30% are assumed likely when surface voltage differentials in excess of 1 kV exist.

TABLE II

SUMMARY OF CHARGE STORED IN DIELECTRICS AND POSSIBLE DISCHARGE LOSSES

NASCAP RUNS FOR THREE-AXIS STABILIZED SPACECRAFT

Simulation	Site	Voltage Differential (kV)	Charge Stored (μC)*	Discharge Loss (μC)
Midnight	Kapton (2 mil) Antenna	-2.0	94.1	28
	Teflon (2 mil)	-1.95	76.4	23
	Optical Solar Reflectors (8 mil)	-1.9	29.8	3
	Kapton-Read (2 mil)	-2.1	98.8	10
	Solar Cell Covers (6 mil)	-0.5	10.5	3
Dawn	Kapton (2 mil) Antenna	-2.1	98.8	30
	Teflon (2 mil)	-2.0	78.4	8
	White Paint (2 mil)	-0.94	44.2	4
	Optical Solar Reflectors (8 mil)	-2.1	32.1	3
	Kapton (2 mil) - Rear	-2.1	98.8	10
	Solar Cell Covers (6 mil)	-0.44	9.2	3

* Per NASCAP CELL of 900 cm^2

4.3 Summary

Both of the generic spacecraft considered here used materials and coatings that are currently considered viable for present-day spacecraft construction. There was no attempt to use conductive coatings (either conductive paints or indium-tin-oxide films) to reduce the charging. The results indicated that discharges are highly probable in the spin-stabilized spacecraft due to the large despun antenna and large cavity. The anticipated charge lost, though, should be relatively low.

FIGURE 14. PREDICTED VOLTAGE DISTRIBUTION - 3 AXIS STABILIZED SPACECRAFT -DAWN SIMULATION-

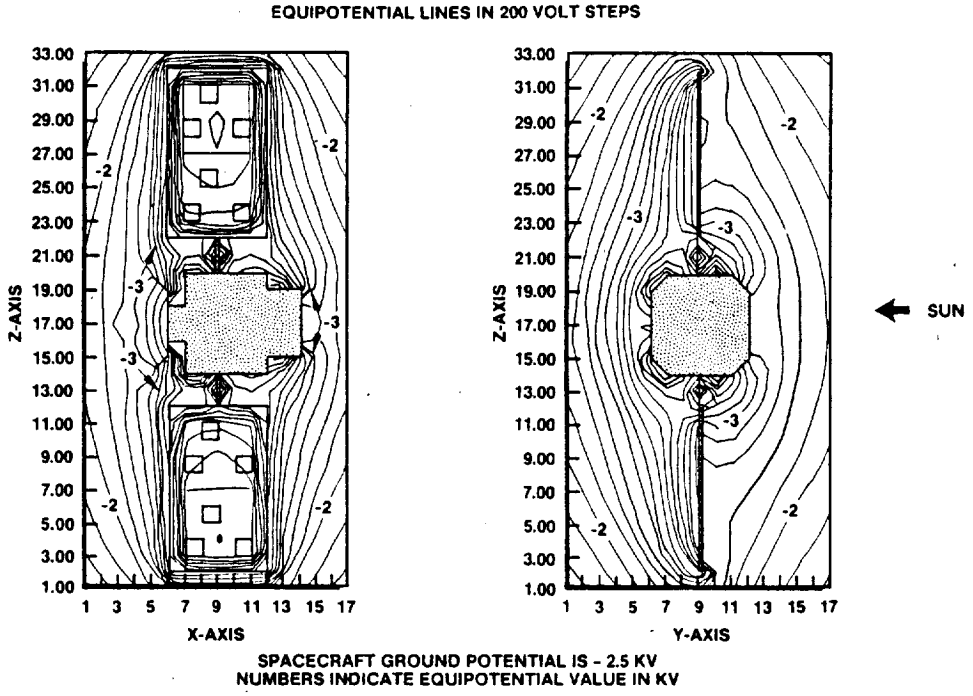

FIGURE 15. 3 AXIS STABILIZED SPACECRAFT - DAWN SIMULATION DIELECTRIC DIFFERENTIAL VOLTAGES

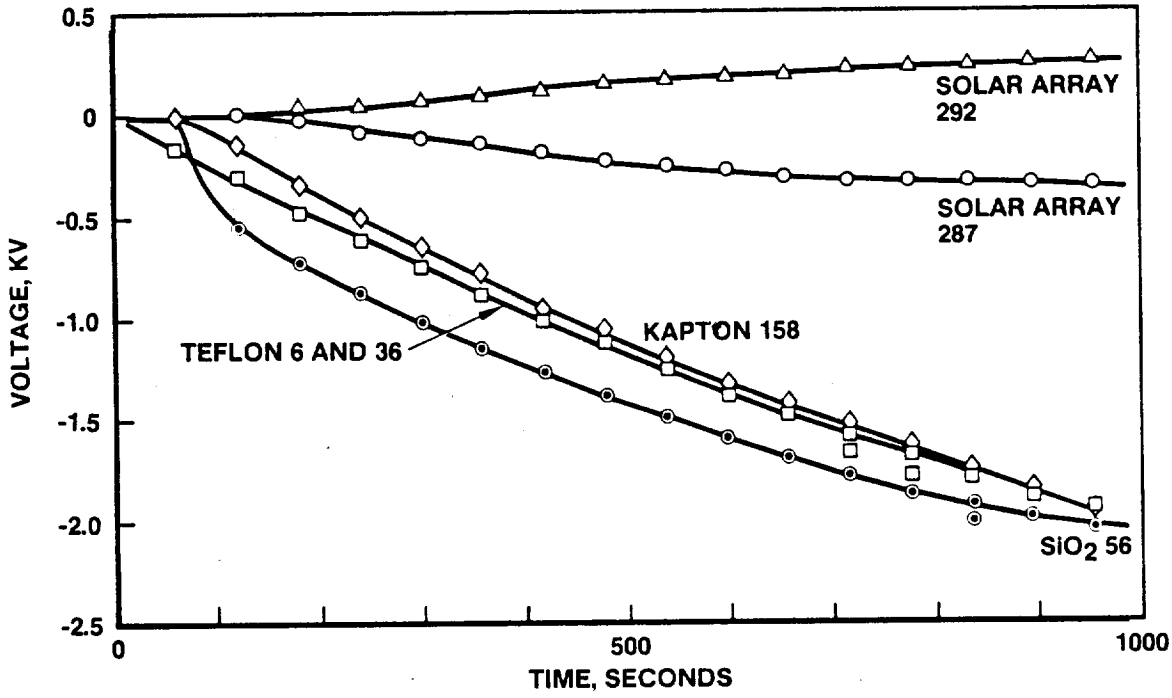

The three-axis stabilized spacecraft, on the other hand, had a more uniformly charged set of surfaces and discharges should not be as probable. However, when these discharges do occur, they could be more severe.

5. INTERNAL TRANSIENT RESPONSE

In order to examine the effects of discharge on the spacecraft interior a detailed lumped element model (LEM) was used. The NASCAP results were used as input to the LEM. In the following sections the detailed and simplified LEM's and the results obtained with them are examined.

In addition, a buffer (interface) circuit typical of those used to filter unwanted transients from power and signal lines was examined to determine its susceptibility to signals generated by electrostatic discharges. Its vulnerability to these signals was studied at both the normal input and the ground point of the circuit.

5.1 Detailed Lumped Element Model Descriptions

5.1.1 General Approach

The coupling of the discharge into the spacecraft structure was computed by means of a lumped element, circuit analysis model or LEM. The LEM was constructed by representing the various spacecraft components and structures by their equivalent capacitance, resistances and inductances.[36,41,42] The model for a typical spacecraft can become quite complex (see Figure 16 for the structural model of a spacecraft).

FIGURE 16. LUMPED ELEMENTS MODEL OF A TYPICAL SPIN STABILIZED SATELLITE (STRUCTURE)

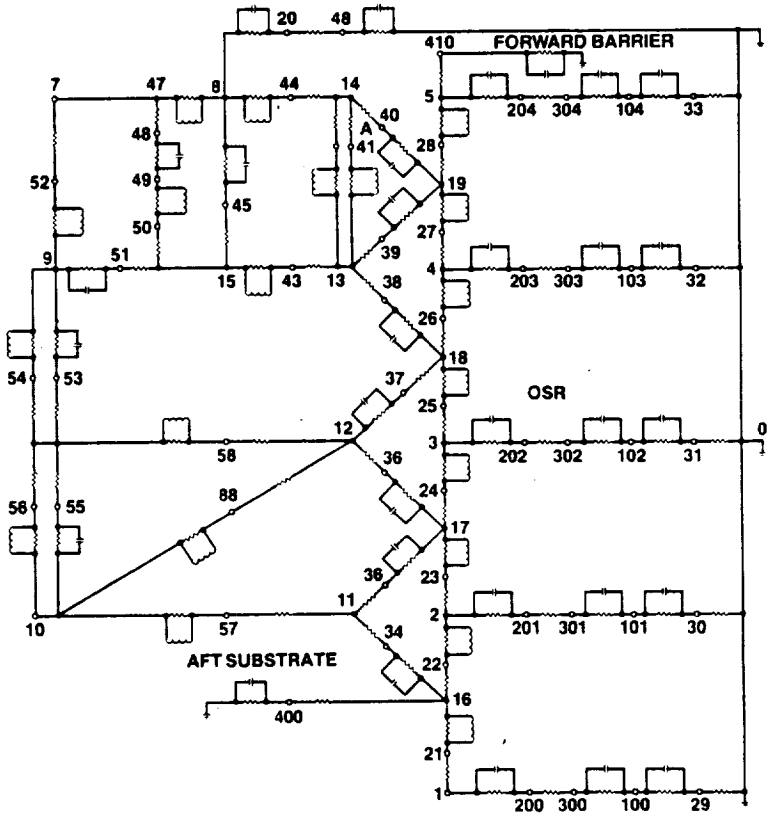

For this study, the LEM of a spin stabilized spacecraft was used in the analysis for the spinner then modified to represent the three axis stabilized satellite. The model was sufficient in detail to provide a realistic response and was made to represent a typical spacecraft configuration. The responses given here therefore give indications of the response for any spacecraft of these general configurations.

5.1.2 Spin Stabilized Spacecraft LEM

The spin stabilized spacecraft had a spun portion containing the solar array, an equipment shelf and the major part of the structure. The despun portion contained the antenna farm and a despun equipment shelf. The two areas were connected electrically by internal power, signal and ground cables. The interface is the bearing and power transfer assembly (or BAPTA). The BAPTA also served as a common point for satellite wiring between the two sections of the spacecraft. The antenna consisted of a single dish and feed, both of which were despun. The major part of the body included a cylindrical structure to which was attached the solar panels.

Included in the LEM was a power return wire between the antenna and the spun shelf. The wire was modelled as a single, unshielded wire and was terminated with 50 Ω at both ends. The wire model was the one to give a worst case response. Figure 17 shows the location of the wire.

FIGURE 17. CROSS SECTION OF SPIN STABILIZED S/C

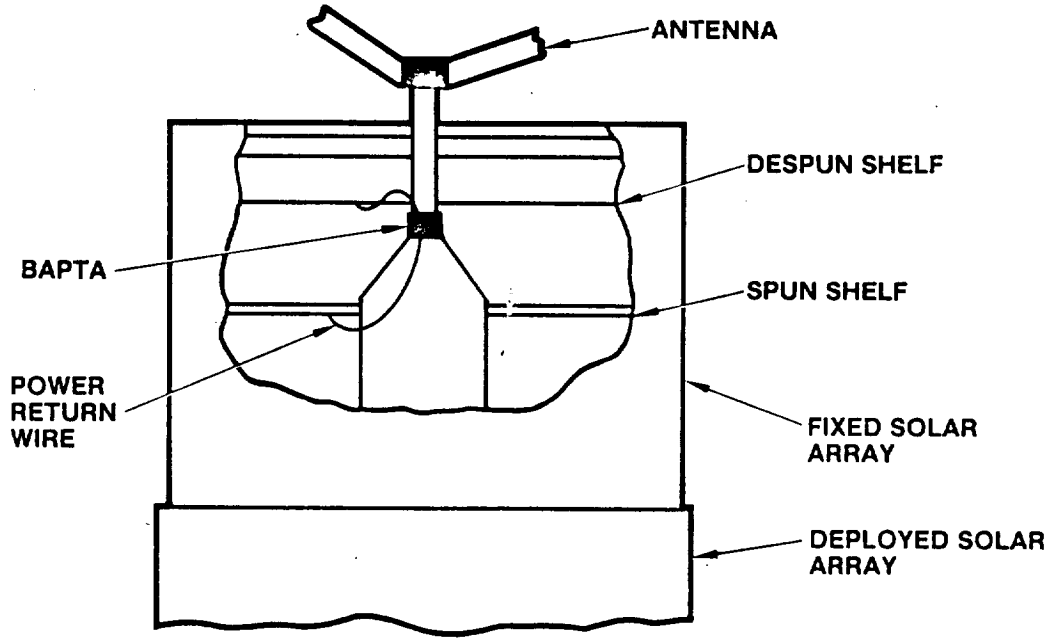

5.1.3 Three Axis Stabilized Spacecraft LEM

The three axis stabilized spacecraft did not have spun portion. The spacecraft body had an equipment shelf within it and the solar panels attached as wings. The antenna was attached to the top of the body.

Several modifications were made to the LEM to model the three axis stabilized spacecraft. The solar panels, the spun shelf and the electrical interface between the spun and despun shelf were removed. The solar panels were added as wings attached to opposite sides of the body. The cable was again modelled as a single, unshielded wire and was connected across the equipment shelf to simulate the return wire for earth sensors located on the outside edge of the shelf. Figure 18 shows the location of this wire.

FIGURE 18. CROSS SECTION OF 3 AXIS STABILIZED S/C

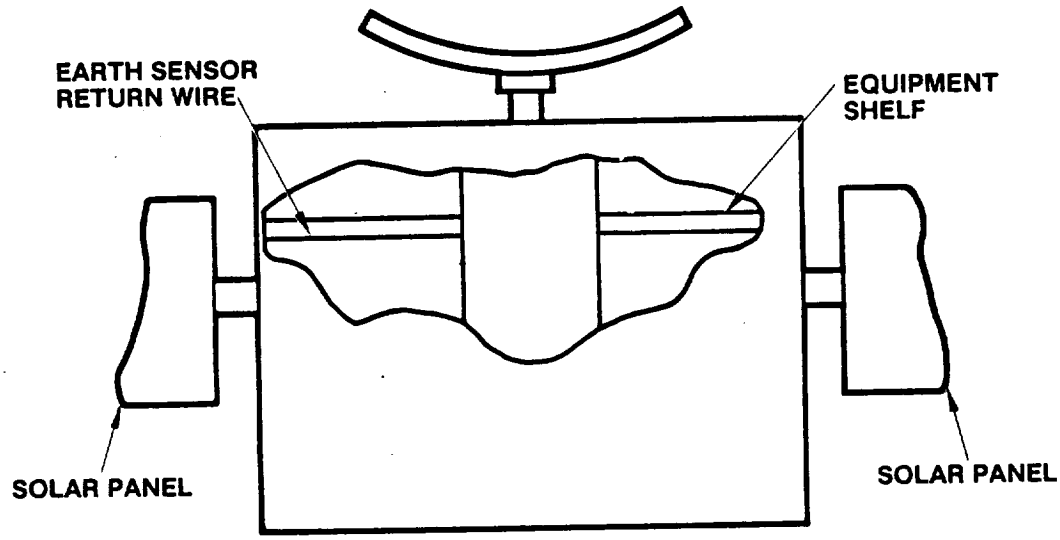

5.2 Detailed Lumped Element Model Analysis

5.2.1 Discharge Simulation

NASCAP results (Tables I and II) indicated highest charge build-up (~100 μC) on the antennas of both the spin and three axis stabilized spacecraft and on the 3-axis solar panels. Since these were the areas with the highest electric fields, the discharges were simulated in those areas. A maximum of 10% charge loss for the spinner and the 3-axis spacecraft was assumed. In addition a lower value (2 μC) was also used for comparision with detailed LEM results. NASCAP indicated a negative charge build-up so the discharges were modelled as positive current pulses input to the circuit at the discharge site to simulate a loss of electrons. Figures 19 and 20 represent the discharge pulses' characteristics.

The response examined was the behavior of the potential relative to the discharge site as a function of distance from the discharge site. Also studied was the magnitude of transient current produced in the satellite wiring due to the discharge. Figure 21 shows a spin stabilized spacecraft and a typical discharge.

FIGURE 19. DISCHARGE CHARACTERISTICS 2 μC DISCHARGE PULSE

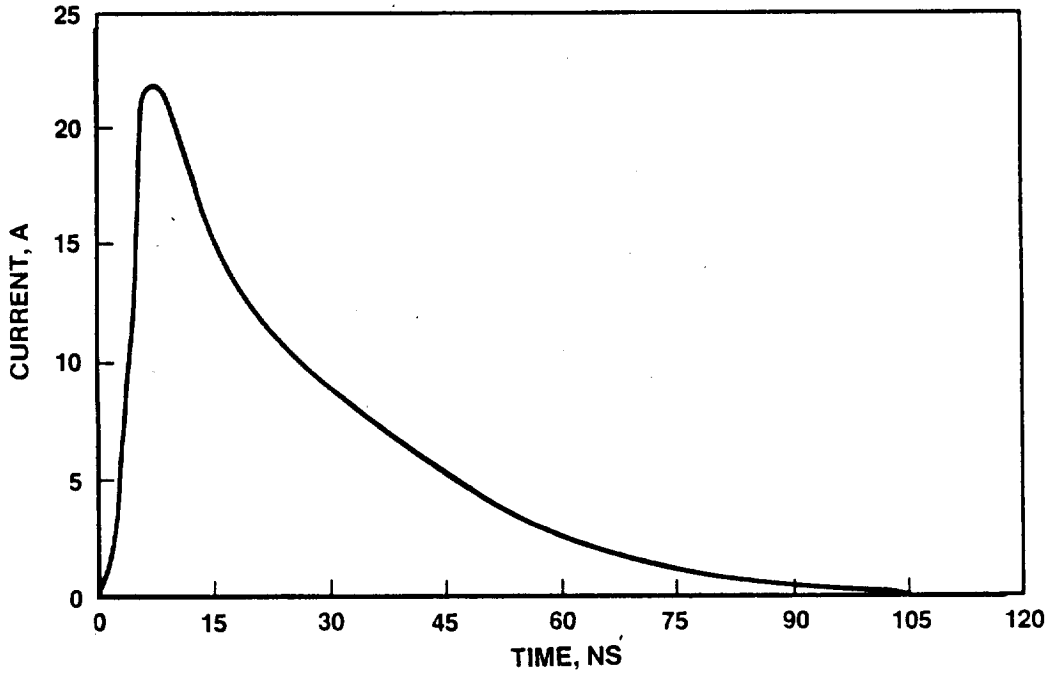

FIGURE 20. DISCHARGE CHARACTERISTICS 10 μC DISCHARGE PULSE

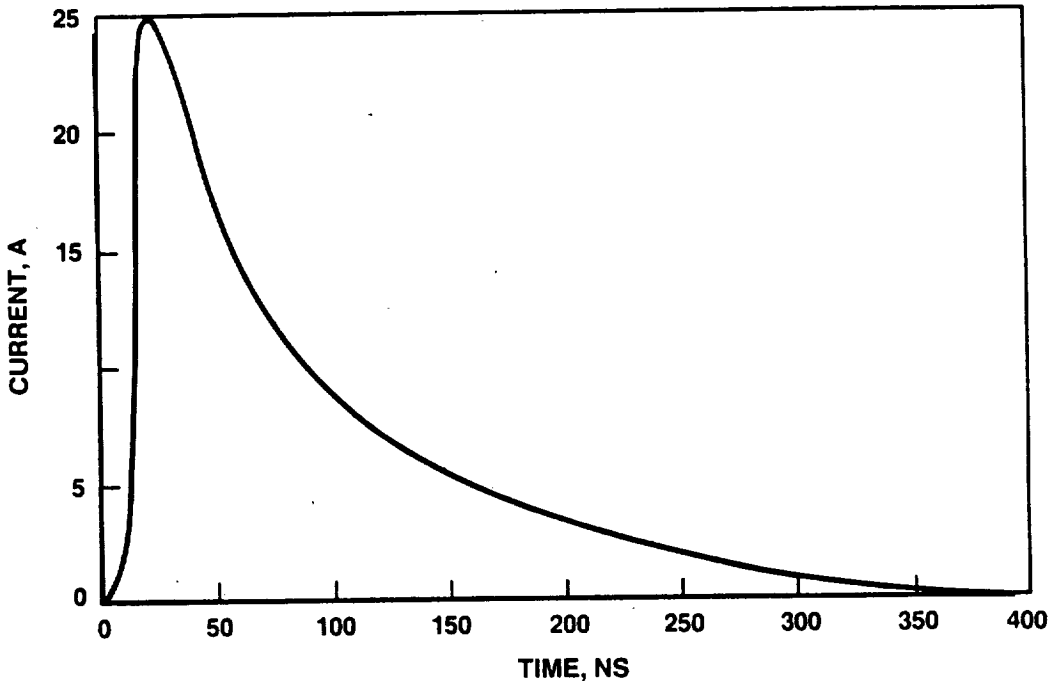

FIGURE 21. CUTAWAY VIEW OF SPACECRAFT

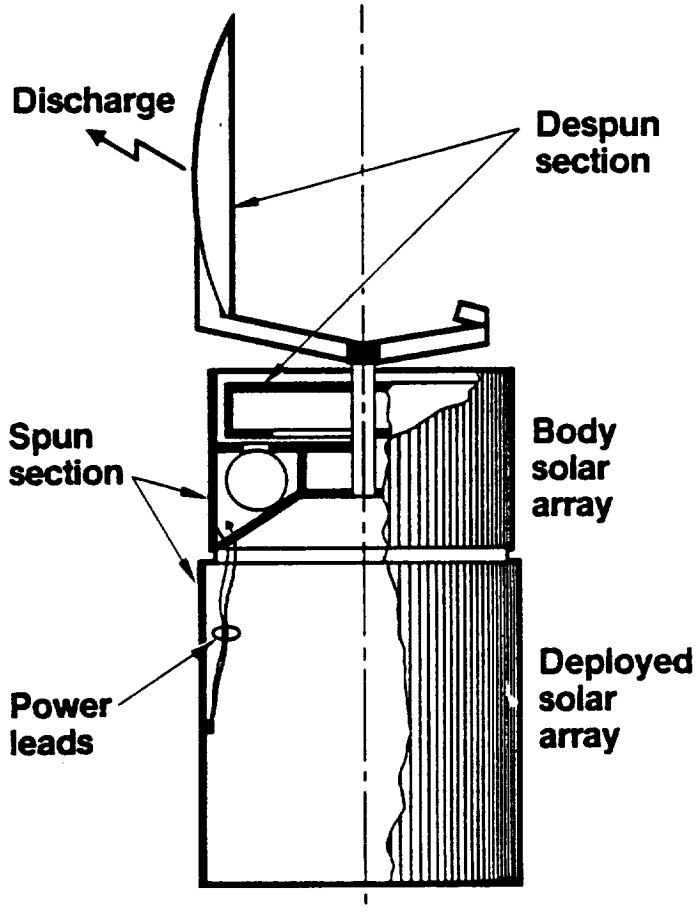

5.2.2 Transient Response Results

5.2.2.1 Potential

Figure 22 shows the potential of the spinner's structure relative to the antenna for 2 μC discharge. In this case the potential is similar for most parts of the structure except for the despun shelf which is lower in magnitude and out of phase with the other potentials. The potential reached a maximum value of about 400 V for the array and spun shelf and about 125 V for the despun shelf. The behavior was oscillatory in nature and damped out in time (Figure 23). For the 10 μC discharge, the results were the same as the 2 μC discharge results except for having higher magnitudes. The shape was the same with the array and spun shelf potentials reaching to about 500 V and the despun shelf 125 V.

An antenna discharge in the three axis stabilized case yielded similar results. Figure 24 shows the top and bottom potentials relative to the discharge site. The differential potential between the top and bottom was oscillatory as seen in Figure 25.

The equipment shelf potential was approximately 800 V initially and damped out quickly since it was not coupled directly to the antenna (Figure 26). The potential between the top and bottom of the 3-axis body was greater when the discharge occurred on the solar panels and is shown in Figure 27. The overall potential relative to the antenna reached about 3 kV in the 2 μC discharge case and about 10 kV in the 10 μC discharge case.

5.2.2.2 Current

Figure 28 shows the current in the spinner's power return wire and Figure 29 shows the current generated by the solar panel discharge in the 3 axis Earth sensor return wire. In the spinner case the current peaks at about 12 A while for the 3 axis sensor return wire the maximum current was about 0.3 A. In both cases the 10 μC discharge produced currents which followed the same damped oscillatory motion but with slightly higher magnitudes.

5.3 Simplified Lumped Element Model Analysis

5.3.1 Model Description

In addition to the detailed LEM studies, the results from simplified dual path models were analyzed. These are gross models that agreed qualitatively with the detailed LEM's and are to be used primarily to determine if detailed models were needed, to understand what is occurring in selected regions or to evaluate possible corrective techniques.

FIGURE 22. STRUCTURAL POTENTIAL

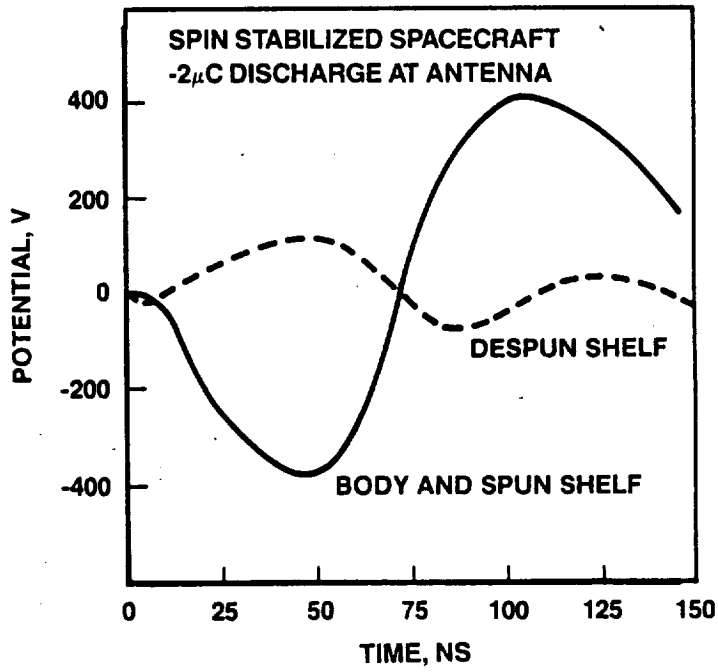

FIGURE 23. DIFFERENTIAL VOLTAGE BETWEEN SPUN/DESPUN SHELVES

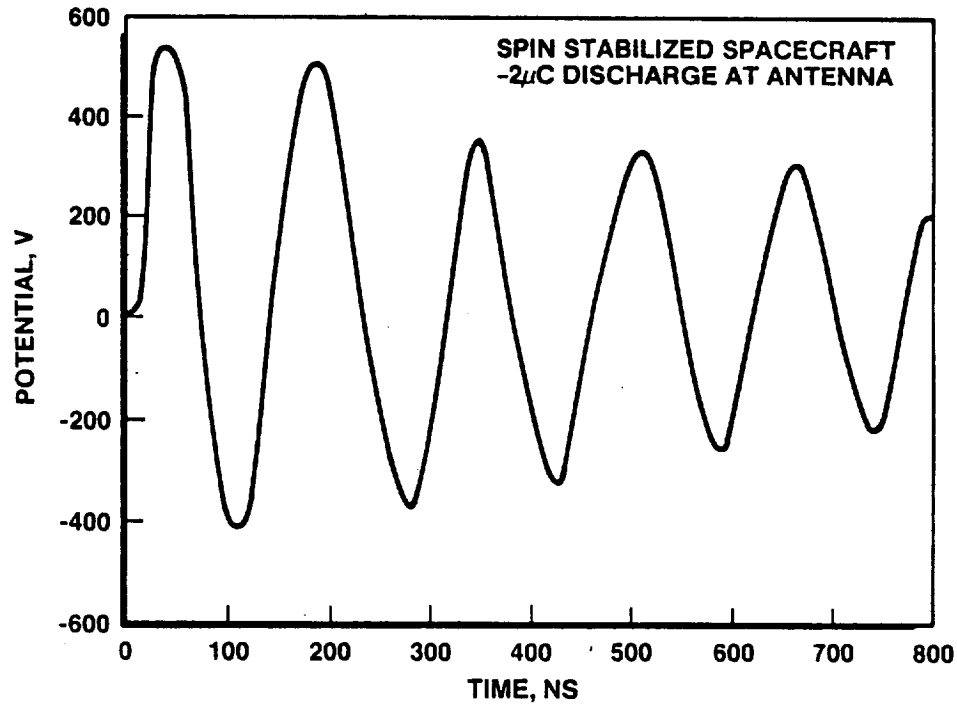

FIGURE 24. STRUCTURAL POTENTIAL

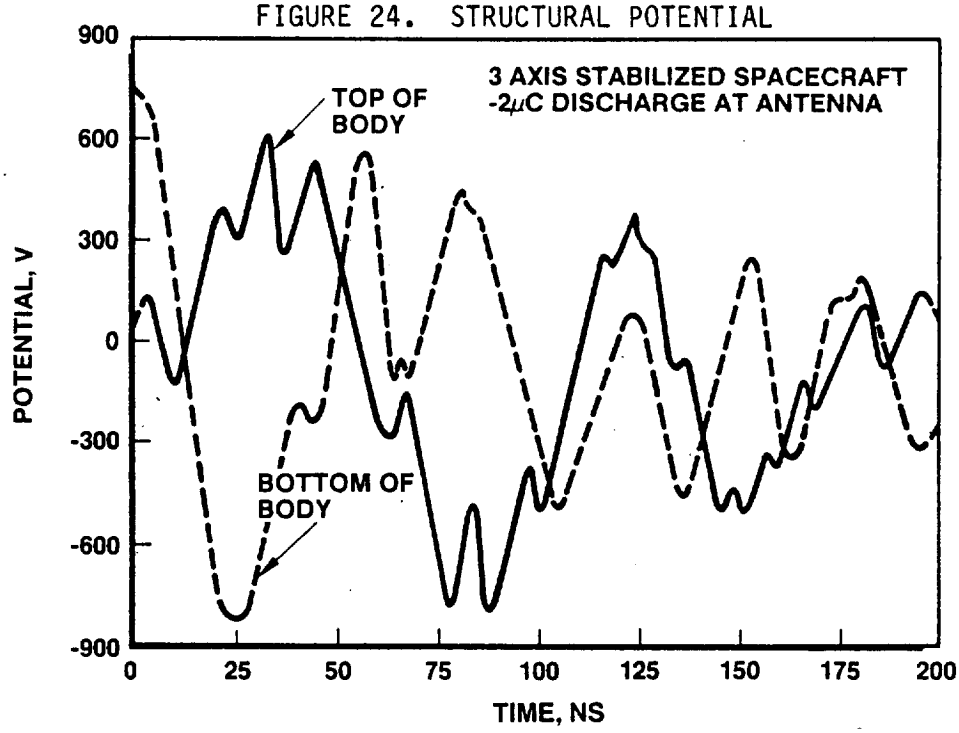

FIGURE 25. DIFFERENTIAL POTENTIAL BETWEEN TOP AND BOTTOM OF SPACECRAFT

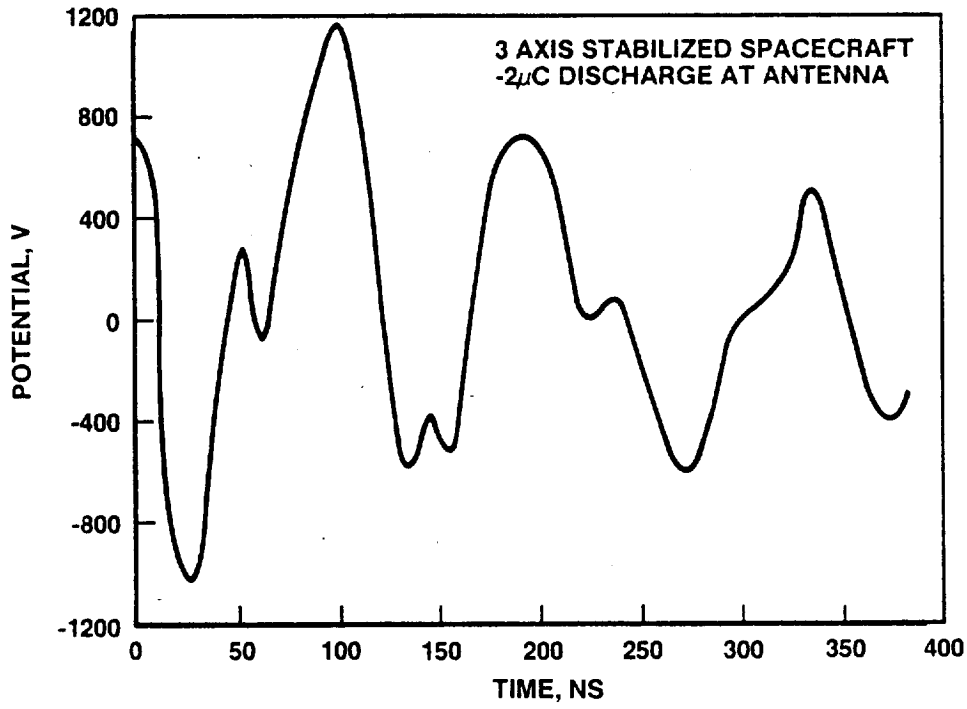

FIGURE 26. EQUIPMENT SHELF POTENTIAL

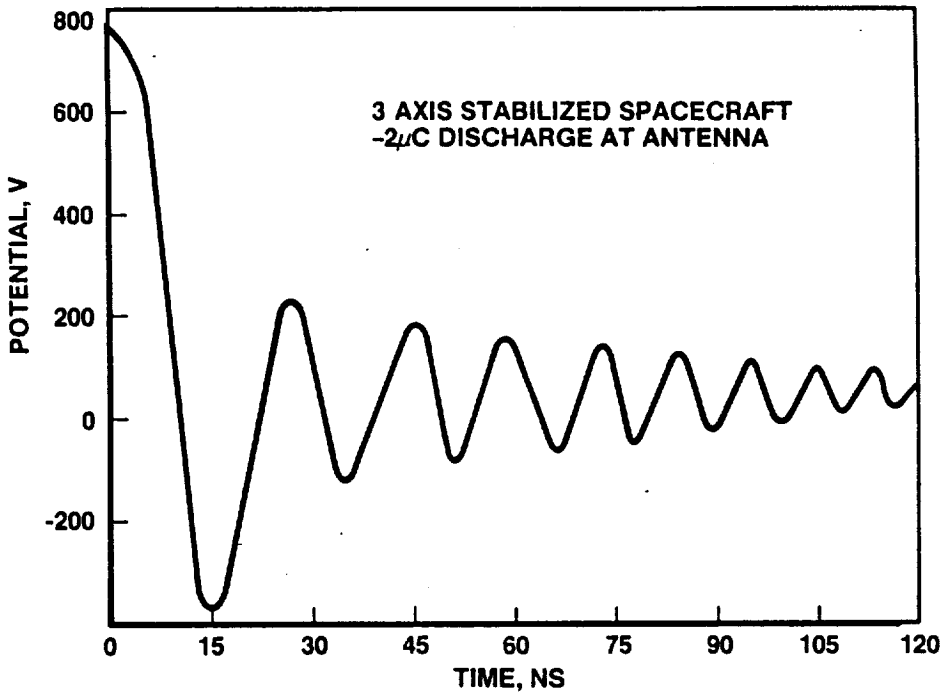

FIGURE 27. STRUCTURAL POTENTIAL

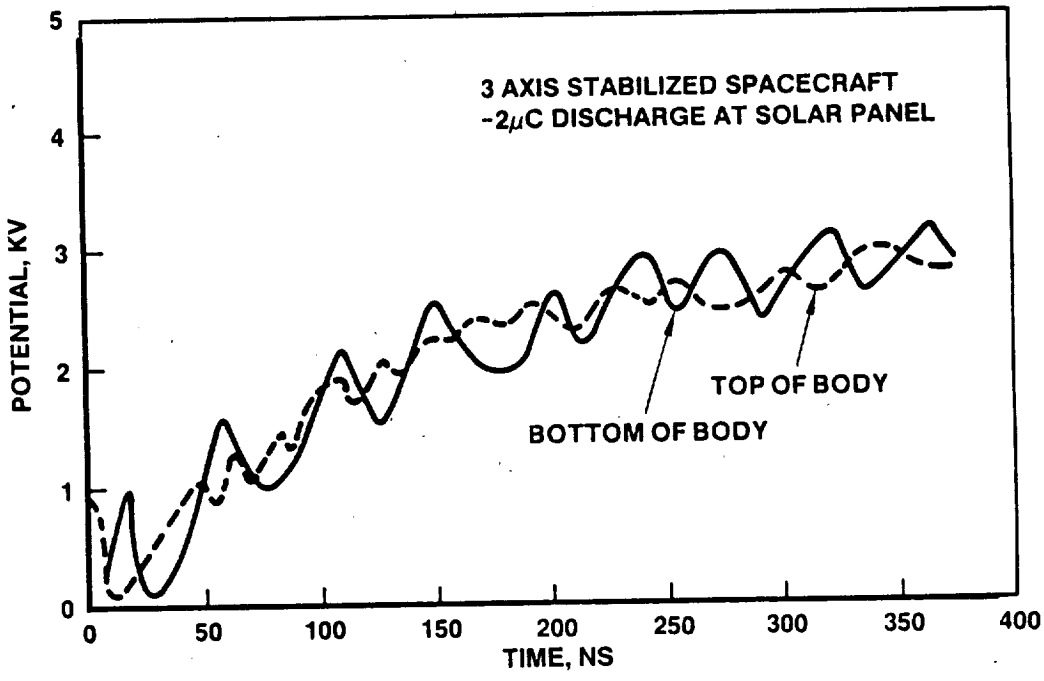

FIGURE 28. CURRENT THROUGH POWER RETURN WIRE

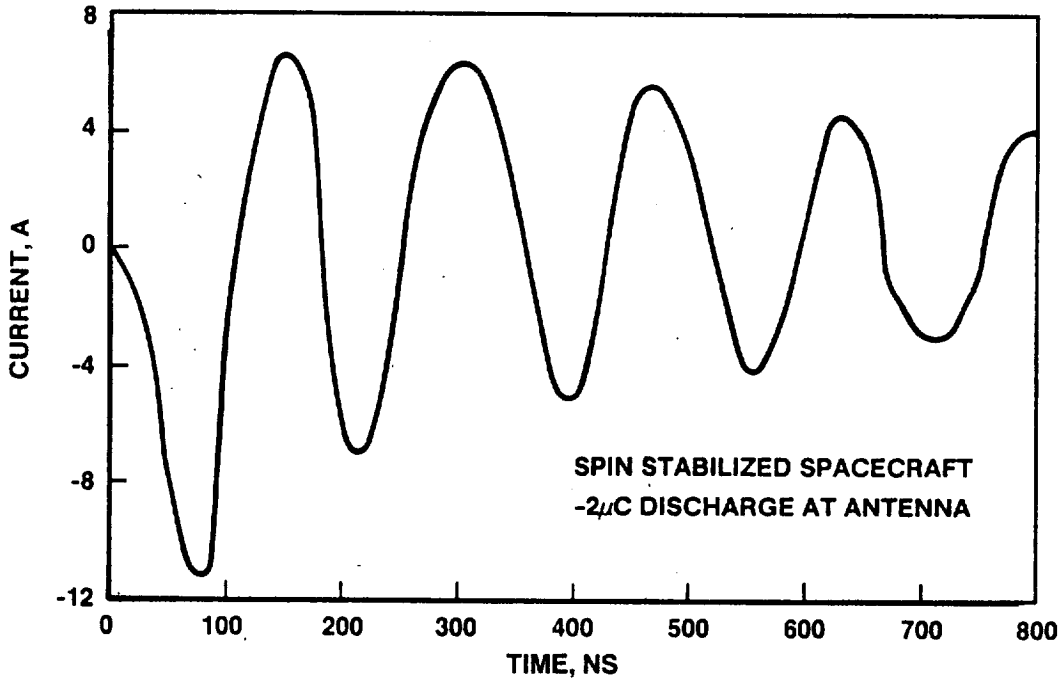

FIGURE 29. CURRENT THROUGH EARTH SENSOR WIRE

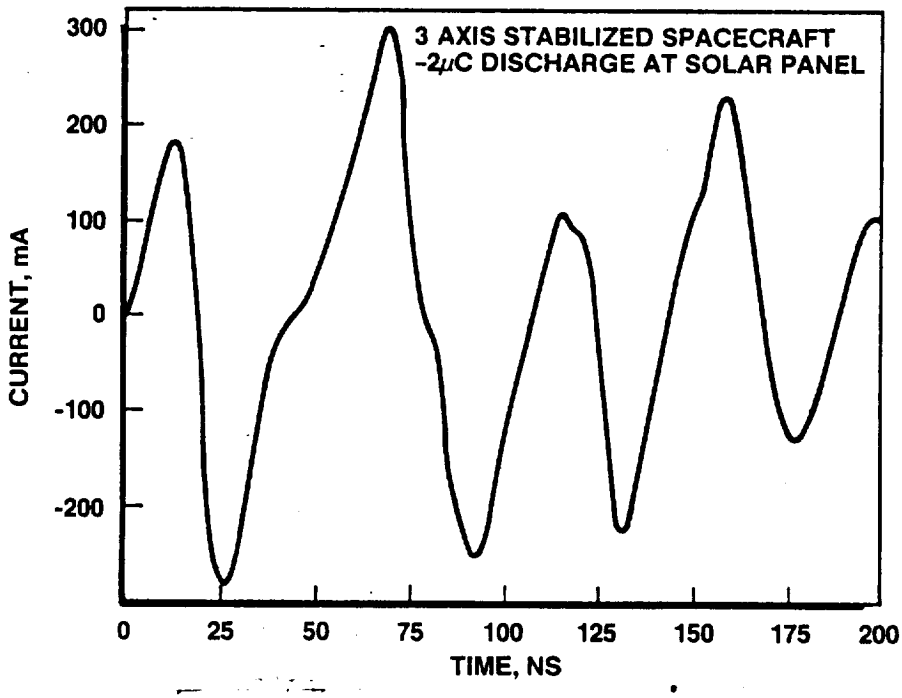

The simplified spin stabilized LEM used here is shown in Figure 30. The despun section was simulated by a single capacitance (C1), resistance (R1), and inductance (L1). There was also an unshielded 50 cm. cable attached to a shelf. The spun section was likewise treated with parameters labeled 2. The discharge response relative to space was treated with a single capacitance to space. Recharging by the substorm was accomplished by exposing the conductive area to the incident electron current. The parameters to simulate the structural elements were chosen to give an underdamped transient with frequencies in the range of 1 to 10 MHz for the spun section and 10 to 20 MHz for the despun.

The discharge was triggered by closing the switch connecting a R-L-C circuit to the discharge site. The values of RD, LD, and CD were chosen to give an overdamped current transient equivalent to the desired charge lost. It was found that the discharge currents dissipate in microseconds which is short compared to the recharging time of the spacecraft by the substorm environment so that the two processes can be considered independently.

FIGURE 30. HIGHLY SIMPLIFIED LEM

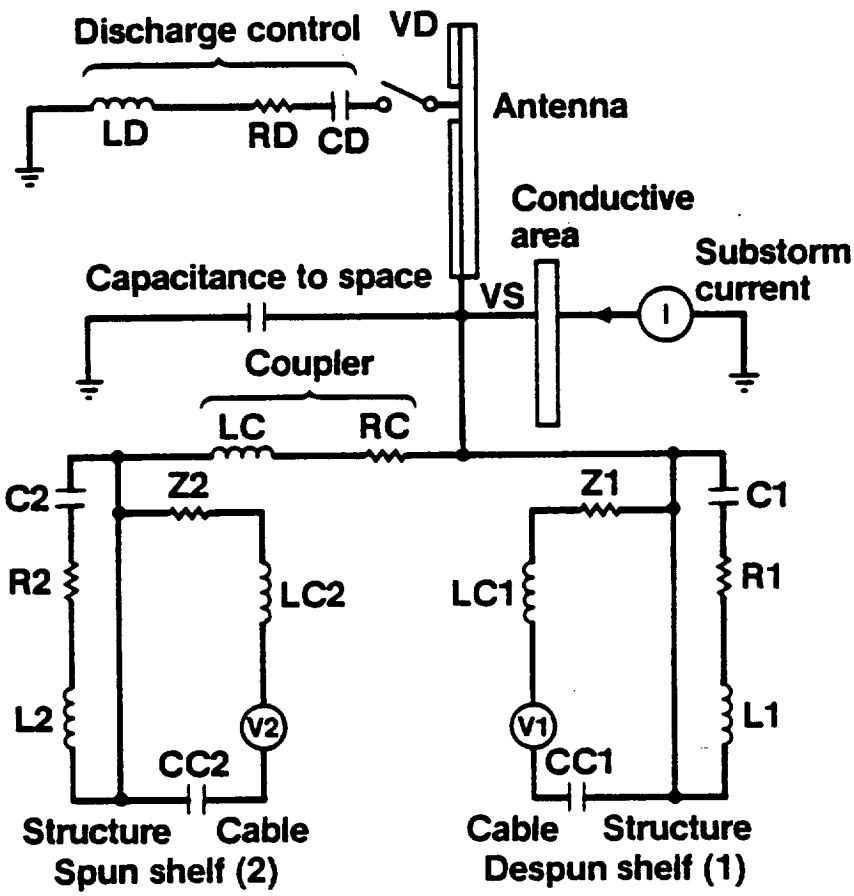

5.3.2 Transient Response Results

The discharge pulse used in this simulation is shown in Figure 31. The values chosen for CD, RD and LD ($2.x10^{-9}$, 50., & $1.x10^{-6}$ respectively) resulted in a discharge current transient that reached 50 Amps, damped out in about a microsecond and ejected 11.5 microcoulombs to space. This charge loss was a little larger than desired, but it is meant only as illustration.

As a result of this charge loss, the spacecraft potential changed as shown in Figure 32. The ultimate rise was determined solely by the charge lost and the spacecraft capacitance to space.

The initial potential was -1550 volts and the final value 26,500 volts. At the 1500 nanosecond time, the structure potential was just starting to be recharged by the milliampere substorm charging current. The differential voltage built up between the despun and spun areas of the spacecraft due to the coupler is shown in Figure 33. The coupler values chosen for this case gave an impedance of about 300 Ohms. The difference peaked at about 760 volts and the curve followed the discharge pulse transient.

The currents induced in each of the cables is shown in Figure 34. Since the termination impedance of each pulse was 50 Ohms, the transient damped out very rapidly; it was over before the discharge pulse ended. The currents peaked at +200 and -400 mA which should not be excessive.

A comparison of the results of simplified and detailed LEM's (Figure 35) show that the agreement between them is quite good for a typical 2 μC discharge.

FIGURE 31. DISCHARGE CURRENT TRANSIENT

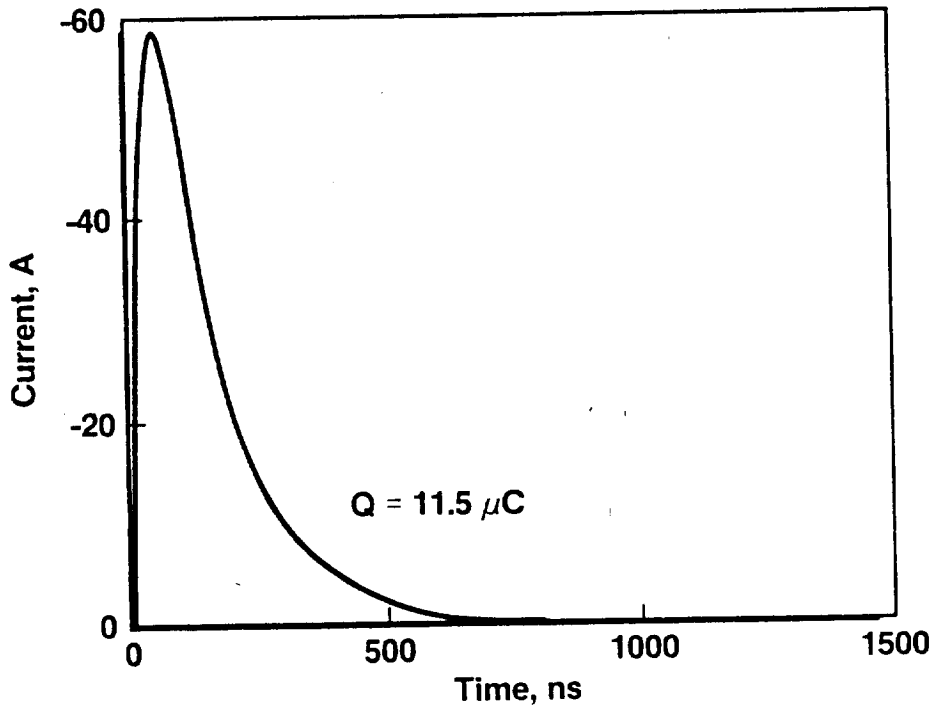

FIGURE 32. STRUCTURE POTENTIAL RELATIVE TO SPACE
11.5 μC DISCHARGE

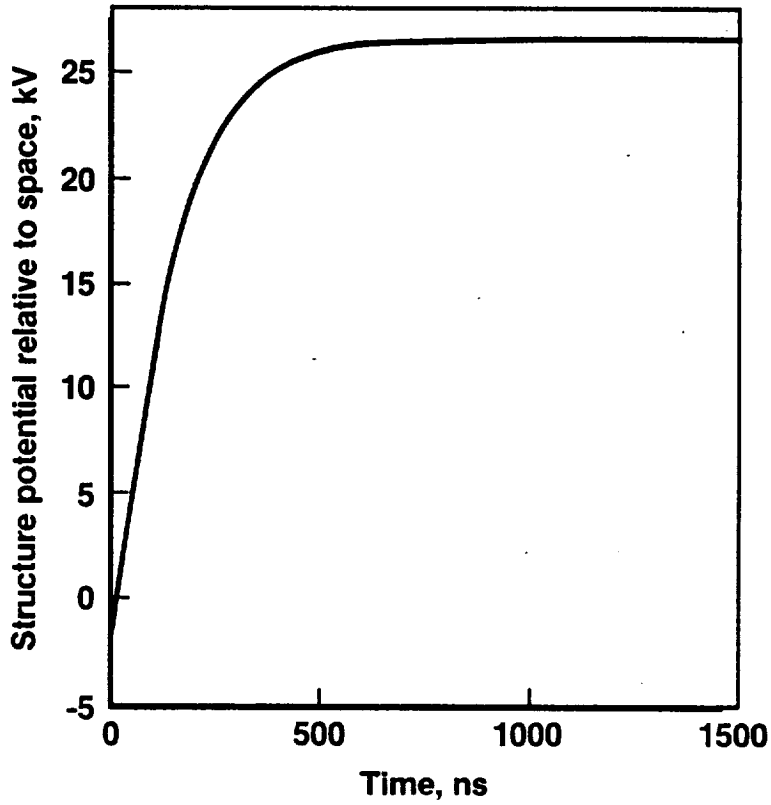

FIGURE 33. DIFFERENTIAL VOLTAGE - RELATIVE TO SPACE
SHELF 1 TO 2

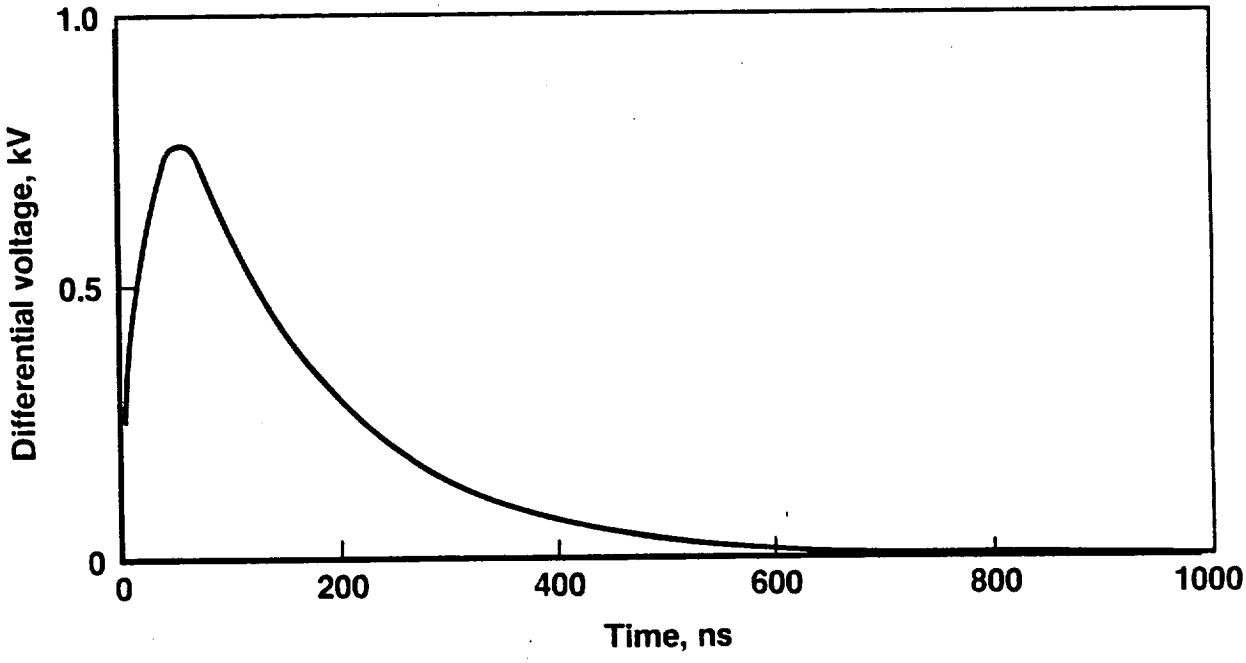

FIGURE 34. CURRENT COUPLED INTO CABLES
SHELF 1 AND 2

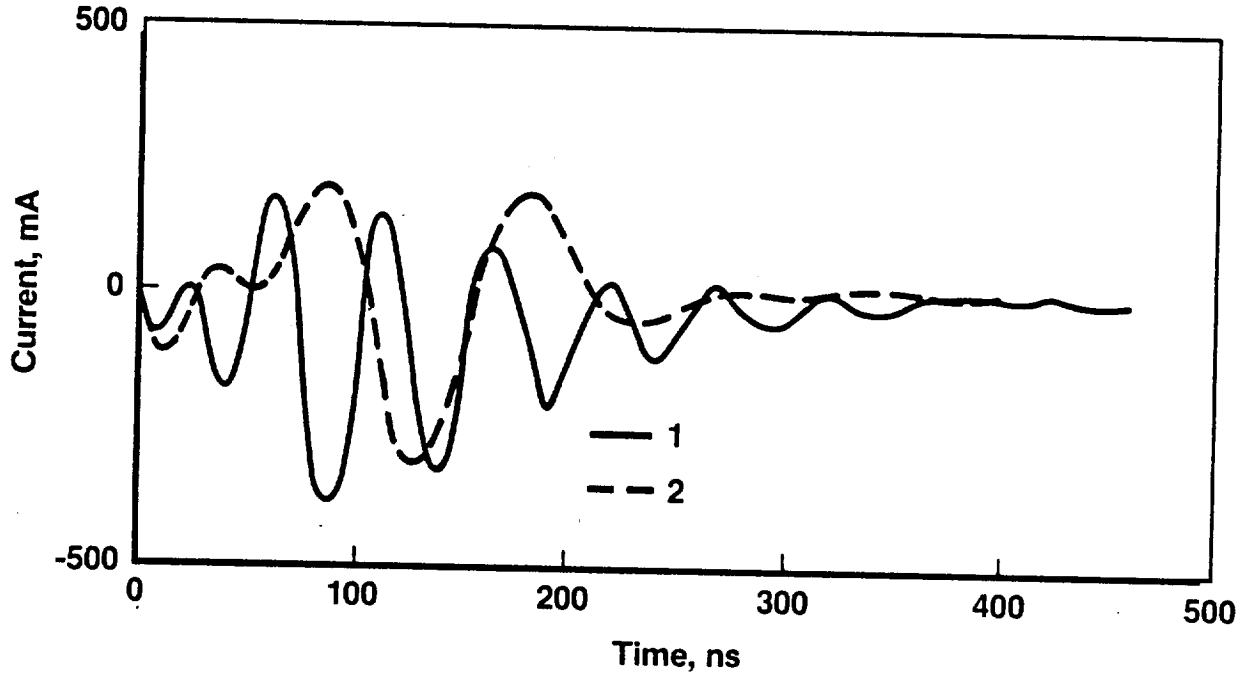

FIGURE 35. COMPARISON OF DETAILED LEM TO SIMPLE LEM
2 μC DISCHARGE

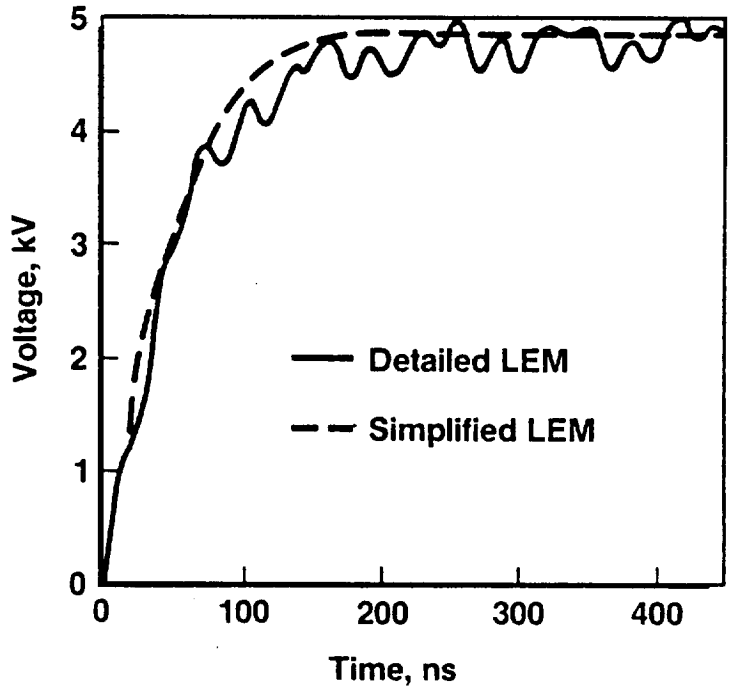

5.4 Interface Circuit

5.4.1 Description

Electronic systems are usually protected by buffer circuits such as those shown in Figure 36. The circuits are used on spacecraft cables to suppress noise signals on the line. The effectiveness and response of the circuit to various inputs were examined as a part of this study. The effects of injecting pulses at the input and the groundpoint were analyzed.

FIGURE 36. TYPICAL INTERFACE CIRCUIT FOR NOISE REJECTION

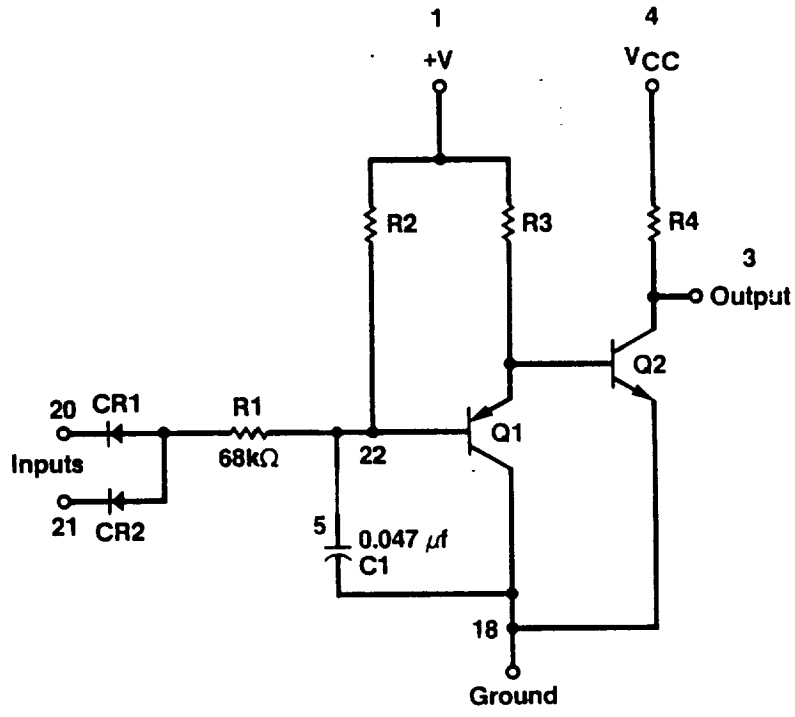

5.4.2 Signals Input At Front End

Only DC voltage signals of negative magnitude turn on the output when signal was applied at input. All other inputs had no effect unless signal was high enough to cause component failures. The exception to this was when the R-C filter was removed. In this case, input signals traveled through the circuit without being greatly affected. The RC filter was needed to keep out unwanted signals. These results are quite typical and well known.

5.4.3 Signals Input At Ground Point

5.4.3.1 Pulses

Negative pulses of both μsec and nsec pulse widths were input at the ground point (Figures 37 and 38). The start of the pulse sent the output to 5 V and it remained there for the duration of the pulse. When μsec pulses of positive magnitude were input to the ground point, the output was unaffected until the input pulse switched off.

After this, the output was driven to 5 V where it remained for ≈700 μsec (Figure 39). This may be explained as the equivalent R-C time constant of the circuit. This affect did not occur until the magnitude of the pulse went above about 20 V. This corresponds probably to the interaction between the capacitor and the transistors.

For nanosecond pulse widths, the results were similar except that the duration of the output signal did not last beyond 100 nsec for the higher magnitude (750 V) pulses and was shorter for the lower magnitude pulses. Here the threshold magnitude was lower (40 V) than in the μsec pulses case.

5.4.3.2 Damped Sine Wave Input At The Ground Point

Detailed LEM results indicated currents with 10-20 MHz transients would be generated in the wiring. In other studies frequencies as high as 50 MHz were seen. To cover these observed frequencies, signals of 1 MHz, 50 MHz and 100 MHz were input to the buffer circuit.

In these cases, the output had positive spikes when the sine wave went positive and negative spikes when the sine wave went negative. These spikes lasted only the duration of the positive or negative going part of the wave. The magnitude of the output spikes were higher in the 50 MHz and 100 MHz cases (~20-30 V), but only lasted a few nanoseconds of each half wave. In the 1 MHz case where each half wave was 5 μsec long, the output spike lasted for this long, but only reached 5 V magnitude. Figures 40 and 41 show the 1 MHz and 50 MHz input signals and the resulting output.

FIGURE 37. INTERFACE CIRCUIT RESPONSE TO NEGATIVE INPUT PULSE

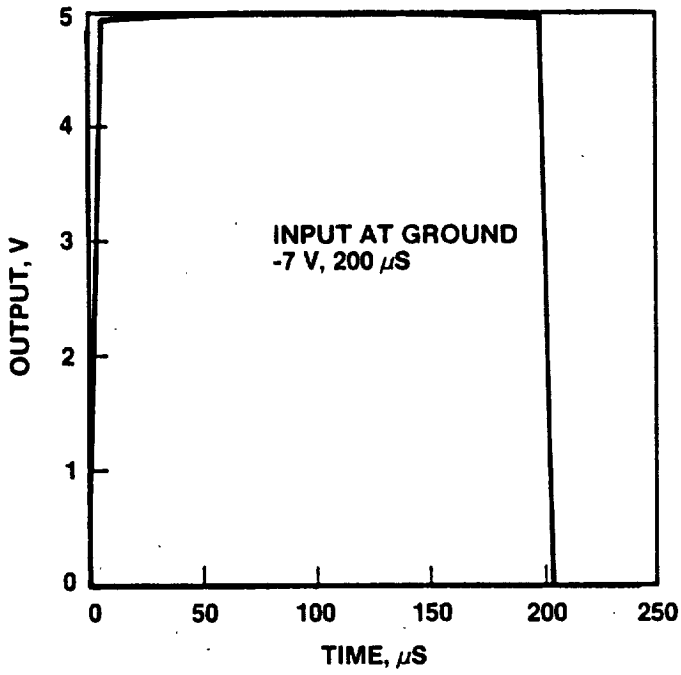

FIGURE 38. INTERFACE CIRCUIT RESPONSE TO NEGATIVE INPUT PULSE

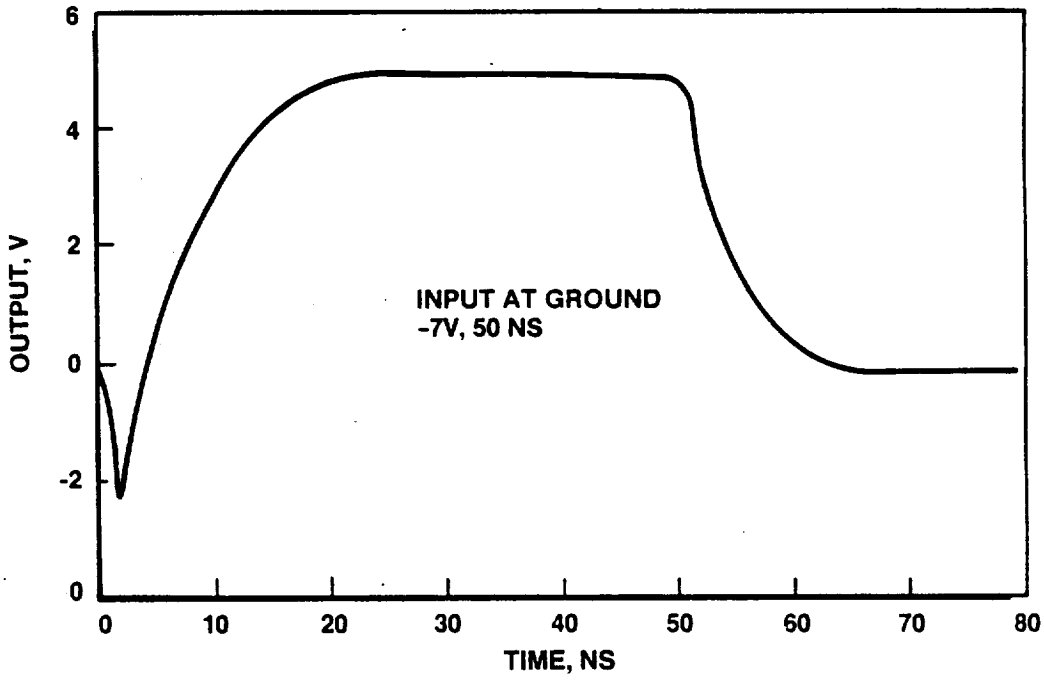

FIGURE 39. INTERFACE CIRCUIT RESPONSE TO POSITIVE INPUT PULSE

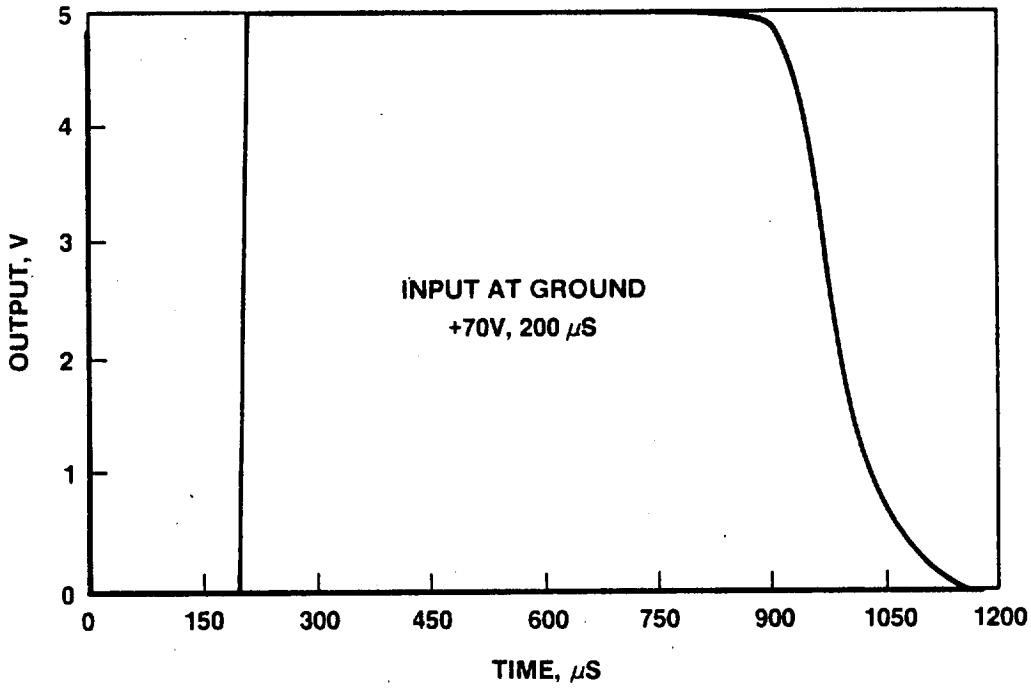

FIGURE 40. INTERFACE CIRCUIT REPONSE TO INPUT VOLTAGE

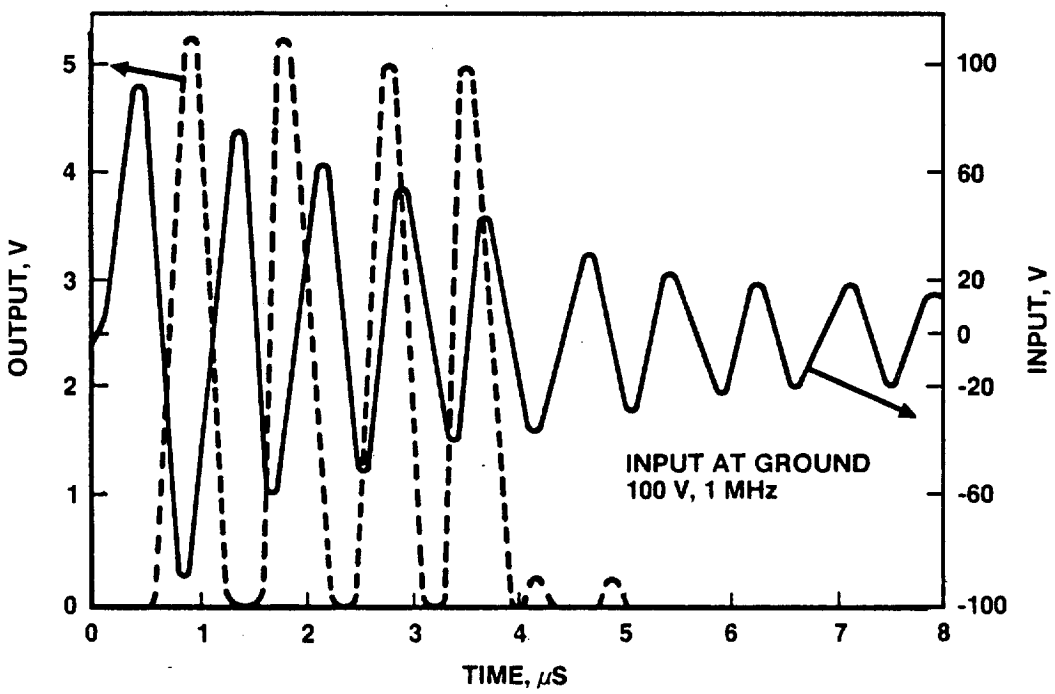

FIGURE 41. INTERFACE CIRCUIT RESPONSE TO INPUT VOLTAGE

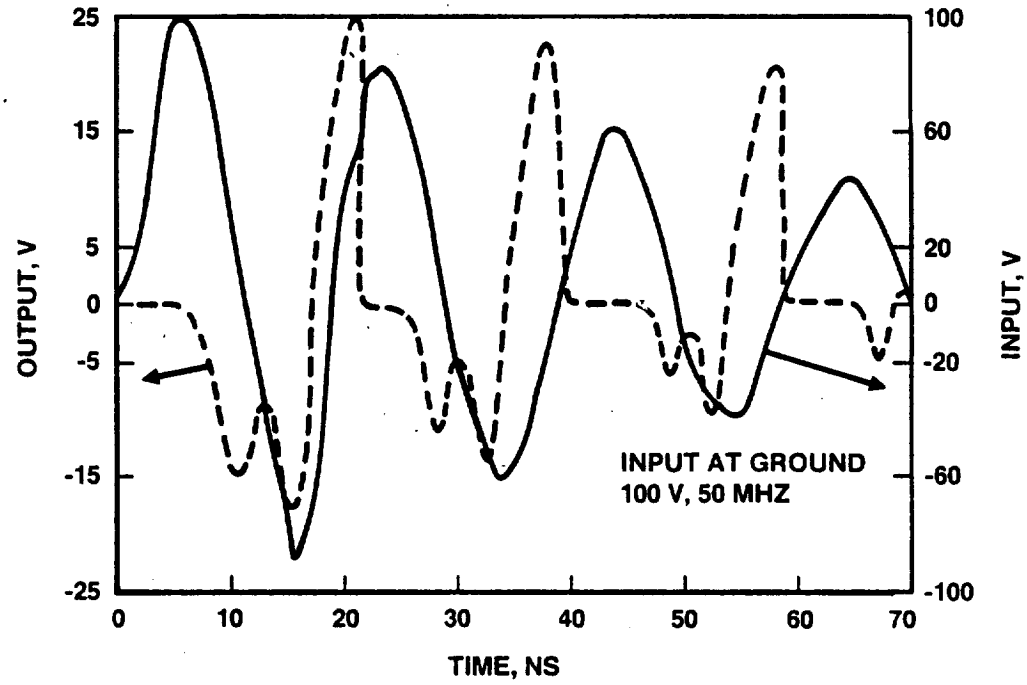

The output as a function of input frequency was also examined. Up to 1 MHz the output acted as if input signals were a string of pulses. The output frequency was the same as the input frequency (Figure 42). As the input frequency rose beyond 1 MHz the magnitude of the output rose, peaked and leveled off at about 50 MHz then decreased as the frequency went beyond 75 MHz (Figure 43). Since transients of greater than 100 MHz have not been predicted, no frequencies above this were studied.

FIGURE 42. EFFECT OF R-C FILTERS ON NOISE REJECTION
FREQUENCY DEPENDANCE OF OUTPUT SIGNAL

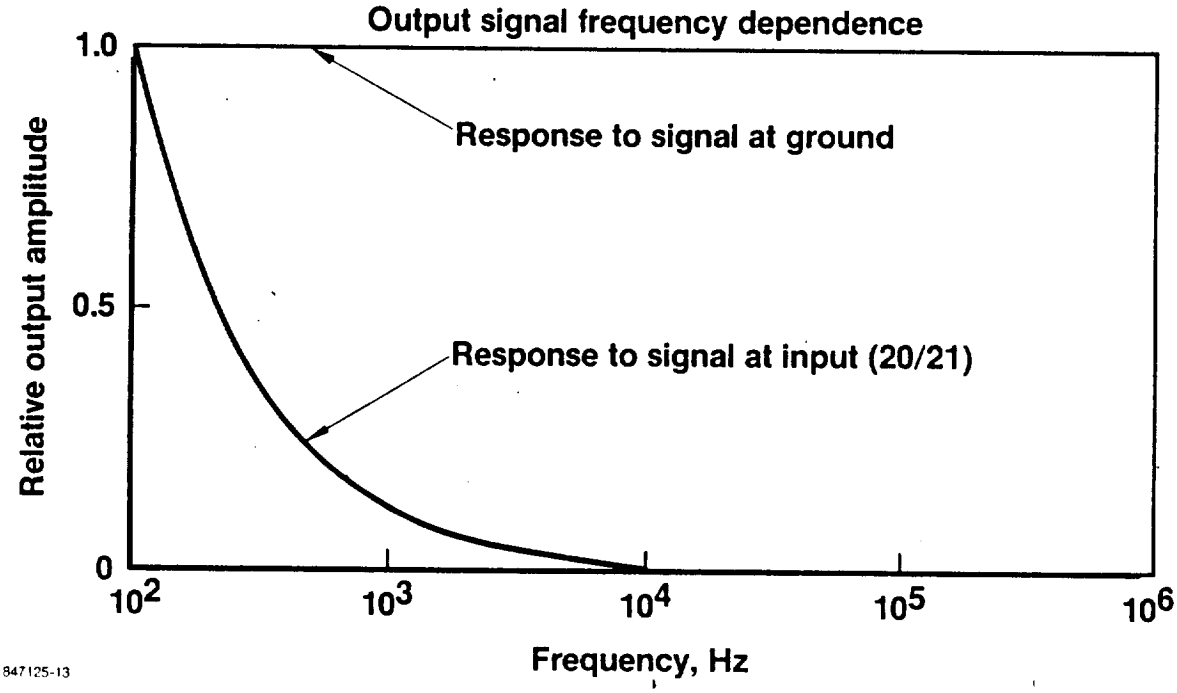

FIGURE 43. INTERFACE CIRCUIT RESPONSE TO INPUT FREQUENCY

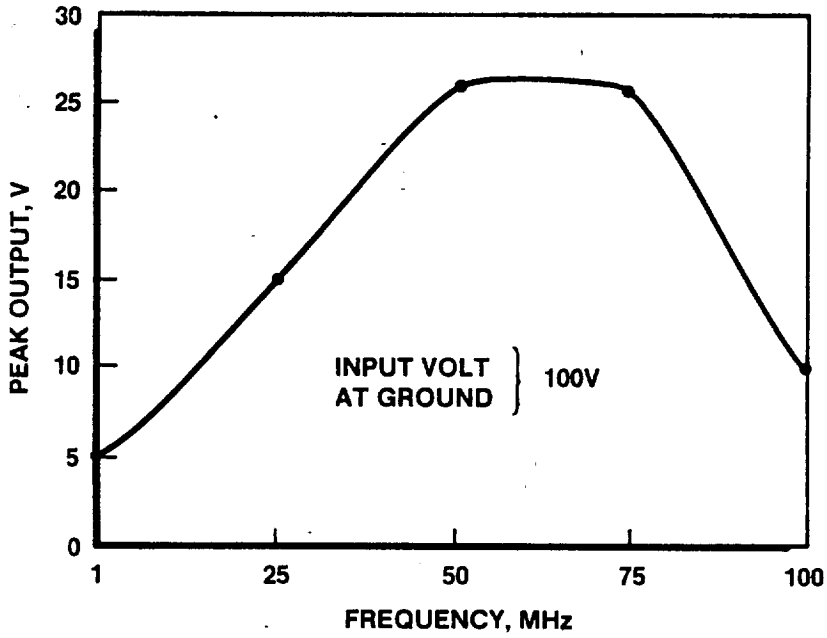

6. BACKGROUND - HIGH VOLTAGE SOLAR ARRAY DISCHARGE TRANSIENTS

A technology investigation of high voltage solar array interactions with plasma environments was launched about 15 years ago to satisfy a preceived need for such power for electric propulsion and advanced communications missions.[43-45] This investigation consisted of analytical and experimental studies and an auxiliary payload satellite program (SPHINX).[46] About the same time the satellite was launched and lost (1974), interest in high voltage system space plasma interaction phenomena decayed.

In the past several years, however, NASA has been conducting mission planning studies calling for large satellites to be placed in low Earth orbits by the Shuttle.[47-50] The culmination of this activity is the proposed Space Station which has a baseline operational power capability of 70 KW. The solar array to provide such power over the mission life must be sized to generate 200 KW initially.[51]

The generation of large power levels require very large solar arrays since the nominal power density is on the order of 100 watts/m^2. Such areas imply long cabling to bring power to the user. If the array is operated at a nominal voltage of 30 to 60 volts, currents on the order of 5000 amperes would be required. Currents of this magnitude can produce either significant cable harness losses (I^2R) or unacceptable increases in weight if the cable loss is reduced by thicker cross-sectional areas.[52] In addition, large currents flowing in the array can generate magnetic fields that can interact with the ambient field. This increases the drag on the system. The alternative is to increase the operating voltages thereby reducing currents. For the Space Station operating voltages in the range of 200 to 1000 volts are being considered. However, the largest operational voltage used in space occured during the relatively short periods of time that the Skylab was configured to operate at 100 volts.[53] The operation of power systems at elevated voltages can give rise to interactions with the space plasma environment that must be considered in designing these systems.

The interactions of concern are illustrated in the conceptual high-voltage space power system illustrated in Figure 44. This system consists of two large solar array wings surrounding a central body or spacecraft. The solar arrays are assumed to be assembled in what is called standard construction techiques. This means that the cover slides do not completely shield the metallic interconnects from the environment. These cell interconnects are at various voltages depending upon their location in the array circuits. Hence, the interconnects can act as plasma probes attracting or repelling charged particles. At some location on the array, the generated voltages will be equal to the space plasma potential. Since the electrons are more mobile than the ions, the array will float at a voltage that is

more negative than positive with respect to space potential. Cell interconnects at voltages above this space plasma potential will collect electrons, while those at voltages below this space potential will collect ions. The voltage distribution at the interconnects relative to space must be such that these electron and ion currents are equal. (i.e., the net current collected is zero).

This flow of particles can be considered to be a current loop through space that is in parallel with the operational system and, hence, is a power loss. In addition, the cover glass used on solar cells must also have a zero net current collection. This interaction with the space plasma forces the cover glass to a small negative potential which can produce large voltage gradients in the gap region between cells. This can give rise to breakdowns to space producing transients in the power lines.

The severity of these plasma interactions depends upon the array operational voltage and the charge-particle environments. The operating voltage will be determined from power system studies, but probably will be less than 1000 volts. The charged-particle environment is determined by the orbital altitude. At the projected operational voltages only the low energy or thermal plasma environment should be of concern since the array voltages are too low to influence the higher energy environmental particles. This thermal plasma environment at the equator is shown in Figure 45. Since the peak density of 3×10^6 cm^{-3} occurs at 300 km, one should expect interactions to be more severe at the lower altitudes.

FIGURE 44. SPACECRAFT HIGH VOLTAGE SYSTEM-ENVIRONMENT INTERACTIONS

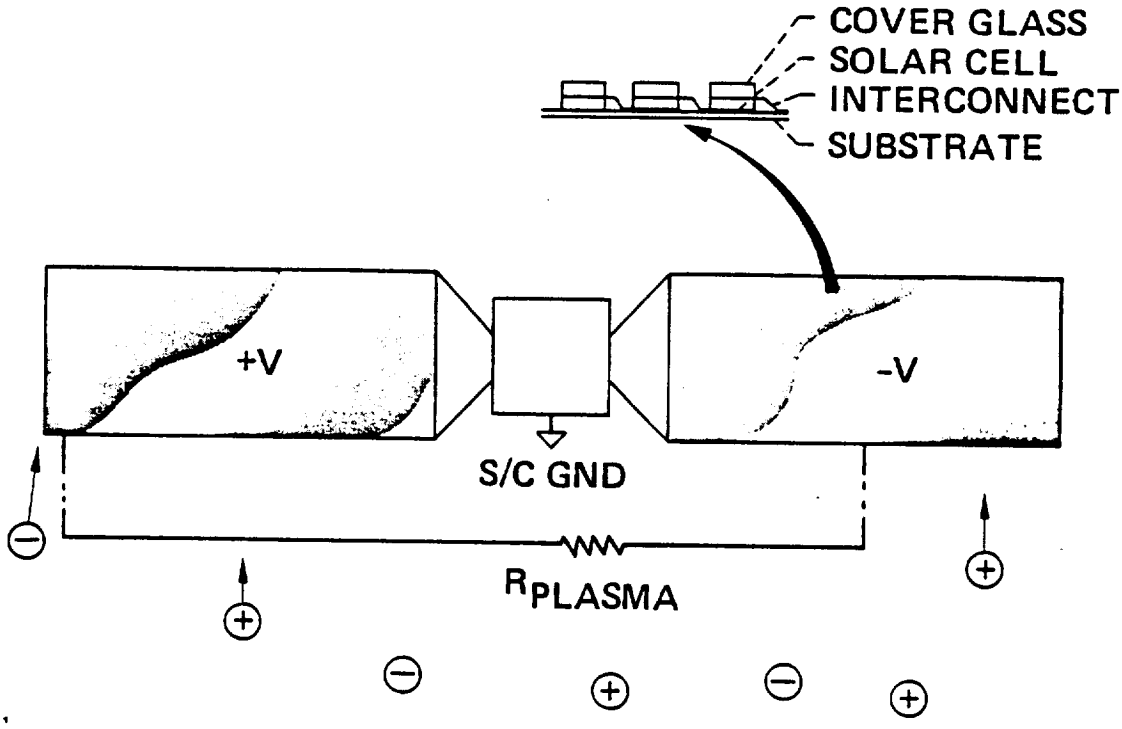

FIGURE 45. PLASMA NUMBER DENSITY VS ALTITUDE IN EQUATORIAL ORBIT

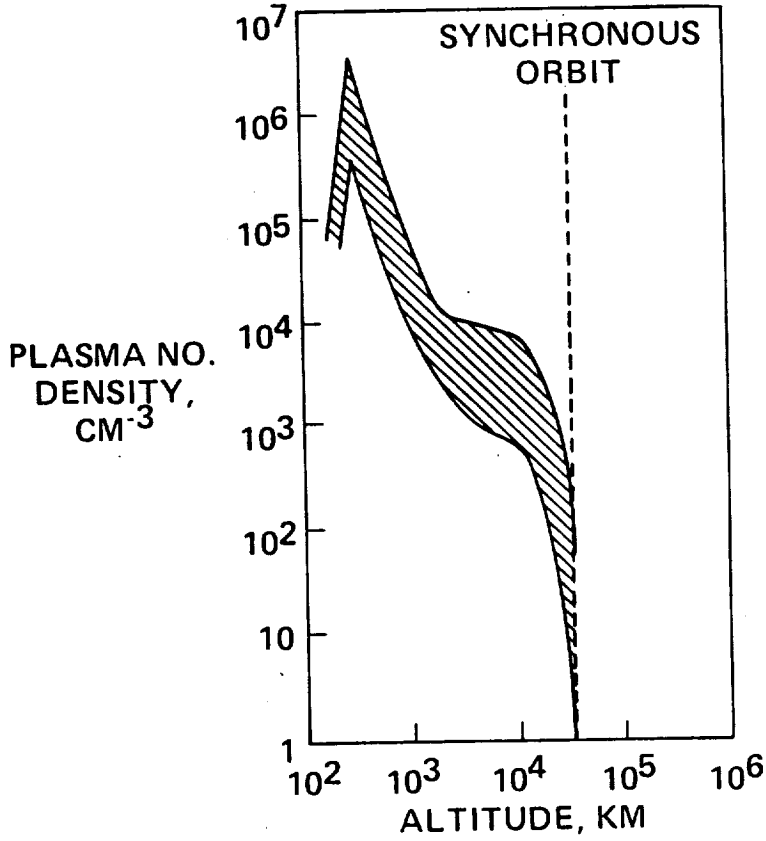

FIGURE 46. SCHEMATIC DIAGRAM OF TEST ARRANGEMENT

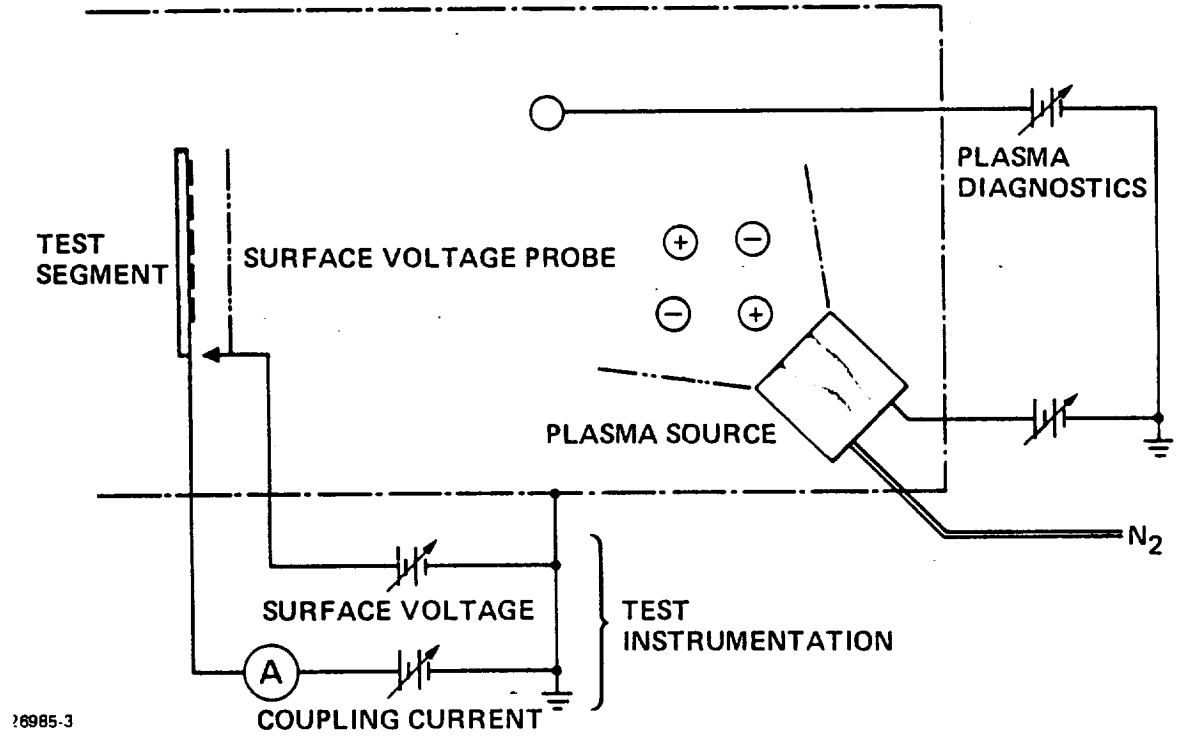

7. GROUND SIMULATION STUDIES

7.1 Introduction

Tests of segments of solar arrays exposed to plasma environments and biased by external power supplies have been conducted for years.[53-61] The philosophy implicit in such a test is that the interaction measured at each individual voltage step in the laboratory can be summed to obtain the performance of a distributed voltage solar array. Hence, it is assumed that there are no interactions between the various parts of the array at different voltages and the phenomena measured should produce worst-case results.

Such plasma interaction tests have been typically conducted in an experimental arrangement shown schematically in Figure 46. The vacuum chamber should be capable of maintaining a background pressure in the 10^{-6} torr range with the plasma source operating. This source creates the environment by ionizing a gas such as nitrogen, argon or helium. The plasma parameters (number density and particle temperatures) are determined with probes usually before and after each test. Determination of plasma properties during a test is impossible since the test surface interaction influences the probe readings. The solar array segment (ranging in size from 100 cm^2 to 10 m^2) is mounted in the chamber electrically isolated from tank ground. A high voltage power supply is connected to one or both ends of the array through an isolated feed through in the table wall. A current sensing instrument is placed between the power supply and the segment to measure the coupling current collected by the segment from the plasma environment. This lead should be shielded to minimize extraneous currents. A surface voltage probe (such as manufactured by TREK)[62] can be used to sense the voltage on the cover glass during the test. Therefore, a surface voltage profile and coupling currents as functions of specific applied voltages are obtained for a given plasma environment. It should be pointed out that the tank ground (at the wall) is not necessarily the plasma potential. This plasma potential is determined from the probe readings and must be added to or subtracted from the applied bias voltage in order to interpret the test data.

It is very important to make this correction at low bias voltages since the plasma potential can be in the range of ±20 volts.

7.2 NASA-Lewis Research Center (LeRC) Test Results

Plasma interaction tests have been conducted in various chambers at the NASA-Lewis Research Center since 1969 to support both technology investigations and space flight experiments.[46,56,57,61] It represents the largest body of test results available. Unfortunately, not all of this information has been published and is available only

as individual plots on separate graphs with brief annotations on plasma conditions. However, the data was complied and used here to form a data base for interactions. The majority of these tests were conducted without solar simulation.

7.2.1 Experimental Results

The following solar arrays were tested in plasma environments with densities ranging from 1×10^3 to 5×10^4 particle/cm^3:

- SPHINX (Space Plasma-Hi Voltage Interaction Experiment) test panel — 100 cm^2
- SPHINX power panel — 1950 cm^2
- SERT (Space Electric Rocket Test) power panel — 1400 cm^2
- PIX-1 (Plasma Interaction Experiment) test panel — 100 cm^2
- PIX-2 test panel - Single Segment — 480 cm^2
- PIX-2 test panel - All four segments — 1920 cm^2
- (4) PIX-1 panels — 400 cm^2
- 9 Panel Array — 13,600 cm^2

SPHINX[4], PIX-1[22] and PIX-2[23] were auxiliary payload experiments that underwent considerable ground testing prior to flight. PIX-1 and 2 both were successful and these results will be discussed in the next section of this report.

In order to minimize the number of variables in these studies the collected current was non-dimensionalized and the voltage used was relative to the plasma potential rather than the applied bias. The results are shown in Figure 47 and 48 for positive and negative biases. The coupling current, I is the experimentally obtained value.

The current, I_o, is the thermal current to the panel (A_p) or:

$I_o = 2.7 \times 10^{-12} n_e \sqrt{T_e} \; A_p$ For positive bias

or

$I_o = K n_i \sqrt{T_i} \; A_p$ For negative bias

where: $K = 9.89 \times 10^{-15}$ if Argon was used in the plasma source.
$K = 1.4 \times 10^{14}$ if Nitrogen was used.

It was hoped that this procedure would minimize the variability of the data but it is obvious that it didn't. The error bars represent the range of results for a specified voltage not a variation about a mean value.

The major uncertaintity in this data is the plasma parameters. The majority of the Lewis data lists only an approximate value for density while values of electron and ion temperatures are rarely listed and the plasma potential is not specified. Density measurement at several locations within the chamber indicates a variable plasma probably due to wall effects. Furthermore, there is no indication that the density always remained uniform throughout the test. The only uncertainty stated in these tests is that the density is known within a factor of two.

In spite of the variation in the data, it is apparent that the positive bias data shows a transition at 100 volts - the snap-over phenomenon.[66] When a large data base is used, this transition is smoother than previously believed based on single data sets. The negative bias data seems to be increasing linearity.

7.2.2 Empirical Model

This LeRC data base can be used to develop empirical relationships for current collection as a function of bias voltage and plasma characteristics. Due to the abrupt transition, the electron current collect would have to be broken into two parts; collection where the voltage is 100 volts or less and collection above 100 volts. The relationships developed are:

$$I_{collected} = j_{eo} A_p (1.25 \times 10^{-3}) \left(1 + \frac{V_+}{T_e}\right) \quad 0 < V_\pm < 100$$

$$I_{collected} = j_{eo} (.25) \frac{A_p}{4} \left(1 + \frac{V_\mp 100}{T_e}\right) \quad V_+ > 100$$

$$I_{collected} = j_{io} (1.25 \times 10^{-2}) A_p \left(1 + \frac{V_-}{T_i}\right) \quad V_- < 0$$

where:

A_p = solar array panel area (cm^2)

j_{eo} = electron thermal current density (amp/cm^2)

j_{io} = ion thermal current density (amp/cm^2)

T_e = electron temperature (eV)

T_i = ion temperature (eV)

FIGURE 47. SUMMARY OF GROUND TEST DATA - LeRC POSITIVE BIAS VOLTAGES

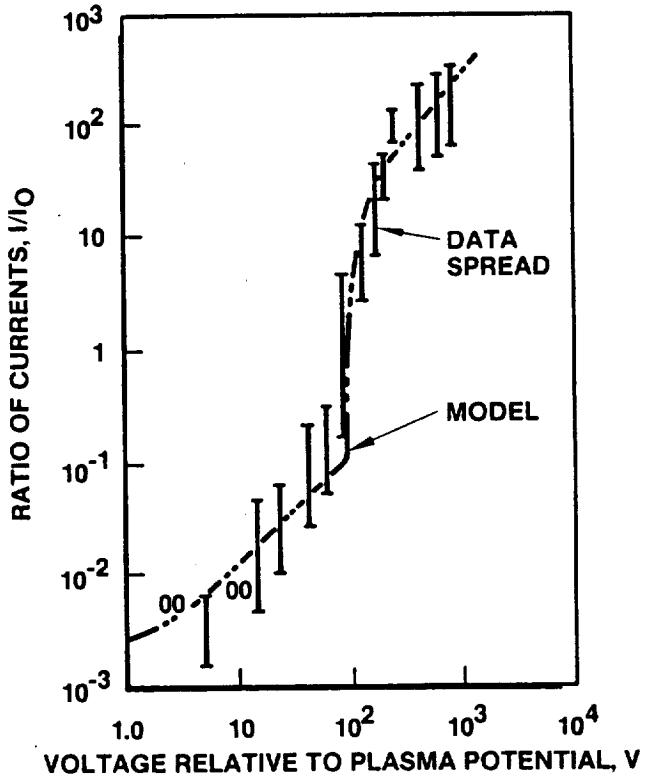

FIGURE 48. SUMMARY OF GOUND TEST DATA - LeRC NEGATIVE BIAS DATA

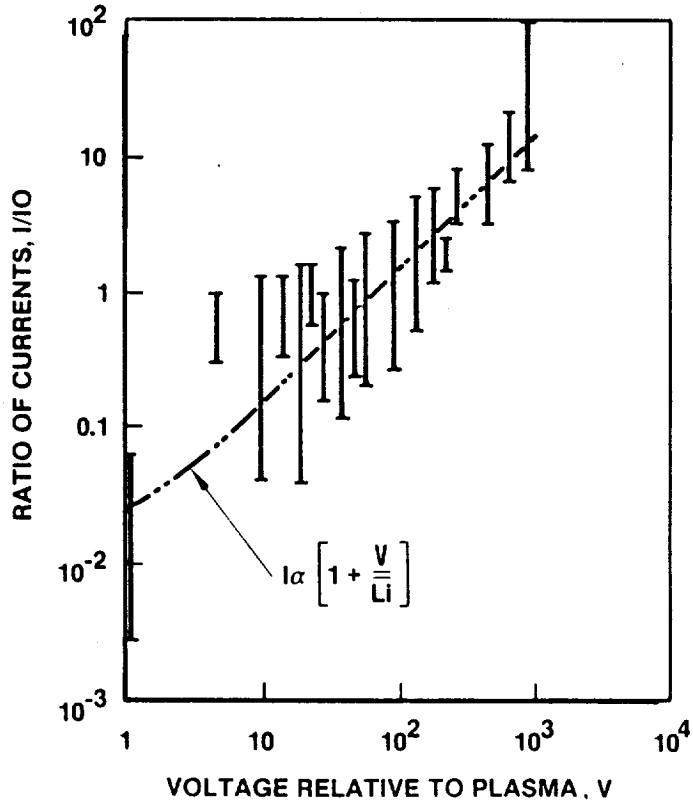

These curves are plotted in Figures 47 and 48 and are in reasonable agreement with the data. The largest discrepancy is in the region between +50 and +100 volts where the collection process is undergoing a transition process to snap-over conditions.

Previous attempts to model the low voltage (<100 volt) positive bias data led to the belief that this collection should correspond to the interconnect region between the solar cells acting as cylindrical plasma probes.[67-69] This lead to a relationship where the current collected would be proportional to the square root of the voltage. This seemed to agree with the results of several sets of data. But, when this data is corrected for a plasma potential and replotted, then the current varies directly with voltage. There is no obvious explanation for the factor 1.5×10^{-3} needed in the current collection model for this low voltage interaction other than it could be due to collection suppression caused by the charged cover glass.

7.3 Effect of Facility on Results

Test have been conducted in facilities other than at the Lewis Research Center (LeRC) and these results should be reviewed and included in the data base. The two sets of data to be discussed here are those obtained at Boeing[13] and Johnson Space Center.[61]

7.3.1 Boeing Test Results

Plasma interaction tests were conducted by Boeing under contract to the Lewis Research Center.[55] These tests were conducted in a similar manner to that previously described and used nitrogen for the plasma environment. The fundamental difference between the LeRC and Boeing facility was the plasma source. The LeRC used a bombardment ionization source in which electrons emitted from a hot wire filament in a cylindrical chamber would spiral out to the outer wall anode ionizing a gas by impact. The electron path was lengthened by a cylindrical magnetic field. The plasma generated would diffuse out of an orfice and fill the chamber. Essentially, it is a point ionization source, but in a large chamber, this should not make much of a difference. The Boeing source was two large screens separated by a small distance. An electrical field was provided across these screens and the ionization process started by a hot wire filament. A gas flow was established into the screen separation and a plasma would exit the device. This device is referred to as a Burrowbridge source.[70]

Each device would generate a plasma but with different characteristics. The Boeing system resulted in plasmas with electron temperatures in the 5 to 10 eV range and ion temperatures in the 25 eV range. The LeRC tests were conducted with particle temperatures in the 1 to 2 eV range.

A second difference was that the Boeing results were obtained in an ion pumped chamber while the LeRc chambers were all oil-diffusion pumped systems. Experimental checks were conducted at Boeing to verify that the pump didn't influence the test results.

The principal difference between the two sets of results is that the Boeing results do not show a snap-over phenomenon (see Figure 49). The electron collection tends to be a fairly uniformly increasing curve with about an order of magnitude larger current at voltages less than 100 volts and about an order of magnitude less at voltages greater than 100 volts. In fact Boeing was able to fit the data with a partially isolated spherical probe theory over the complete range. The negative bias data obtained by Boeing falls within the scatter of the LeRC results.

FIGURE 49. COMPARISON OF GROUND TEST RESULTS

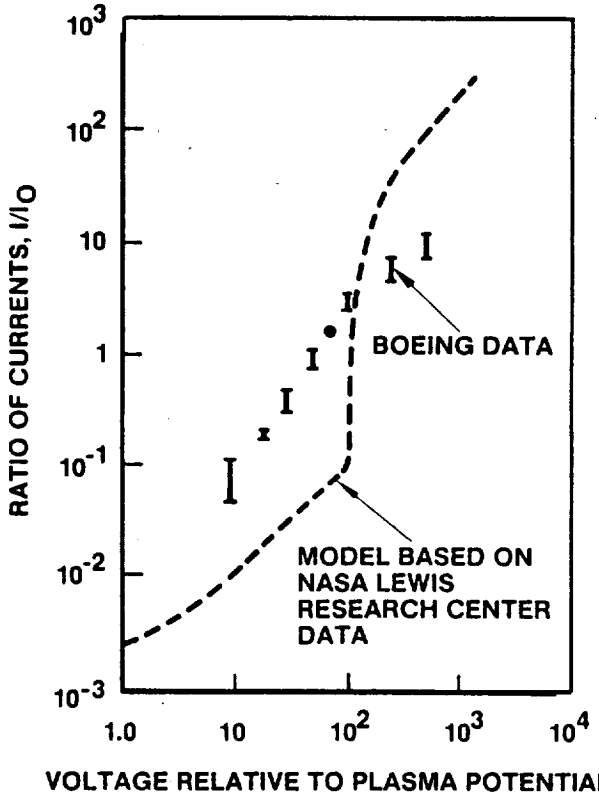

7.3.2 Johnson Space Center (JSC) Results

There have been several tests conducted on high voltage solar array interactions in the 40 foot diameter chamber at JSC.[58,60] The test that will be discussed here is the one that was conducted jointly by JSC and LeRC personnel to evaluate the effect of facilities on plasma-high voltage surface interactions.[61] The same samples were used in both tests and the same personnel did both tests. Tests were run both with and without solar simulation.

The plasma source used in the JSC tests was a 30 cm ion thruster with the accelerator grids floating; no voltages were applied to the accelerator. Argon was used to provide the plasma environment. The solar array test articles consisted of the 9 separate panel array (13,600 cm^2) and a single 1400 cm^2 panel.

The determination of facility effects can best be shown by comparing the results of positive bias voltage collection on the 1400 cm^2 panel. The coupling current collected as a function of voltage in the LeRC and JSC chambers is shown in Figure 50. Both tests used Argon for the plasma but the densities were slightly different: 3×10^3 cm^{-3} at LeRC and 1.6×10^3 cm^3 for JSC. The initial collection characteristics indicate a positive plasma potential in the JSC facility

FIGURE 50. COMPARISON OF TESTS IN DIFFERENT FACILITIES

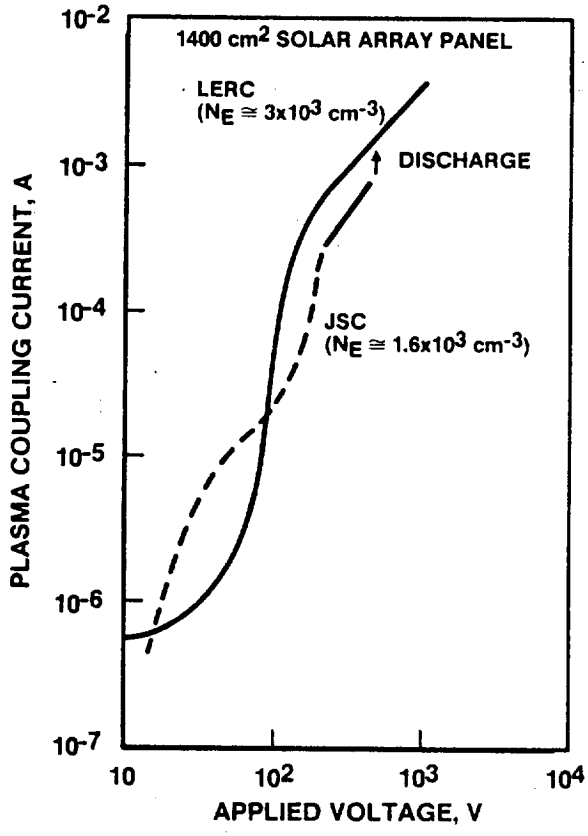

(about 8 to 12 volts) whereas the LeRC facility had a negative plasma potential (usually -5 to -10 volts). The low voltage collection (10 to -60 volts) in the JSC chamber is about an order of magnitude larger than the LeRC results even though the panel was identical and the plasma density was about a factor of two higher in the LeRC chamber.

Snapover occurred, as usual, at about 100 volts in the LeRC chamber whereas a smaller version occured at about 150 volts in the JSC chamber. The current collection above 200 volts is considerably lower in the JSC results compared to the LeRC.

Finally, the JSC chamber results terminated in a discharge at about 400 volts positive. This positive voltage breakdowns did not occur in the LeRC tests. Similar results were found in the positive voltage collection phenomena with the 13,600 cm^2, nine panel array.

In the solar simulation test in the JSC chamber, the nine panel array was connected in series and illuminated providing data on the operation of reasonably large solar array operating in an open circuit mode at about 250 volts in a plasma environment corresponding to an altitude of about 500 km. The voltage of each panel relative to tank ground were measured as was the current flow between each segment. The results indicated that the array floated with one panel at an average voltage of +35 volts positive and decreasing to an average of -190 volts negative relative to the tank ground. Assuming that the plasma potential was the same as before (+10 volts), then the most positive panel was +25 volts and the most negative was -200 volts. A model based on cylindrical probe electron collection and spherical probe ion collection was constructed that appeared to match this data exceptionally well.[68] However, when the models developed as part of this study were applied, the electron collection was down by an order of magnitude while the ion collection was the same.

7.4 Current Collection Models

As shown in the previous summary of ground test results, there are questions about the electron collection data. The low voltage (<100 volts) electron collection data from the LeRC tests always seems to be suppressed compared to the Boeing and JSC results. The data above 100 volts in the LeRC tests tends to be greater than that obtained in the other tests. The combination of these two conditions tends to make snap over much more pronounced in the LeRC tests compared to the others. The cause of this discrepancy is not understood. It could be related to electron temperatures (they were different in all tests) or to magnetic field effects (the large chamber at the LeRC attenuates the local magnetic field). On the other hand, the ion

collection phenomena appears to be reproducible and to be independent of the gas used for the environment, plasma sources and facilities.

Since the purpose of this review is to develop current collection models, the following relationships are assumed:

$$I_{Collected} = \frac{j_{eo}}{10} A_p \left[\frac{.05}{4}\right] \left[1 + \frac{V_+}{T_e}\right] \quad \text{amps} \quad 0 < V_+ < 100$$

$$I_{Collected} = j_{eo} A_p \frac{1}{4} \left[1 + \frac{V_+ - 100}{T_e}\right] \quad \text{amps} \quad V_+ > 100$$

$$I_{Collected} = j_{io} A_p \left[\frac{.05}{4}\right] \left[1 - \frac{V_-}{T_i}\right] \quad \text{amps} \quad V_- < 0$$

where: A_p is the solar array area (cm^2)
j_{eo} and j_{io} are the electron and ion thermal current densities (amp/cm^2)
V_+ and V_- are the positive and negative voltages with respect to the plasma potential.

These current collection models are basically spherical probe relationships. Dividing the panel area by 4 accounts for the difference between a spherical surface area and a disk. The factor 0.05 is used to compute the interconnect area; taken as 5 percent of the total panel area. The factor of 10 in the electron collection at voltages less than 100 volts accounts for the low voltage charging of the cover glass.

These equations are, at best, good to an order of magnitude for electron collection, but considerably better for ion collection.

These relationships were based on the LeRC results only. The validity of the facility effects noted previously will have to be established by further studies.

8. COMPARISON TO FLIGHT DATA

8.1 Introduction

There are only two sets of experimental data obtained in flight, Plasma Interaction Experiments 1 and 2 (PIX - 1 and 2).[64,65] Both of these flights were auxiliary payload experiments flown on the Delta second stage in polar orbits. They were classic examples of low cost experiments and, as such, provided limited information. Interpretations of the results required a major effort and were not necessarily unique.

The most disheartening result in these flights was that the Delta second stage charged during the electron collection phases of the experiment making the positive voltage readings difficult to interpret. There also was a drift in the electron current meter in PIX-1 and some of the low voltage currents were too small to be read in PIX-2. Due to the limited effort available in this contract, it was decided to concentrate on the negative bias results for this comparison.

8.2 PIX -1 Results

The PIX-1 package was flown in February, 1978 on the Delta second stage used to launch Landsat C.[64] PIX-1 operated for about 4 hours in a 900 kilometer polar orbit. The PIX used the Delta telemetry unit so its life was limited by the Delta battery. Since only real time data transmission was available, only about two hours of data was obtained.

The PIX contained three test surfaces; a 10 cm diameter disk mounted on the electronics housing, a 10 cm diameter disk on a 30 cm dia sheet of kapton and a 100 cm^2 solar array segment. The disk-on-kapton and solar array segment were mounted on an experiment plate located 90° around the Delta from the electronics unit (see Figure 51). Each test surface was connected to its own electrometer and all three were connected to the same high voltage power supply. The two experimental surfaces on the plate could be switched to the power supply one at a time.

The experiment was preprogrammed to operate continuously stepping through four positive and five negative voltages in one minute steps. The plain disk was constantly on and was used as an environment monitor. Either the solar array or disk-on-kapton was selected. Discharges were determined when the current input to the power supply exceeded a predetermined level, shutting off the supply for 10 seconds. The power supply could restart after this delay.

Due to the limitations discussed above there were only five negative voltage cycles obtained during this flight. The approach used in the analysis was to use the plain disk data as an indicator of plasma density and velocity and then use the negative voltage current collection model developed here to determine the experiment plasma density and velocity mode (ram, wake or thermal). If the current trends could be matched using reasonable values of density and particle energies, then it could be said that the current collection model was reasonable. Since it was known from ground test results that the disk and disk-on-kapton ion current collection was identical, analysis of this experiment was also conducted.

The comparison of the models to the flight data for the disk, disk-on-kapton and solar array is shown in Figure 52. The agreement is very good and is typical of the other cycles. The results for all cycles are summarized in Table III. The negative voltage current collection model appears to be a reasonable approximation based upon these results.

FIGURE 51. PLASMA INTERACTION EXPERIMENT (PIX)

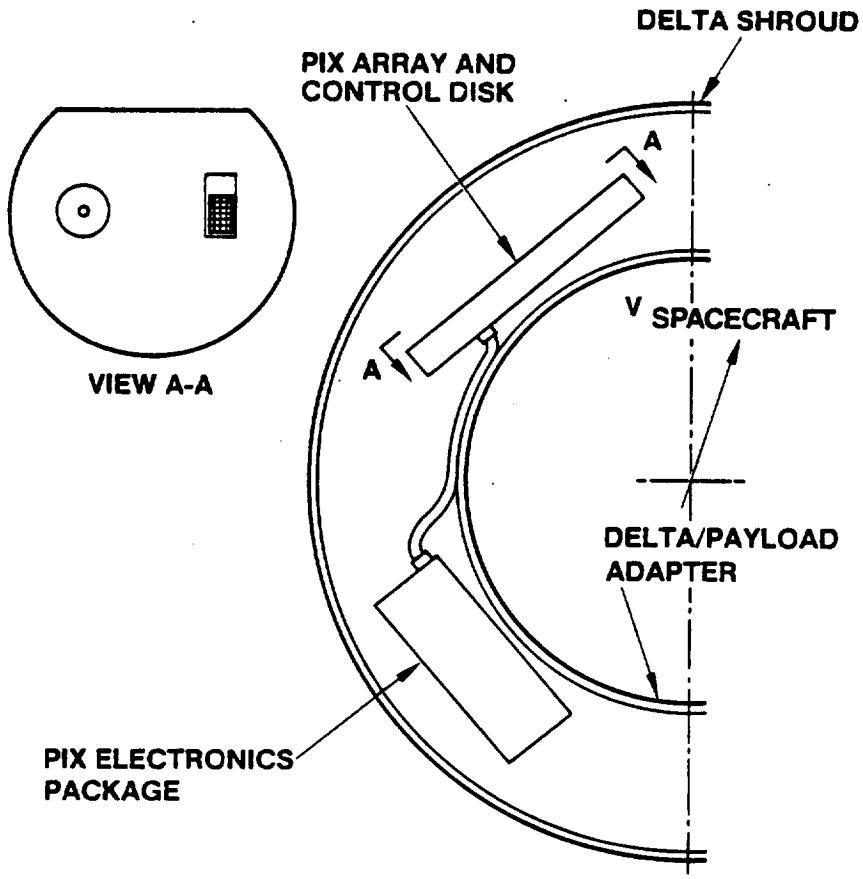

8.3 PIX-2 Results

8.3.1 Introduction

The PIX-2 package flew on the IRAS Delta second stage in January, 1983.[65] It also had a 900 kilometer, polar orbit. The experiment consisted of four, 480 cm^2 solar array segments that could be biased separately or collectively to either plus or minus 1 kilovolt in 10 steps. This array was mounted on the experiment plate 180° away from the electronics enclosure (see Figure 53). The Delta telemetry system was used but additional battery capacity was added. In addition, a data storage system was included which increased the information from this experiment. It operated for about 11 hours and most of the data were recovered. The plasma diagnostics were improved to the extent of carrying a Langmuir probe which could be swept from -20 to +100 volts when the experiment was off or held at 50 volts during the experiment to monitor density changes. The probe was mounted on the electronics enclosure. An electron emitter was also incuded to try to limit the charging of the Delta during the higher positive voltage steps.

FIGURE 52. COMPARISON OF MODEL TO PIX-1 DATA
NEGATIVE BIAS DATA

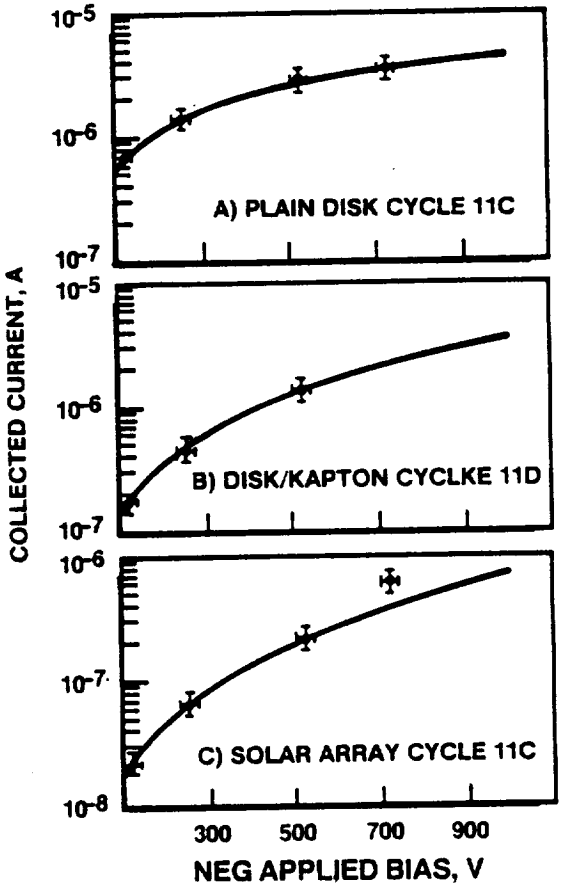

TABLE III

SUMMARY OF PIX -1 ANALYSIS
NEGATIVE BIAS DATA

CYCLE NO	EXPERIMENT	PLASMA CONDITIONS DENSITY (CM -3)	TEMPERATURE (EV)
1C	PLAIN DISK	3.5×10^{4}	.09
	SOLAR ARRAY	1.0×10^{3}	.07
1D	PLAIN DISK	3.8×10^{4}	.07
	KAPTON/DISK	$2 - 7.5 \times 10^{3}$	.07
6D	PLAIN DISK	3.9×10^{4}	.07
	KAPTON/DISK	3.9×10^{4}	.2
9C	PLAIN DISK	3.6×10^{4}	.08
	SOLAR ARRAY	3.6×10^{4}	.5 - 1.0
9D	PLAIN DISK	4.8×10^{4}	.07
	KAPTON/DISK	4.8×10^{4}	1.0 - 0.1
11C	PLAIN DISK	3.8×10^{4}	.07 - .1
	SOLAR ARRAY	$5 \quad -10 \times 10^{3}$	.07
11D	PLAIN DISK	3.8×10^{4}	0.2
	KAPTON/DISK	$1 - 2.5 \times 10^{4}$	.07
12C	PLAIN DISK	$3.6 - 3.8 \times 10^{4}$	.12 - .05
	SOLAR ARRAY	3.6×10^{4}	2.4 - 1.5
12D	PLAIN DISK	4.2×10^{4}	.07
	KAPTON/DISK	4.2×10^{4}	1.5

As part of this contract study, the Langmuir probe data was briefly reviewed. The main effort was concentrated on the negative bias data with the comparisons between models and data limited to segment 1 data only.

FIGURE 53. PIX II/DELTA

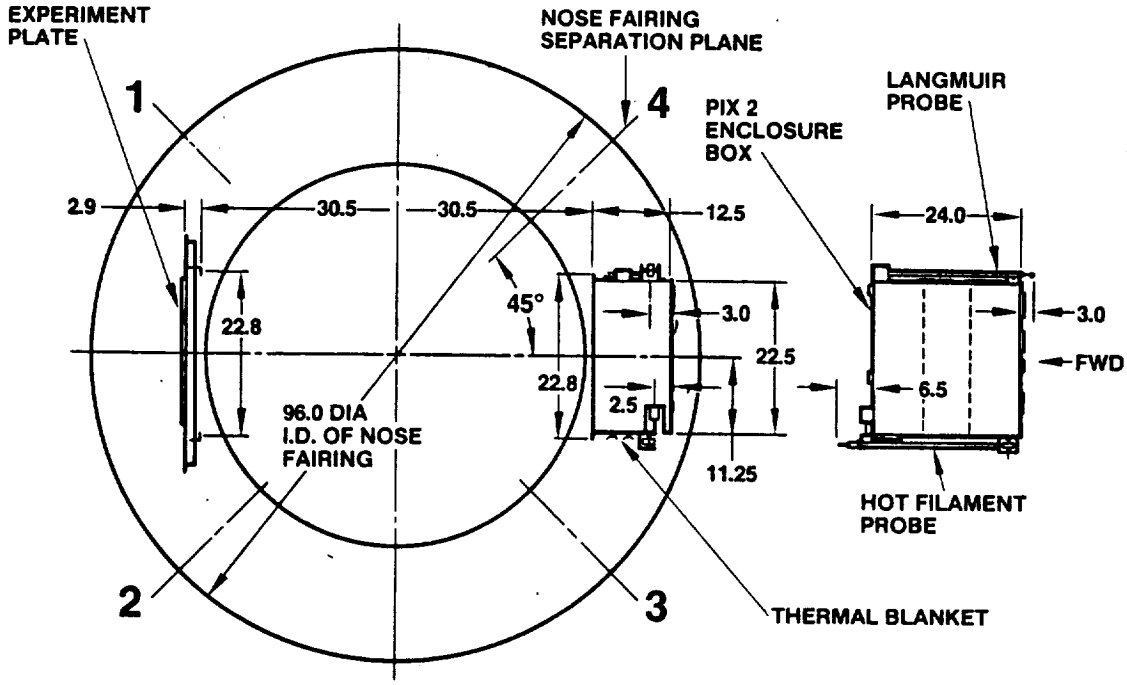

8.3.2 Langmuir Probe Results

The currents collected for positive bias voltage steps in the first three Langmuir probe sweeps are shown in Figure 54. In the first sweep, conducted before initiation of the solar array experiments, the current is linear as expected. Analysis of these results indicates a plasma density of about 4×10^3 cm^{-3} with an electron temperature of about 0.3 eV. Results like these were anticipated. The negative voltage data for this sweep was lost. The next two sweeps taken after the experiment started indicate that the current is proportional to the voltage to some power between 1.2 and 1.6. This is not what was anticipated for the probe operation, but could be explained by a variable density and temperature such as that shown in Figure 55. Here the first probe sweep results is shown for comparison with a later sweep. It is interesting to note that the ion collection portion of the curve matched reasonably well with the expected density and temperature. Unfortunately the ion collection phenomena is very strongly dependent on whether the probe is in the ram, wake or thermal positions and can be difficult to interpret.

Since the probe data was questionable and since the LeRC personnel were concentrating on interpreting these results, no further work on the Langmuir probe data was attempted as part of this contract study. Instead, the density data supplied by the LeRC was used.[71]

FIGURE 54. PIX - 2 LANGMUIR PROBE DATA
1st THREE PROBE SWEEPS

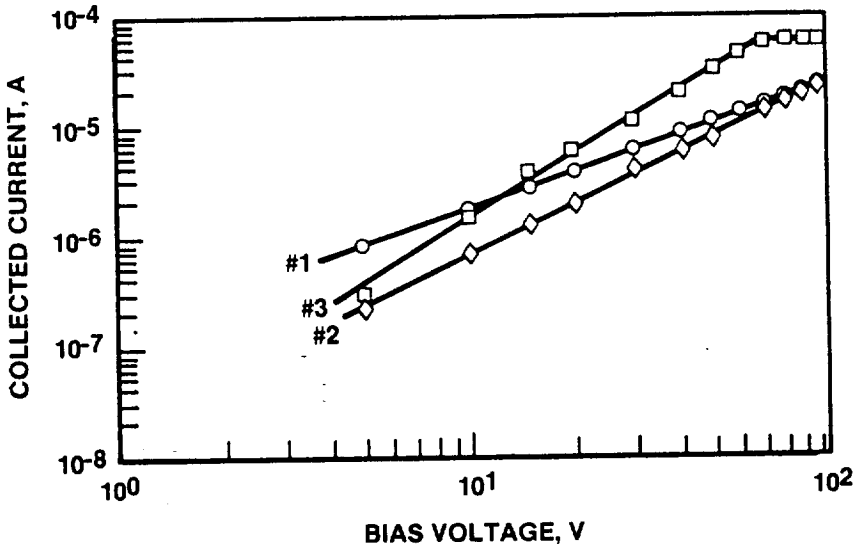

FIGURE 55. PIX-2 LANGMUIR PROBE DATA

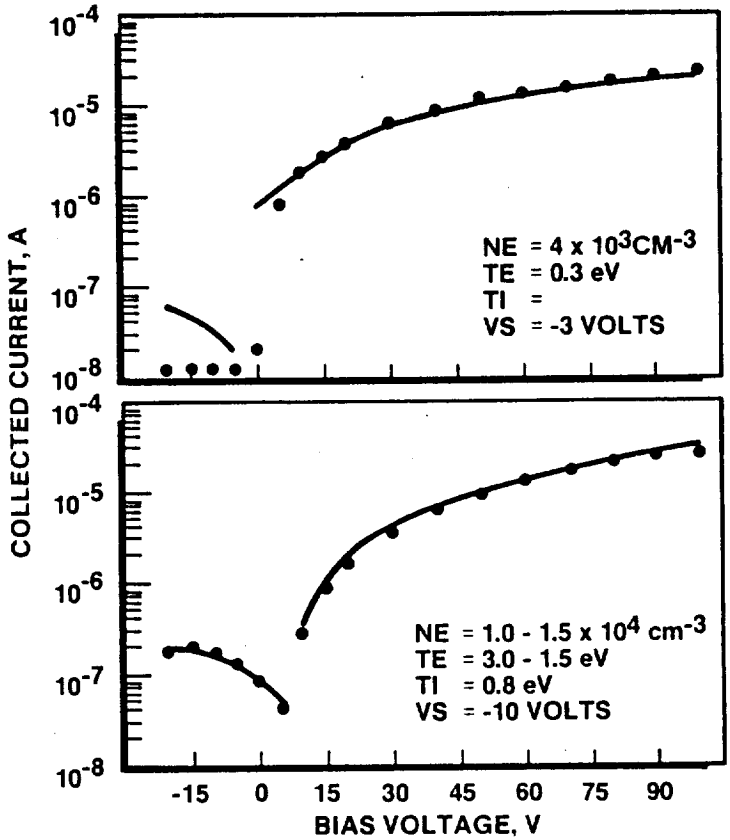

8.3.3 Negative Bias Data

As stated previously the principal effort here was concentrated in the analysis of segment 1 negative bias data. Of the 19 possible segment 1 runs, 12 were selected for analysis. The first step was to separate out the velocity mode effects. This was accomplished by plotting the equilibrium currents for the first four or five voltages and extrapolating the curve back to zero. The number of voltage steps used depended upon the linearity of the curve. The results are shown in Figures 56 and 57. There are two distinct regimes; one in which the current at zero volts is less than 0.05 μA and the second in which the zero volt current is greater than 0.20 μA. Since the current at zero volts is proportional to the square root of the ion temperature and since the temperature in the ram mode can be up to 60 times the temperature in either wake or thermal modes, it is asserted that those runs in the second catagory have a ram component while the first can either be in thermal or wake modes. Extrapolating the curve back through zero also gives an indication of the spacecraft voltage. This latter point should be treated cautiously since values up to 80 volts can be obtained and these are difficult to justify. It is apparent, though, that spacecraft voltages are larger than those normally expected.

The next phase of the analysis is to use the current collection mode to verify that the trends can be predicted with reasonable values of density and particle temperatures. The first step is to verify that the ground test data can be so treated. Typical results of this matching process is shown in Figure 58. Note that the match of the initial -30 volt step requires a plasma potential of about -8 volts this value is typical for the LeRC tank tests. The comparisons for the flight data are illustrated in Figure 59 a for a "ram" condition (program step 690) and Figure 60 for a thermal condition. The difference between "thermal" and "wake" modes is assumed to occur when the density inferred from the mode is considerably lower than that supplied by LeRC. In order to match the first data point, spacecraft voltages in the order of -20 to -50 volts had to be assumed. The summary of the results of all twelve runs is given in Table IV. As an output from this analysis the plasma density dependance on the negative voltage for shut-down can be determined. This data is presented in Figure 61. The error bars here indicate that shutdown occured between voltage steps or that the density was varying. This result indicates that overcurrent shutdown is a function of plasma density and will occur at a value slightly lower than that previously obtained. Whether this is real or a function of this particular power supply capability still has to be determined.

FIGURE 56. CURRENT COLLECTED FOR INITIAL NEGATIVE BIAS VOLTAGES
-PIX 2 FLIGHT DATA-
THERMAL AND WAKE CONDITIONS

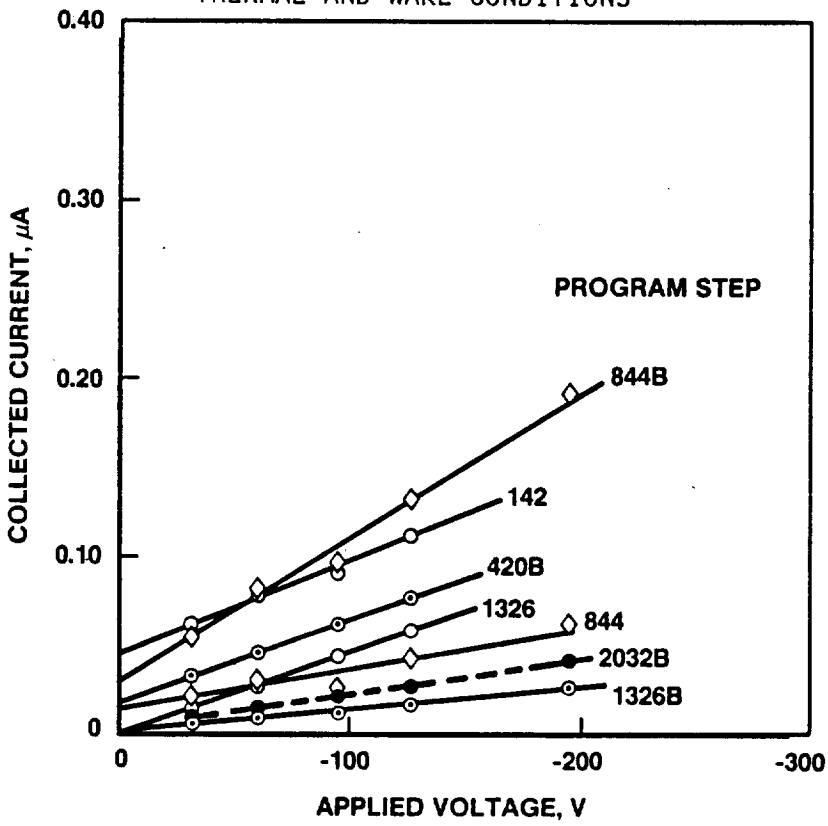

FIGURE 57. CURRENT COLLECTED FOR INITIAL NEGATIVE BIAS VOLTAGES
-PIX 2 FLIGHT DATA-
RAM CONDITIONS

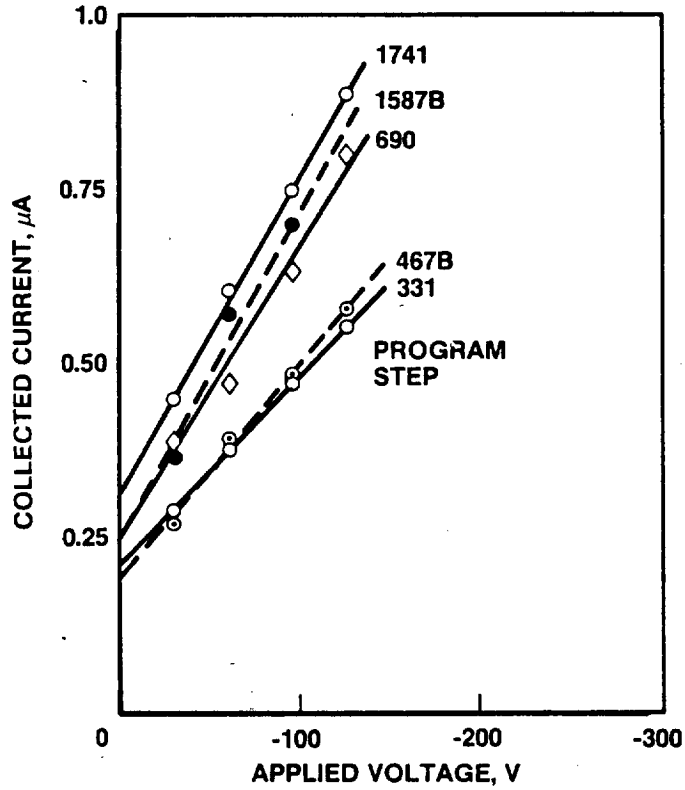

These results indicate that the negative bias current collection model works reasonably well for both ground test and space environmental conditions. There is a fundamental difference between the ground test results and flight data that has yet to be resolved. In the ground test conducted with plasma densities on the order of 10^4 cm,$^{-3}$ negative voltage shut-downs were very rare. In the flight experiment, negative voltage shutdowns were very frequent.

FIGURE 58. COMPARISON OF MODEL TO PIX-2 GROUND TEST DATA

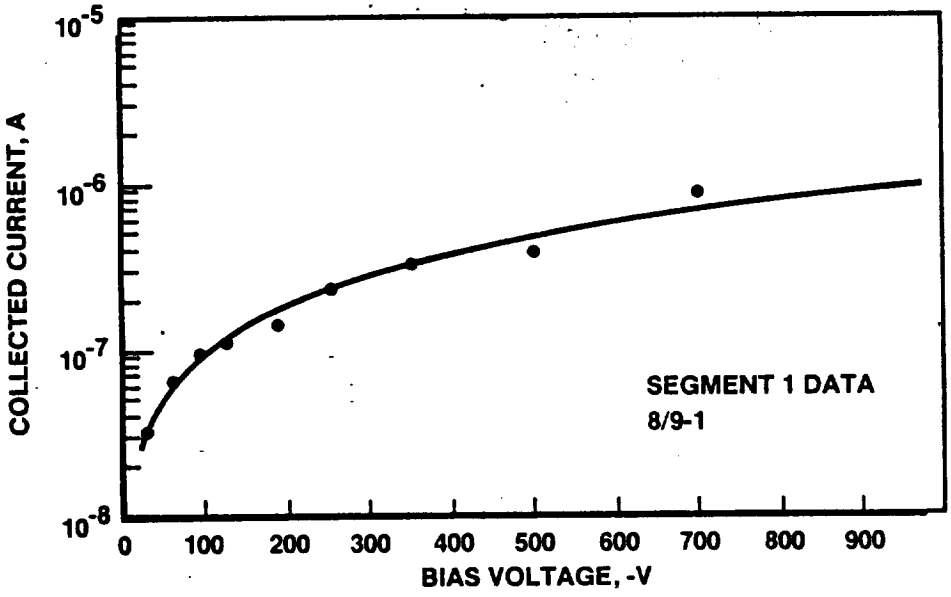

NUMBER DENSITY	INIT 1.5×10^4	FINAL 1.7×10^4
ION TEMPERATURE	1.0 ev	
PLASMA POTENTIAL	-8 V	

FIGURE 59. COMPARISON OF MODEL TO PIX-2 FLIGHT DATA RAM MODE

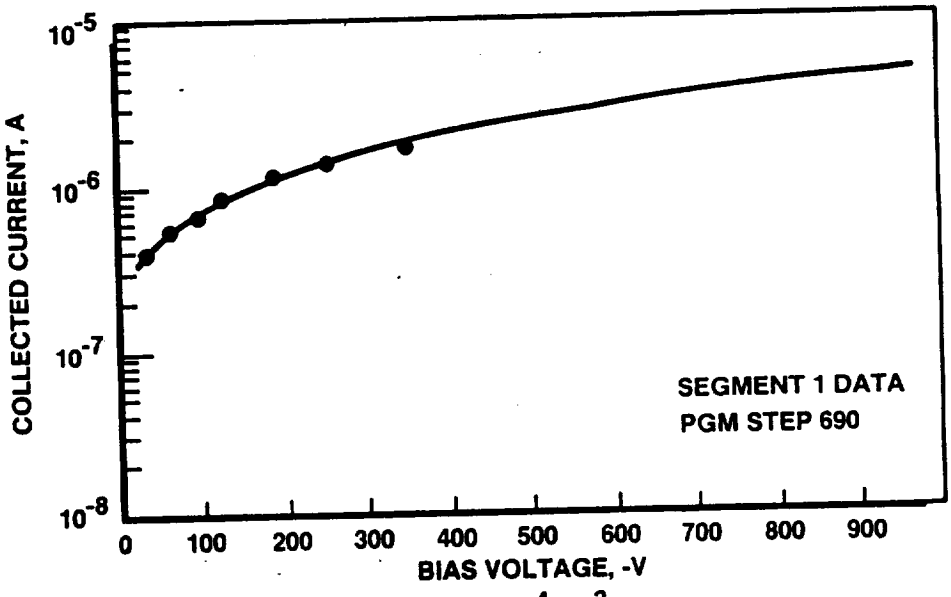

PLASMA DENSITY	$6 \times 10^4 cm^{-3}$
TEMPERATURE	1.5e V
SPACECRAFT VOLTAGE	-50 V

FIGURE 60. COMPARISON OF MODEL TO PIX-2 FLIGHT DATA
THERMAL MODE

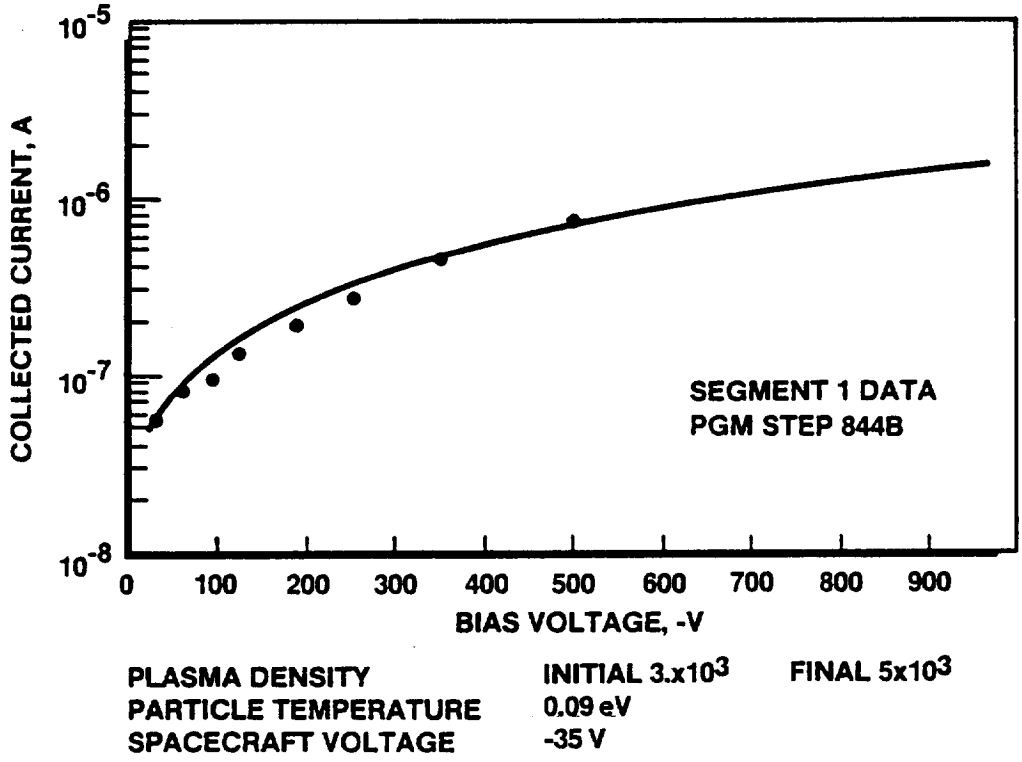

FIGURE 61. SHUT-DOWN THRESHOLD PIX-2 DATA

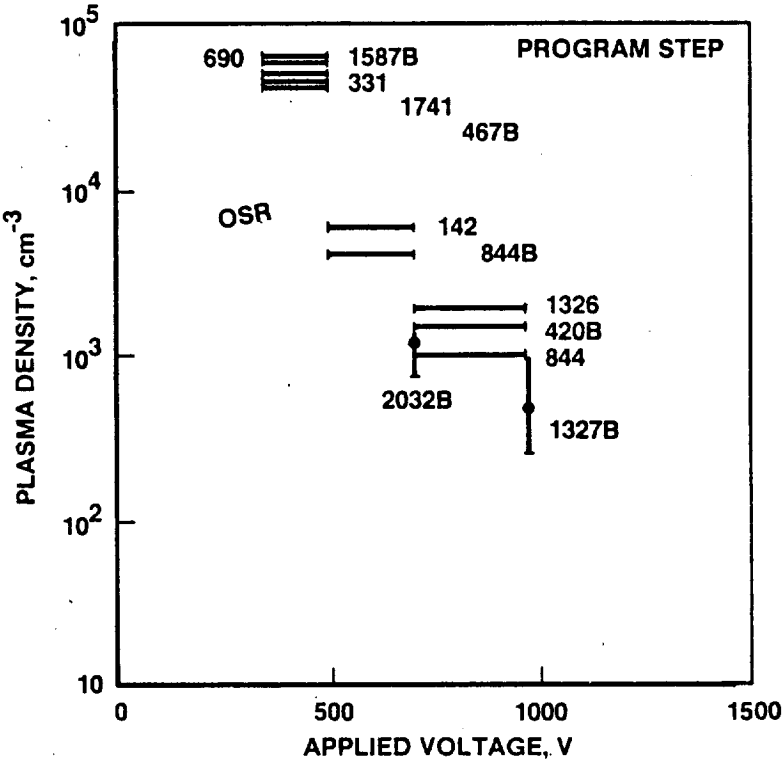

TABLE IV

SUMMARY OF PIX-2 FLIGHT DATA ANALYSIS

PGM Step	Inferred Plasma Properties				Velocity Mode
	Density (cm^{-3})		Temp (eV)		
	Initial	Final	Initial	Final	
142	6×10^3		.5		Ram/Thermal
331	5×10^4		2.0		Ram
690	6×10^4		1.5		Ram
844	1×10^3		.07		Thermal
1326	2×10^3	3×10^3	.09		Wake
1741	3×10^4	6.3×10^4	1.0	2.5	Ram
420B	2×10^3	1×10^3	.09		Wake
467B	3×10^4	5.5×10^4	2.5		Ram
844B	3×10^3	$5. \times 10^3$	.09		Thermal
1327B	250	1×10^3	.09		Wake
1587B	6×10^4		1.5		Ram
2032B	750	1.5×10^3	.09		Wake

9. APPLICATION TO LARGE SPACE POWER SYSTEMS

9.1 Introduction

There have been several studies conducted in the past few years in which space power system interactions with plasma environments have been estimated.[66,68,69,72,73] The major hurdle in these studies was that no one had a realistic model of the plasma current collection processes.[73] While this study does not claim to have developed the best possible model, the collection phenomena is based upon a review of several years of experimental results. The main extrapolation used here relates to extending information obtained with samples up to 1 m^2 to systems ranging in size up to 1000 m^2.

Any power system operating in space plasma environments must come into equilibrium such that the net current collected from the plasma is zero. This forces the array to float predominantly negative to achieve this balance. Furthermore, this floating potential changes as the system moves in its orbit due to velocity effects. These must be considered before the impact of discharges on the power load can be assessed.

In this section of the report, the current collection models developed will be applied to a 100 kilowatt solar array operating in space at various voltages. The effect of possible discharges on this system's operation will be reviewed and means of reducing the threat discussed.

9.2 Power System Floating Potentials

9.2.1 Power System Description

The 100 kilowatt solar array used in this study is assumed to consist of ten modules in parallel; each module consisting of ten blocks in series (see Figure 62). The voltage builds up within each module from 0 to the operating voltage. Each module is assumed to be identical, contributing an equal current to the load. The array is also assumed to consist of 6 x 6 cm solar cells with an open circuit voltage of 0.6 volts and a short circuit current of 1.1 amperes each. The back side of the array is assumed to be a dielectric surface so that the only interactions occur on the solar cell side.

This system is assumed to operate in a 400 km equatorial orbit having the plasma characteristics given in Table V. The motion induced effects on this system in its orbit are illustrated in Figure 63. At local midnight the system is in eclipse; the power will be off and the array will cool down. Upon reentering sunlight

FIGURE 62. SPACE POWER SYSTEM CONCEPT
100 KW GENERATED AT 500 V

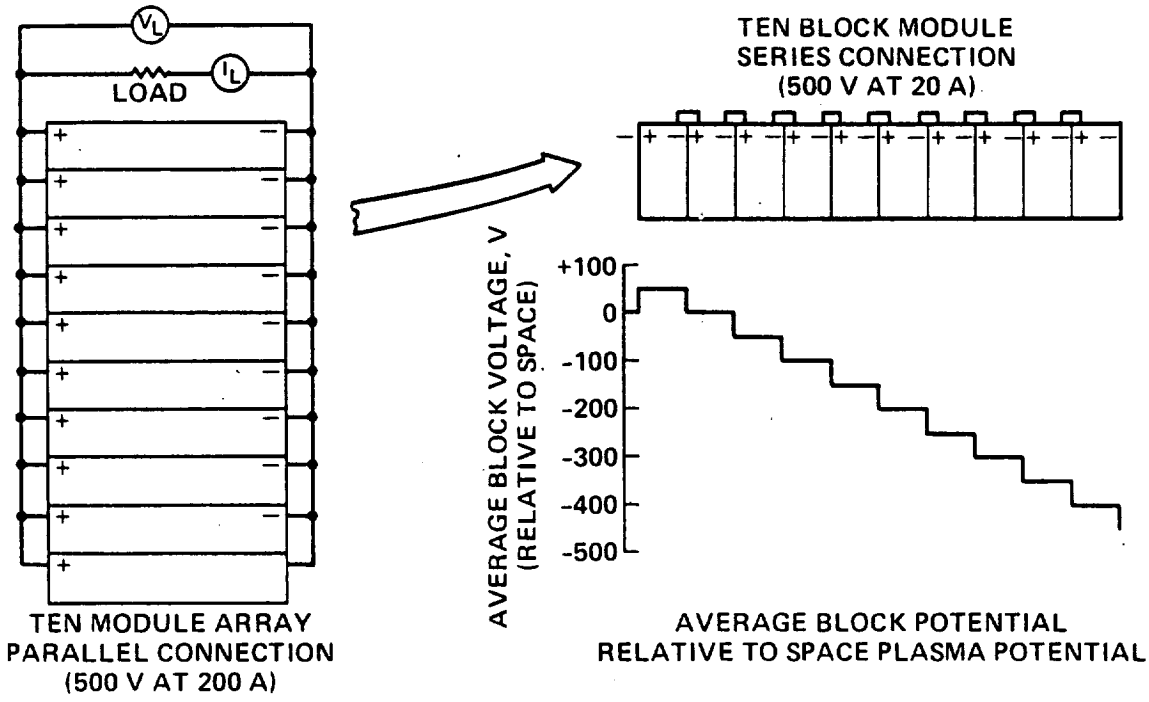

FIGURE 63. CHANGES IN ENVIRONMENTAL CONDITIONS
OVER ORBIT

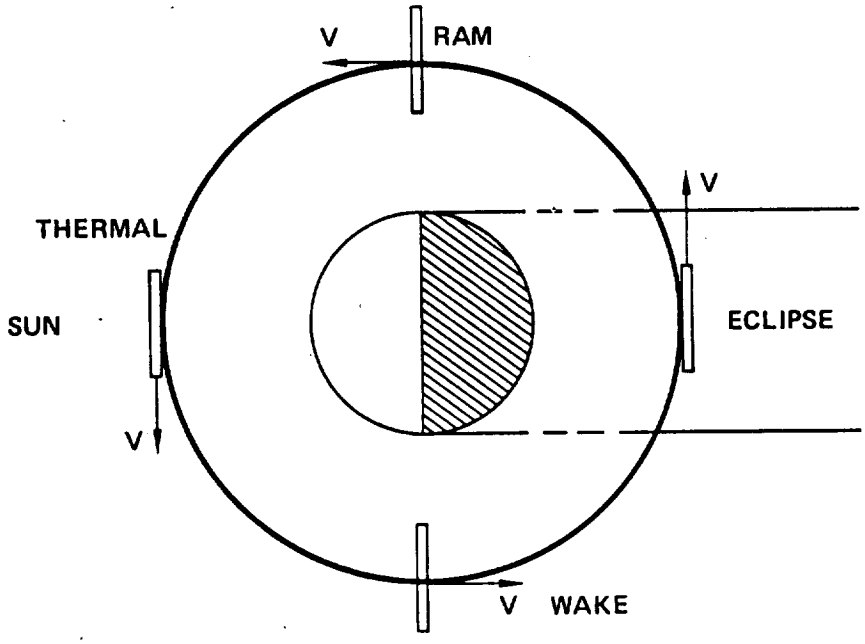

the cold array will generate about twice its normal voltage until the temperature returns to normal (usually within a few minutes). The array will enter the "ram" mode: the active side of the array faces the velocity direction. In this case the spacecraft velocity is much greater than the ion thermal velocity; the ion current collection is then assumed to be based on the higher energy.

The PIX results demonstrated that ram mode collection is at a higher partical energy than thermal or wake mode. In the local noon region of the orbit, the velocity is perpendicular to the array normal and current collection is based upon the plasma thermal properties. In the local evening region, the active side of the array is in the "wake." Here, it has been found from the PIX data that both the electron and ion densities are substantially lower and current collection reduced. The orbit period is about 100 minutes with about 25 minutes each in ram, thermal, wake and eclipse.

The solar array block characteristics are computed from a simple diode approximation for each of the desired operating voltages of 300, 500, 750 and 1000 volts (see Figure 64). From these characteristics the maximum power point voltage and current are chosen for the current balance computations.

9.2.2 Plasma Current Calculations

Based on the ground test data review given in Section 3 of this report, the following are the current collection equations to be used:

$$I = j_{eo}\, Ap\, (1.25 \times 10^{-3})\, (1 + \frac{V_+}{Te}) \quad \text{amps} \qquad 0 \leq V_+ \leq 100$$

$$I = j_{eo}\, Ap\, (0.25)\, (1 + \frac{V_+ - 100}{Te}) \quad \text{amps} \qquad V_+ > 100$$

$$I = j_{io}\, Ap\, (1.25 \times 10^{-2})\, (1 + \frac{V_-}{Ti}) \quad \text{amps} \qquad V_- < 0$$

where j_{eo} and j_{io} are the plasma thermal current density (amp/cm^2)
Ap is the block panel area (cm^2)
V_+ and V_- are the block average voltages (positive and negative)
Te and Ti are the electron and ion temperatures (eV)

At the 400 km orbit of this system, the predominant ion specie is oxygen and this will be used in the calculations. There is also an implicit assumption that the plasma collection phenomena can be characterized by the average potential of each block rather than a distributed voltage over the face. This seems to be true, based on a very limited data base of large panel tests.[68] Finally, it is assumed that each block behaves independently of its neighbors. This is based upon the PIX-2 flight data which appears to indicate this independence.

TABLE V

PLASMA ENVIRONMENT PARAMETERS

(400 KM. ORBIT)

	RAM	THERMAL	WAKE
Electrons	2×10^5	2×10^5	2×10^4
Number Density (CM^{-3})			
Particle Energy (eV)	0.2	0.2	0.2
Oxygen Ions	2×10^5	2×10^5	20
Number Density (CM^{-3})			
Particle Energy (eV)	5.0	0.09	0.09

FIGURE 64. BLOCK SOLAR ARRAY CHARACTERISTICS
6X6 CM CELLS

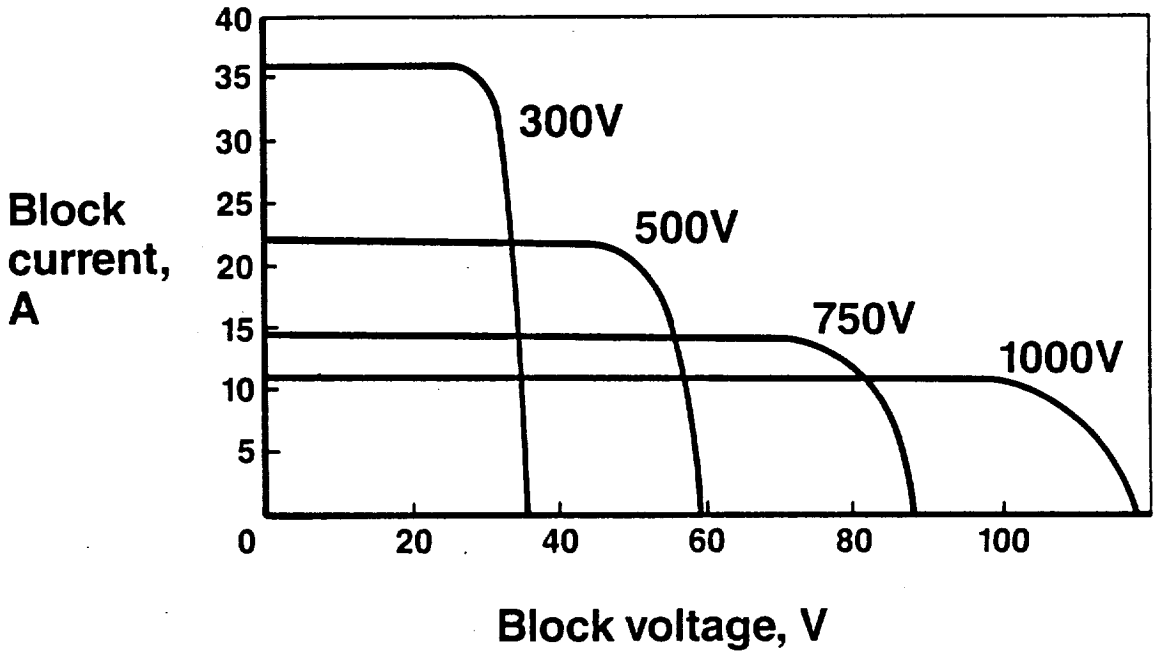

There is still an open question on the extrapolation to these large areas, that is, the electron current collection is above 100 volts. The ground test data indicates a spherical relationship but if this is extended to very large areas, huge currents can results. Another option proposed is that every large array array would collect as a flat plate with a curved edge sheath.[66] Such a current collection model has been developed and has the following form:

$$I = (j_{eo}\ Ap)\ (1 + K\ V_{+}^{\ 3/4})\ \text{amps}$$

where K is a constant (9.8)

Some of the data obtained in ground tests indicates that the current collection above 100 volts does depend upon a power of the voltage that is less than one. However, this can not be stated positvely at this time and the option of either a spherical model or plate model is available.

9.2.3 Floating Potentials

The above relationships are used to compute the floating potential of the array when operating at 300, 500, 750 and 1000 volts. This is done to assess the plasma power losses and the probability of arcing in the array. The procedure used is first to compute the environmental currents and then compute the collection for each block in the module. The block characteristics are taken at the maximum power point as determined from the curve in Figure 64. The balancing process starts with a first guess potential for the most negative block with the others indexed by the block voltage. The currents collected for each block are computed sequentially and summed. If the currents do not balance, the most negative block voltage is increased by one volt and the current recomputed. This process is continued until the sign of the net current changes. Hence, the balance is within 1 volt.

The results of these floating potential computations are shown in Figure 65 for the ram (R), thermal (T) and wake (W) regions and the selected operational voltages. It is interesting to note that the positive voltages did not exceed 100 volts in any of these cases so that the choice between plate and spherical collection did not have to be made. For the thermal collection regions the usual guide is that the array should be about 10 percent positive. This study indicates that the percentage positive is about 4 percent for all cases.

The plasma currents collected are exceptionally small compared to the operating currents. In the 1000 volt operations the electron current collected is on the order of 55 milliamps whereas the load current is 11.5 amps. This represents a loss of 0.5 percent. No other condition was found to be worse. Hence, it should be concluded that plasma coupling power losses are negligible.

FIGURE 65. FLOATING POTENTIALS FOR 100 kW ARRAY
MAXIMUM POWER POINT OPERATION

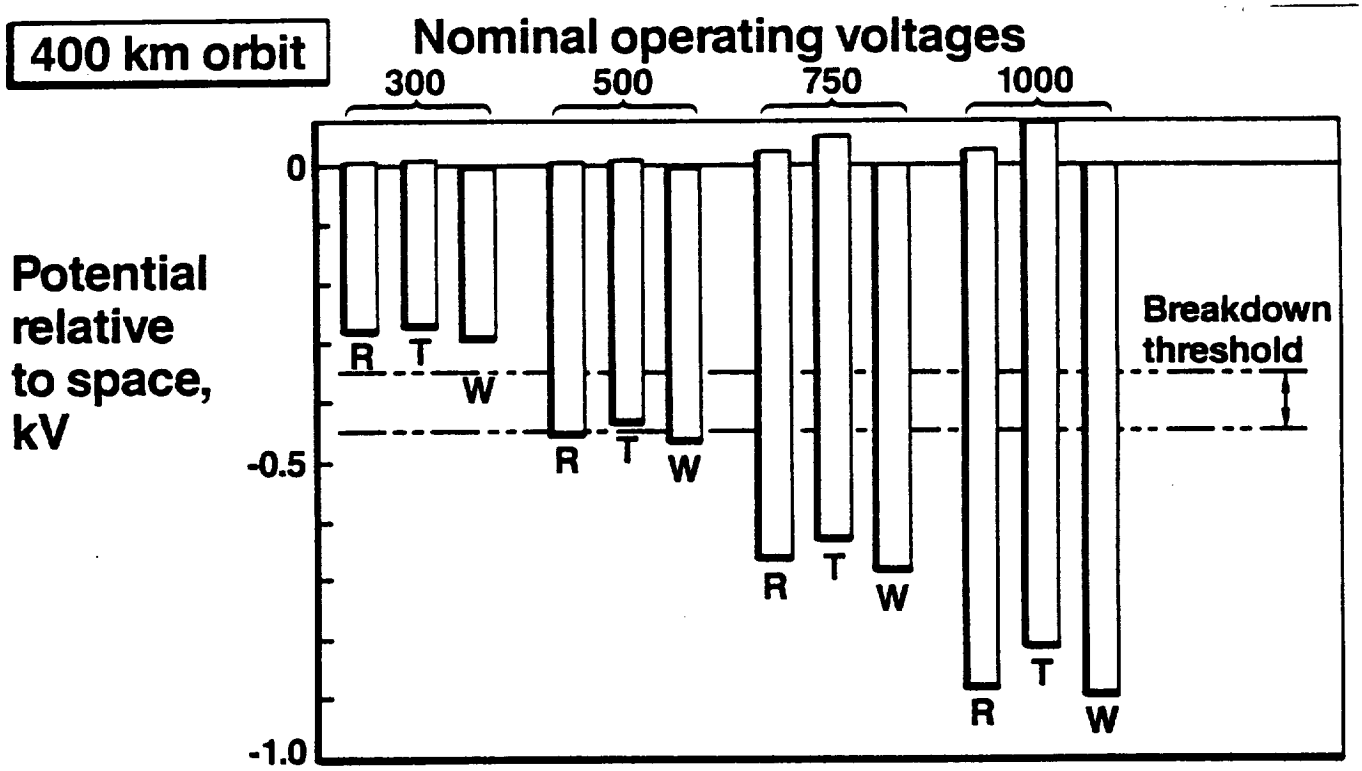

There appears to be a real possibility of discharges occurring in these arrays. The PIX-2 data would indicate a possible discharge threshold at these densities of about -350 volts (extrapolated from data given in Figure 15). Previous ground test summaries extrapolate to a value of -450 volts for breakdowns at these densities. If one were to design a system based on present knowledge, then the maximum operating voltage to be considered would be 250 volts which would result in the most negative block at about -240 volts. This would provide an estimated safely margin for no discharges of about 1.5 to 1.9. However, when the array exits eclipse, the array voltage will double and discharges would occur then. The question to be resolved, then, is to determine the impact of discharges on the power system performance.

9.3 Discharge Behavior

That high voltage solar arrays discharge has been known for 15 years. However, what is not known are the discharge pulse characteristics. Attempts to determine these have usually ended in the characterization of a power supply. Recently, some progress has been made in cataloging such discharge characteristics for small solar array segments.[32-34]

In this study a discharge will be assumed to involve a breakdown of the plasma sheath in the negative voltage portions of the array between the interconnects and space. The process will involve a charge loss to space causing the array to become more

positive. Furthermore, it is assumed that the discharge current is supplied by the array at the expense of the load current, if necessary. The increased current demand in the series circuit between blocks will cause the block voltage to change to maintain the block V-I characteristics. The plasma coupling current is negligible until the array becomes sufficiently positive to collect an electron current large enough to drive it back to its normal voltage relative to space. The discharge current transient is assumed to be characterized by an overdamped pulse. Eventually, this pulse terminates allowing the array to return to its original voltage distribution and to discharge again. If the discharge current demand is sufficient to exceed the array short-circuit current, then the array would shut down temporarily. If this doesn't happen, then there will be power loss in the load which may or may not be tolerable.

The computation procedure used in this discharge effects study is illustrated in Figure 66. This shows a module of 10 blocks in a 500 volt array. Each block is at ~50 volts and a small fraction of the module is positive with respect to the space plasma potential. A discharge is assumed to occur in the negative portions of the array where the threshold is exceeded. The discharge is modeled as an overdamped pulse produced by the breakdown of the capacitance of the plasma sheath (between the array and space), C_S. An assumed value of resistance and inductance is used to complete the pulse definition. Capacitance values from 10^{-10} farads (small localized discharge) to 10^{-7} farads (major discharge involving whole array) were used. Two different pulse durations were also used: a short pulse generated by making the resistance 50 ohms and a long pulse resulting from a resistance of 100 ohms. The short pulse would be comparable to a spacecraft charging type of discharge while the long pulses (μseconds in duration) would be representative of those recently measured. In both cases the discharge threshold was assumed to be -350 volts and hence would involve the possibility of three blocks discharging at once.

The results of this study can be summarized by considering the array performance in the ram mode. In this mode the sheath is thinner making the capacitance larger. The results for a major discharge, short pulse is shown in Figure 67. The discharge pulse had a maximum current of about 6.5 amps occuring at about 70 nanoseconds with a decay to zero in about 600 nanoseconds. The voltage distribution in the module, block 1 to 10, is shown beneath the pulse. The discharging blocks start to become more positive relative to space plasma potential due to the charge lost in the discharge. The block voltage is reduced due to the increased current demand. This reduces the module output voltage. At about 30 nanoseconds the short-circuit capability of the block is exceeded driving the module to zero volts. The simulation followed here assumed the pulse to be continuous and therefore, the module would be off until the current demand was reduced to below the short-circuit limit. This occurred at about 60 nanoseconds. The module became increasingly more positive due to

FIGURE 66. SIMPLIFIED CIRCUIT MODEL FOR HV ARRAY/PLASMA INTERACTION

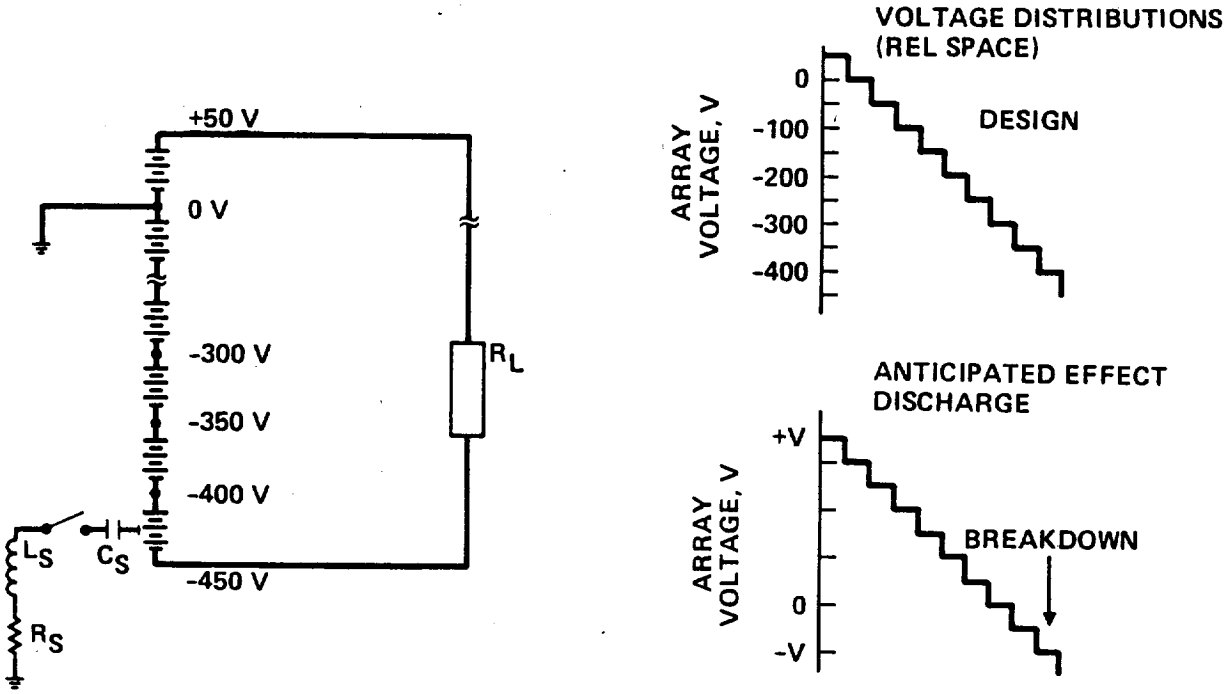

FIGURE 67. PREDICTED DISCHARGE BEHAVIOR SHORT PULSE

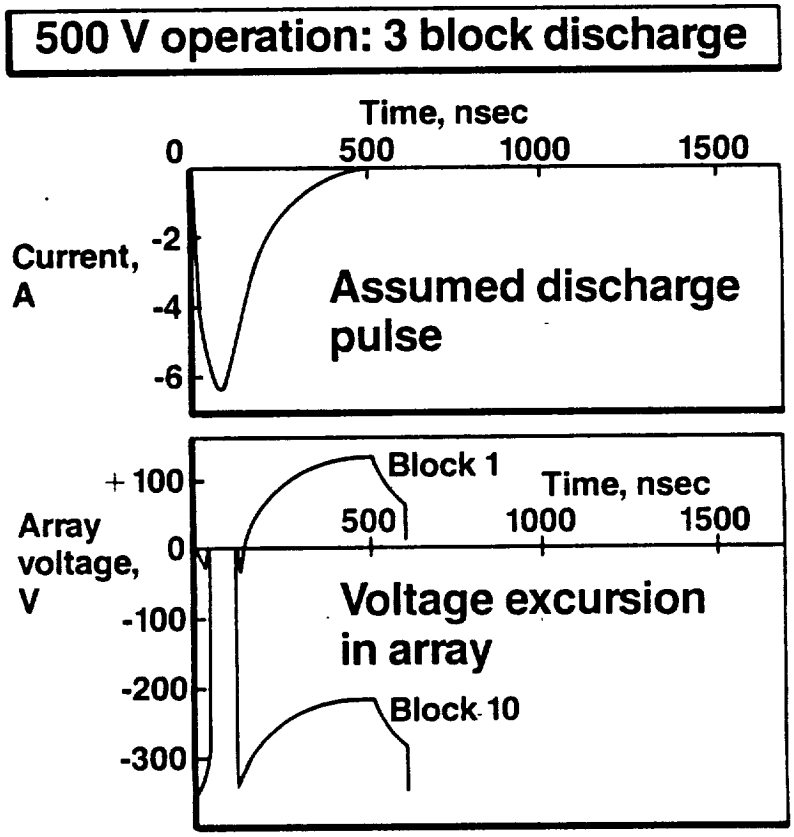

the continued loss of charge until, at about 500 nanoseconds, the plasma currents collected exceeded the computed discharge currents and the module was driven more negative. At the discharge termination (about 600 nanoseconds), the process was stopped and the module was returned to its initial state where it could discharge again.

In reality, once the module went to zero voltage due to the current demand exceeding the short-circuit capability of the block, the discharge should have terminated. The module voltage would then be reestablished and a discharge ignited again. This could give rise to a possible continuously noisy output rather than an interrupted power output. In either case this is a serious concern.

The long pulse results are shown in Figure 68. Here the discharge pulse peaks at 3 amps but runs out to 1500 nanoseconds (the charge loss is the same as in the short pulse). The voltage distribution in the module is shown below the pulse. In this case the current demand never exceeds the capability of the blocks and the module doesn't shut down. The potential of block 1 rises to +200 volts (relative to space plasma potential) before the plasma coupling current forces the potential back towards the normal values. To compensate for the discharge current, the current to the load is decreased reducing the power to the load by about 2 percent.

FIGURE 68. PREDICTED DISCHARGE BEHAVIOR LONG PULSE

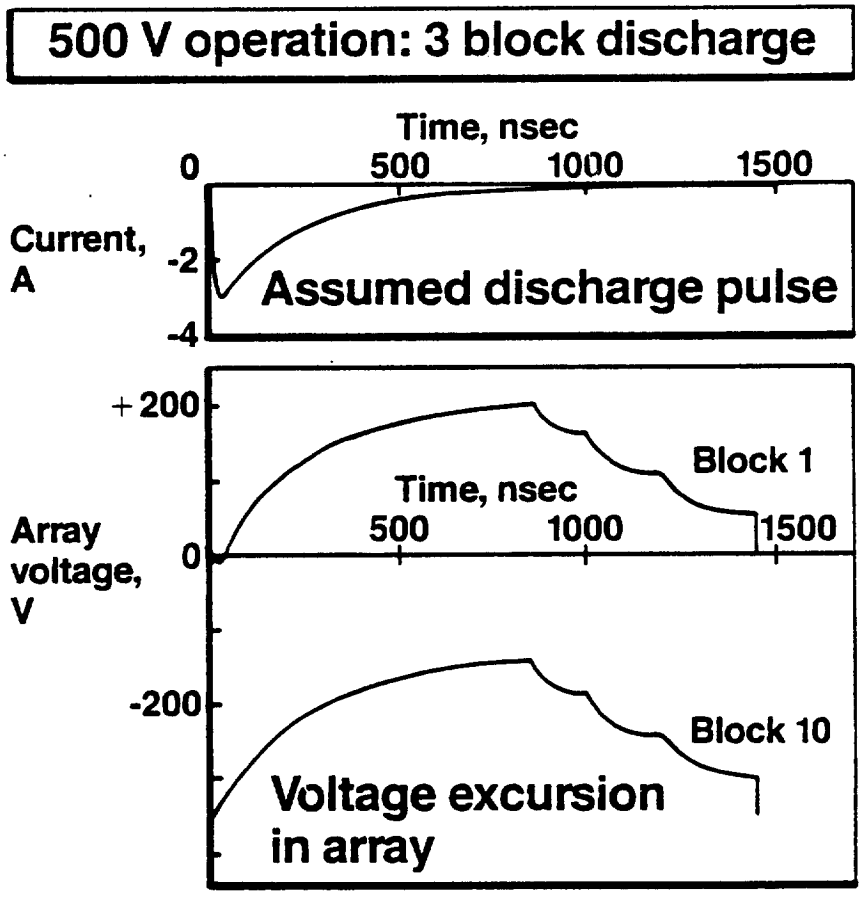

In the data presented here, the plate model for current collection above +100 volts was used. If a spherical collection model is used, the most positive voltages of the blocks was limited to between 100 and 130 volts.

In the thermal and wake modes the sheath capacitances are lower and hence, the discharge pulses have lower amplitudes. This results in behavior analogous to the long pulse case already presented; a small loss of power to the load. In addition, small discharges result in very brief transients in the power line (less than 100 nsec duration).

In summary then, if the discharge characteristic has a current peak greater than 5 amperes, then the array can be driven into an interrupted or noisy mode of operation. If the pulse amplitude is less than 5 amperes, then the load current will oscillate at a reduced current representing a power loss of less than 2 percent (per module breakdown). If all modules broke down simultaneously, then the loss could be driven to 20 percent. The pulse amplitude could exceed the 5 amp threshold only if the pulse were relatively short. Long pulses characterized by kilohm resistances would not allow large currents. Since the discharge is assumed to result from a sheath capacitance breakdown, then the worst case breakdowns should be expected when the array is in the ram mode where this capacitance is the largest.

It should be stated that this analysis is still speculative since discharge characteristics are still being defined and no one has yet shown that breakdowns would occur in operational arrays.

Furthermore, no one has demonstrated what happens to the array when discharges occur. If the discharge is damaging to the array, then it must be prevented. If the process involves only charge loss to space, then filtering would probably reduce the effect on the load to tolerable levels.

9.4 Design Modifications

In this section some techniques to minimize the effects of discharges are discussed.

9.4.1 Operating Points

One means of minimizing the possible module shut-down is to increase the current margin by changing the operating point on the V-I curve. If, instead of the maximum power point, an 80 percent point (lower current, higher block voltage) were chosen, then the short-circuit current capability might not be exceeded. The normal procedure is to operate off-optimum initially to allow for array degradation with time in space. A complete system analysis should be done to see if an operating point could be found that would help minimize discharges while satisfying the mission power requirements.

9.4.2 Conductive Substrate

The study discussed here assumed that the rear side of the substrate was a thin dielectric film. There is a possibility of making this surface conductive and tieing it to part of the array. A brief study was made of this concept with the conductive surface tied to the negative, positive or center-tapped terminal of the array. These results are shown in Figure 69 for a 500 volt array. The entire back of the module (10 blocks) is assumed to be the conductive area. As shown here, this approach does not lift the array beyond the discharge threshold throughout the entire orbit. In addition, the plasma collection and current now are on the order of 20 percent of the load currents and no longer be neglected.

9.4.3 Gap Fillers

The use of gap fillers has been considered for some time. In a brief test of a small solar array segment with RTV covering the interconnects between the cells, it was apparent that discharges were suppressed (see Figure 70). However, it did not hinder electron collection. This must be considered only an indication of a possible result. Additional testing is required to verify the results at the plasma density of interest and to demonstrate the lifetime of the filler. Furthermore, a study is required to determine the weight penalty of such fillers and to evaluate the effectiveness of using fillers only on selected areas of the array.

FIGURE 69. FLOATING POTENTIALS OF SOLAR ARRAY AS A FUNCTION OF SUBSTRATE BACKING

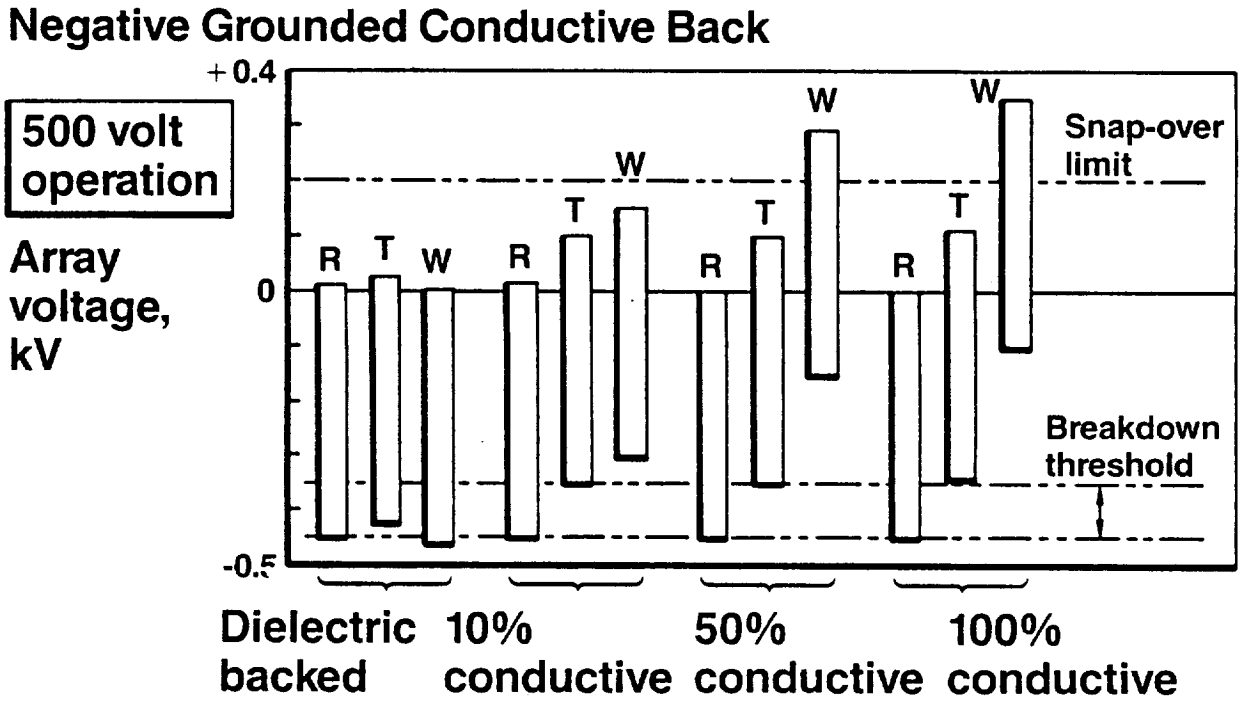

FIGURE 70. GROUND TEST RESULTS - SOLAR ARRAY SEGMENT
EFFECT OF INSULATING INTERCONNECTS

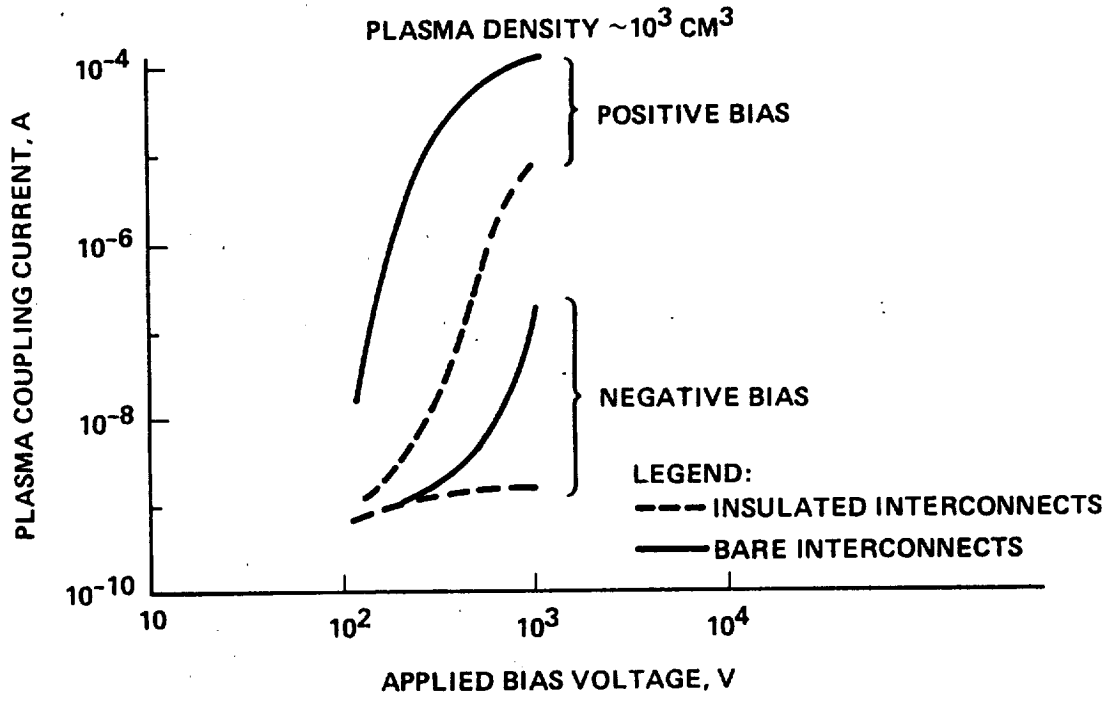

10. CONCLUSIONS AND RECOMMENDATIONS

10.1 Spacecraft Charging and Coupling Studies

The natural radiation environment is harsh. It has been shown how the environment can charge spacecraft surfaces. NASCAP gives quantitative results for the amount of charge buildup on various spacecraft surfaces. Discharges to space can then occur. The effects to the interior systems and how these effects are coupled into the spacecraft was the object of this study.

There is now an established link between the discharge on the exterior of the spacecraft and the internal transient noise signals that arise because of the discharge. This study shows how the discharge, by varying structure potentials, can cause transient signals to arise in spacecraft wiring.

If inputs (signal and ground) to spacecraft systems are not adequately protected then these transients can enter those systems resulting in possible upsets.

10.1.1 Detailed LEM

It has been shown that discharges on the exterior of satellites can cause internal structure potentials to vary which turn can cause transients in wiring. Differential voltages as high as 3 kv can occur in 3-axis stabilized spacecraft. Currents as large as 12 A can be generated in spin stabilized spacecraft.

10.1.2 Simplified LEM

The simplified LEM of a Spin Stabilized Spacecraft gave results very similar to detailed LEM and thus could be used for gross initial evaluation of transients coupling into spacecraft.

10.1.3 Interface Circuits

It has been shown that buffer or interface circuits are vulnerable to induced signals in the ground paths. These circuits are designed to prevent unwanted signals in the power lines from entering satellite systems. In this, these circuits are successful.

The circuit quickly damps out high frequency, for signals entering through the front end, input-point. However, these signals entering through ground points can get through to the output and therefore enter the satellite electronic systems.

10.2 High Voltage Solar Array Discharge Transient Coupling Studies

10.2.1 Ground Based Test Results

In this study the data obtained in the past 15 years was compiled and used to develop empirical models for electron and ion current collection phenomena. This data base has turned out to be inadequate to provide an absolute set of equations. There are major differences between facilities, experimenters and test philosophy that have to be resolved. It appears that collection processes can be modeled as:

$$I = j_{eo}\, Ap\, (1.25 \times 10^{-3})\, (1 + \frac{V_+}{Te}) \quad \text{amps} \qquad 0 < V_+ < 100$$

$$I = j_{io}\, Ap\, (1.25 \times 10^{-2})\, (1 + \frac{V_-}{Ti}) \quad \text{amps} \qquad V_- < 0$$

$$I = j_{eo}\, Ap\, (0.25)\, (1 + \frac{V_+ - 100}{Te}) \quad \text{amps} \qquad V+ > 0$$

or

$$I = (j_{eo}\, Ap)\, (1 + K\, V^{3/4}) \quad \text{amps} \qquad V > 0$$

where the terms are defined in the text.

This is based on the comparison between LeRC and other test results. The extrapolation to very large areas still leaves a choice between spherical and plate models.

10.2.1.1 Recommendations

a. A series of test should be conducted over a wide voltage range with all of the plasma properties provided. Parameters such as plasma density, electron and ion temperature, sunlight/shade effects, magnetic field, type of vacuum pumping, solar array construction and instrumentation should all be systematically evaluated. Then, it may be possible to worry about size extrapolations.

b. The discrepancy between the LeRC electron collection data and others should be resolved. The LeRC data is a factor of 10 lower at voltages less than 100 volts and a factor of ten higher above 100 volts. This comparison is with Boeing data and tests run at JSC. It is vital to know why these discrepancies exist.

c. Current collection of large areas should be determined for voltages beyond snapover to determine whether or not the behavior follows the spherical or plate models.

10.2.2 Flight Data Comparisons

The negative current collection models developed above have been applied to the flight data obtained in the PIX-1 and 2 missions. Basically, the models seem to work well and in turn, give information on the plasma characteristics during flight.

10.2.2.1 Recommendations

a. Continue the data reduction process for both positive and negative bias data. It should be possible to evaluate the interactions between the segments, if any, by completing the analysis of each segment separately and looking for any differences when the segments were run together. The data would have to be reviewed critically to find those runs when the density did not jump. This would resolve the concept that various parts of the array can be considered to respond to the plasma independently of its neighbors.

b. Resolve the differences between the ground test and flight data In the negative bias data, the ground test indicated few shutdowns; the flight data showed many. There may be discrepancies in the positive voltage data also.

10.2.3 Extrapolation to Large Space Power Systems

The current models developed here have been used to estimate the behvior of large space power systems in plasma environments. It was found that these arrays would float predominantly negative, that plasma coupling current losses are negligible and that discharges are probable on all systems operating at or above 300 volts. These discharges might not be serious if the discharge pulse is spread out over a long time period (μseconds) and if the discharge does not damage the array. Both of these points need to be verified.

10.2.3.1 Recommendations

a. A self-generated voltage solar array test should be conducted to verify that such a system could discharge and to determine the characteristics of such discharges. Since there seems to be an unresolved difference between ground and space flight results, this test should be run both in space and on the ground.

b. Discharge characteristics must be determined. The characteristics must be measured in the solar array circuit and not inferred by another probe. This is vital to determining whether or not a problem exists.

11. REFERENCES

1. McPherson, D. A. and Schober, W. R., "Spacecraft Charging At High Altitudes: The SCATHA Satellite Program"; in Spacecraft Charging By Magnetospheric Plasmas, ed. A. Rosen, Progress in Astronautics and Aeronautics, Vol. 47, AIAA, N.Y., 1976, pp. 15-30.

2. Sharp, R. D., Shelleym E. G., Johnson, R. G. and Paschman, G., "Preliminary Results of a Low Energy Particle Survey at Synchronous Altitude", JGR, Vol. 75, 1970, p. 6092.

3. DeForest, S. E. and McIlwain, C. E., "Plasma Clouds in the Magnetosphere", JGR, Vol. 76, June 1971, pp. 3587-3611.

4. DeForest, S. E., "Spacecraft Charging at Synchronous Orbits", JGR, Vol. 77, Feb. 1972, pp. 651-659.

5. Bartlett, R. O., DeForest, S. E., and Goldstein, R., "Spacecraft Charging Control Demonstration at Geosynchronous Altitude", AIAA Paper 75-359, 1975.

6. Lovell, R. R., Stevens, N. J., Schober, W. R., Pike, C. P. and Lehn, Wm., "Spacecraft Charging Investigation: A Joint Research and Technology Program", in Spacecraft Charging By Magnetospheric Plasma, ed. A. Rosen, Progress in Astronautics and Aeronautics, Vol. 47, AIAA,, N.Y., 1976, pp. 3-14.

7. Proceeding of the Spacecraft Charging Technology Conference, ed. C. P. Pike and R. R. Lovell, AFGL-TR-77-0051/NASA TMX-73537, Feb. 1977.

8. Spacecraft Charging Technology-1978, NASA CP-2071/AFGL-TR-79-0082, 1979.

9. Spacecraft Charging Technology-1980, NASA CP-2182/AFGL-TR-81-0270, 1981.

10. Eighteenth Aerospace Sciences Meeting, Pasadena, CA, Jan. 1980.

11. Twentieth Aerospace Sciences Meeting, Orlando, CA, Jan. 1982.

12. Mullen, E. G., Hardy, D. A., Garrett, H. B. and Whipple, E. C.; "P78-2 SCATHA Environmental Atlas", Spacecraft Charging Technology-1980, NASA CP-2182/AFGL-TR-81-0270, 1981, pp. 802-813.

13. Katz, I., Cassidy, J. J., Mandell, M. J., Schneulle, G. W., Steen, P. G. and Roche, J. C., "The Capabilities of the NASA Charging Analyzer Program", Spacecraft Charging Technology-1978, NASA CP-2071/AFGL-TR-790082, 1979, pp. 101-122.

14. Stannard, P. R., Katz, I., Gedeon, L., Roche, J. C. Rubin, A. G. and Tautz, M. F., "Validation of the NASCAP Model Using Spaceflight Data", AIAA Paper #82-0269, Jan. 1982.

15. Holman, A. B., "Military Standard for Spacecraft Charging-Status Report" in Spacecraft Charging Technology-1980, NASA CP-2182/AFGL-TR-81-0270, 1981, pp. 772-788.

16. Frankos, D. T., "Military Standards and SCATHA Program Update of MIL-STD-1541", ibid, pp. 768-771.

17. Purvis, C. K. Garrett, H. B., Whittlesay, A. E. Stevens, N. J., "Design Guidelines for Assessing and Controlling Spacecraft Effects", NASA Technical Paper, 1984.

18. Purvis, C. K., "Evolution of Spacecraft Charging Technology", AIAA Paper 82-0273, Jan. 1982.

19. Sanders, N. L. and Inouye, G. T., "NASCAP Charging Calculations for a Synchronous Orbit Satellite", Spacecraft Charging Technology-1980, NASA CP-2182/AFGL-TR-81-0270, 1981, pp. 648-708.

20. Stevens, N. J., "Analytical Modeling of Satellites in Geosynchronous Orbits", ibid, pp. 717-729.

21. Stevens, N. J., "Environmentally-Induced Discharges on Satellites", NASA TM-82849, May 1982.

22. Mullen, E. G. and Gussenhoven, M. G., "SCATHA Environmental Altas" AFGL-TR-83-0002, Air Force Geophysics Lab., 1983 and "High-Level Spacecraft Charging Environments Near Geosynchronous Orbit" AFGL-TR-82-0063, Air Force Geophysics Laboratory, 1982.

23. Mizera, P. F., "Natural and Charging-Results from the Satellite Surface Potential Monitor Flown on P78-2", AIAA Paper 80-0334, Jan. 1980.

24. Koons, H. C., "Characteristics of Electrical Discharges on the P78-2 Satellite (SCATHA)", AIAA Paper 80-0333, Jan. 1980.

25. DeForest, S. E., "Spacecraft Charging at Synchronous Orbit", J. Geophys Rese., Vol. 77, No. 2, Feb. 1972, pp. 651-659.

26. Reasoner, D. L., Lennartsson, W. and Chappell, C. R., "Relationship Between ATS-6-Spacecraft Charging Occurrences and Warm Plasma Encounters", Spacecraft Charging By Magnetosphere Plasmas, A. Rosen, ed. Prog. Astronaut. Aeronautics, vol 47, AIAA, 1976, pp. 89.

27. Katz, I., Cassidy, J. J., Mandell, M. J., Schneulle, G. W., Steen, P. G., Steen, P. G., Parks, D. E., Rotenberg, M., and Alexander, J. H., "Extension, Validation and Application of the NASCAP Code, "NASA CR-159595, 1979.

28. Katz, I., Cassidy, J. J., Mandell, M. J., Schnuelle, G. W., Steen, P. G. and Roche, J. C. "The Capabilites of the NASA Charging Analyzer Program", Spacecraft Charging Technology-1978, NASA CP-2071/AFGL-TR-79-0082, 1979, pp. 101-122.

29. Stannard, P. R., Katz, I., Gedeon, L., Roche, J. C., Rubin, A. G., and Tautz, M. F., "Validation of the NASCAP Model Using Spaceflight Data", AIAA Paper 82-0269, Jan. 1982.

30. Vampola, A. L., "P78-2 Engineering Overview", Spacecraft Charging Technology-1980, NASA CR-2182/AFGL-TR-0270, 1981, pp. 439-460.

31. Stevens, N. J., Lovell, R. R. and Gore, J. V., "Spacecraft-Charging Investigation for the CTS Project", Spacecraft Charging by Magnetosphere Plasmas, A. Rosen, ed., Prog. Astronaut. Aeronatics, vol. 47, AIAA, 1976, pp. 263-275.

32. Meulenberg, A. Jr., "Evidence for a New Discharge Mechanism for Dielectrics in a Plasma", Spacecraft Charging by Magnetosphere Plasmas, A. Rosen, ed., Prog. Astronuat. Aeronautics, vol. 47, AIAA, 1976, pp. 237-246.

33. Frederickson, A. R., "Bulk Charging and Breakdown in Electron-Irradiated Polymers", Spacecraft Charging Technology-1980, NASA CR-2182/AFGL-TR-810270, 1981, pp. 33-44.

34. Stevens, N. J., Klinect, V. W., and Gore, J. V., "Summary of CTS Transient Event Counter Data After One Year of Operation", IEEE Trans. Nucl. Sci., vcl/NS-24, Dec., 1977, pp. 2270-2275.

35. Woods, A. J., Treadway, M. J., Grismore, R., Leadon, R. E., Flanagan, T. M., and Wenaas, E. P., "Model of Coupling of Discharges Into Spacecraft Structures", Spacecraft Charging Technology-1980, NASA CR-2182/ AFGL-TR-81-0270, 1981, pp. 745-754.

36. Elkman, W. R., Brown, E. M., Wadsworth, D. V. Z., Smith, E. C., and Adams, P. F., "Electrostatic Charging and Radiation Shielding Design Philosophy for Hughes Satellites", AIAA Paper 82-0116, January 1982.

37. Whittlesey, A. C., "Voyager Electrostatic Discharge Protection Program", Internation Symposium on Electromagnetic Compatibility Proceedings, IEEE, 1978, pp. 377-383.

38. Whittlesey, A., and Inouye, G., "Voyager Spacecraft Electrostatic Discharge Testing", J. Environ. Sci, vol. 23, Mar-Apr, 1980, pp. 29-33.

39. Rosen, A., Sanders, N. L., Sellen, J. M., Jr., and Inouye, G. T., "Effects of Arcing Due to Spacecraft Charging on Spacecraft Survival", NASA CR-159593, Nov 1978.

40. Inouye, G. T., "Implications of Arcing Due to Spacecraft Charging on Spacecraft EMI Margins of Immunity", NASA CR-165442, March, 1981.

41. Wennas, E. P., Bloom, G. E., Duncan, L. W., Keyser, L. C., Liu, Y. P., Swift, W. D., "DEMP Analysis of HS-3XX Spacecraft", Intelcom Rad Tech Report No. INTEL-RT 6045-004, 29 January 1974.

42. Shaw, L. E., Sheppard, T. J., Webb, R. M., "System Generated Electromagnetic Pulse Subsystem Susceptibility Study" AFWL-TR-75-85, September 1976.

43. Cole, R. W., Ogawa, H. S. and Sellen, J. M., Jr., "Operation of Solar Cell Arrays in Dilute Streaming Plasmas", NASA CR-72376, Mar. 1968.

44. Knauer, W., Bayless, J. R., Todd, G. T. and Ward, J. W., "High Voltage Solar Array Study", NASA CR-72675, May 1970.

45. Springgate, W. F., "High Voltage Solar Array Study", NASA CR-72674, May 1970

46. Stevens, N. J., "Solar Array Experiments on the SPHINX Satellite", NASA TMX-71458, 1973.

47. "Outlook for Space", NASA SP-386, 1976.

48. Johnson, R. D. and Howlbrow, C. eds., "Space Settlements, A Design Study", NASA SP-413, 1977.

49. Bekey, I., "Big Comsats for Big Jobs at Low User Costs", Astronautics and Aeronautics, Vol 17, Feb. 1979, pp. 42-56.

50. Snoddy, Wm C., "Space Platforms for Science and Applications", Astronautics and Aeronautics, Vol 19, April 1981, pp 28-36.

51. NASA Space Power Workshop, NASA Lewis Research Center, April 20-12, 1984. Proceedings to be published.

52. Stevens, N. J., "Interactions Between Spacecraft and the Charged-Particle Environment", Spacecraft Charging Technology-1978, NASA CP-2071/AFGL-TR79-0082, 1979, pp 268-294

53. Woodsey, A. P., Smith, O. B. and Nassen, H. W., "Skylab Technology Electrical Power System", ASME Paper 74-129, August 1974.

54. Herron, B. G., Bayless, J. R., and Worden, J. D., "High Voltage Solar Array Technology", AIAA paper 72-443, Apr 1972.

55. Kennerud, K. L., "High Voltage Solar Array Experiments", NASA CR-12180, Mar 1974.

56. Domitz, S. and Grier, N. T., "The Interaction of Spacecraft High Voltage Power Systems with the Space Plasma Environment", Power Electronics Specialists Conference, IEEE, N.J., 1974, pp 62-69.

57. Stevens, N. J., Berkopec, F. D., Purvis, C. K., Grier, N. T. and Staskus, J. V., "Investigation of High Voltage Spacecraft System Interactions with Plasma Environments", AIAA Paper 78-672, Apr 1978.

58. McCoy, J. E. and Konradi, A., "Sheath Effects Observed On A 10-Meter High Voltage Panel in Simulated Low Earth Orbit Plasmas", Spacecraft Charging Technology - 1978, NASA CP-2071/AFGL-TR-79-0082, 1979, pp 315-340.

59. Bebermeir, H., Eggers, G. Nurnberger, R. and Golz, W., "Technology of Elevated Voltage Solar Arrays-Key Items Test and Evaluation", Final Report for ESA Under ESTEC Contract 3662/78/NL/HP, AEG-Telefunken, West Germany.

60. McCoy, J. E. and Martucci, D. T., "Experimental Plasma Leakage Currents To Insulated and Uninsulated $10M^2$ High-Voltage Panels", Spacecraft Charging Technology-1980, NASA CP-2182/AFGL-TR-81-0270, 1981, pp 931.

61. Grier, N. T., "Experimental Results on Plasma Interactions with Large Surfaces at High Voltages", NASA TM-81423, Jan 1980.

62. Konradi, A., McIntyre, B., and Polter, A. E., "Experimental Studies of Scaling Laws for Plasma Collection at High Voltages", Journal of Spacecraft and Rockets, Vol 21, No. 3, May-June 1984, pp 287-292.

63. Berkopec, F. D., Stevens, N. J. and Sturman, J. C., "The Lewis Research Center Geomagnetic Substunu Simulaton Facility", Procedings of the Spacecraft Charging Technology Conference, C. P. Pike and R. R. Lowell eds, AFGL-TR-77-0051/NASA TMX-73537, Feb 1977, pp 423-430.

64. Grier, N. T. and Stevens, N. J., "Plasma Interaction Experiment (PIX) Satellite Results", Spacecraft Charging Technology-1978, NASA CP-2071, 1979, pp 295-314.

65. Grier, N. T., Roche, J. C. and Ferguson, D., "The Plasma Interaction Experiment II (PIX-2) Flight Results", AIAA Paper 84-0331, Jan 1984.

66. Purvis, C. K., Stevens, N. J. and Berkopec, F. D., "Interaction of Large, High Power Systems with Operational Orbit Charged-Particle Environments", NASA TMX-73867, 1977.

67. Stevens, N. J., "Review of Biased Solar Array-Plasma Interaction Studies", NASA TM-82693, Apr 1981

68. Stevens, N. J., "Interactions Between Large Space Power Systems and Low Earth Orbit Plasmas", AIAA Paper 83-0310, Jan 1983.

69. Stevens, N. J., "Environmentally-Induced Voltage Limitations in Large Space Power Systems", IEEE Space and Nuclear Radiation Effects Conference, Colorado Springs, CO, July 1984.

70. Burrowbridge, D. R., "A Technique for Simulating the Ionospheric Plasma", NASA Report X-325-68-172, May 1968.

71. Ferguson, D. C., "Ram/Wake Effects on Plasma Current Collection of the PIX-II Langmuir Probe", and Metz, R., Private Communication Paper presented at the AF/NASA Environmental Interactions Conference, Colorado Springs, CO, Oct 1983

72. Stevens, N. J., "Effect of Space-Environmental-Induced Discharges on High Voltage Solar Array Performance", Paper D-6, 20th Annual Conference on Nuclear and Space Radiation Effects, IEEE, July 18-20, 1983, Gotlinburg, TN.

73. Domitz, S. and Kolecki, J. C., "Effect of Parasitic Plasma Currents on Solar Array Power Output", Spacecraft Charging Technology - 1978, NASA CP-2071/AFGL-TR-79-0082, 1979, pp 385-375.

74. Leung, P., "Discharge Characteristics of a Simulated Solar Cell Array", IEEE Transactions on Nuclear Science, Vol NS-30, No 6, Dec 1983, pp 4311-4315.

75. Snyder, D. B., "Discharges on a Negatively Biased Solar Array in a Charged Particle Environment", NASA TM 38644, Oct 1983.

76. Snyder, D. B., "Characteristics of Arc Currents on a Negatively Biased Solar Cell Array in a Plasma", NASA TM 83728, Jul 1984.